EVOLUTION OF AFRICAN EASTERLY WAVES AND THEIR RELATIONSHIP TO TROPICAL CYCLOGENESIS

by

Alan Brammer

A Dissertation

Submitted to the University at Albany, State University of New York

in Partial Fulfillment of

the Requirements for the Degree of

Doctor of Philosophy

College of Arts and Sciences

Department of Atmospheric and Environmental Sciences

2015

ABSTRACT

The research in this thesis explores the relationship between African easterly waves (AEWs) and tropical cyclogenesis over the eastern Atlantic. This research utilises 33 years of reanalysis and satellite data to investigate the interaction between AEW troughs, the surrounding environment and the embedded vortex.

Through the use of an objective tracking methodology and a logistic regression model, AEWs were objectively characterised based on a combination of variables with respect to their likelihood for tropical cyclogenesis over the eastern Atlantic. This characterisation of waves revealed that around 75% of AEW troughs leaving West Africa do not possess a structure conducive for genesis. Analysis of developing and non-developing waves that were favourable for genesis revealed the importance of the low-level environment over the eastern Atlantic as the troughs left West Africa.

Streamline and trajectory analysis showed that for up to 3 days after leaving West Africa, the AEW troughs were ingesting this low-level air from the northwest. Developing waves were associated with anomalously moist conditions, whereas non-developing waves were in the presence of low-level dry air. Back trajectories revealed that the low-level dry air observed in the non-developing cases was predominantly associated with low-level northerly flow over the subtropical Atlantic

Case study analysis of 2 developing and 2 non-developing waves showed patterns matching the composite results. As the troughs left West Africa, the low-level circulation was initially open to the environment from the northwest. The 2 developing waves although in the presence of jet-level dry air, were ingesting moist air at low-levels and sustained deep

convection within the trough. The 2 non-developing waves also had dry-air at the jet-level but were ingesting low-level dry air, thus inhibiting deep convection. Observed in all 4 cases was a consistent vertical tilt towards the southwest of the vortex. This tilt acted to extend the period of time the troughs remained sensitive to the environment. Therefore, even an AEW trough with an especially strong vortex may benefit from anomalously favourable environmental conditions through the lower troposphere over the eastern Atlantic.

ACKNOWLEDGEMENTS

I would like to first thank Dr. Chris Thorncroft for his role as my advisor over the years of this research. His support and advice not only greatly improved this research but my also my knowledge and understanding. Chris also provided the opportunity for me to come to Albany and experience the wonders of the USA.

Thanks also extends to Ryan Torn, John Molinari, Lance Bosart and Andreas Fink for their position on my committee and their valuable feedback in this research. Ryan is thanked in particular for the many discussions relating to a variety of topics; some of which in the end did not make it into the dissertation.

This work would not have been possible without the support of the faculty, staff and fellow graduate students at Albany. In particular, Kevin Tyle for responding to server issues or restarts at almost any hour of the day and Barbara Zampella who has saved me many hours and dollars while trying to resolve administrative issues.

Personal thanks extend to the friends I have gained while at Albany within and outside the department and to Erika in particular. Special thanks to my mother for the continued support over the years, even after I emigrated. Also to coffee and beer for sustaining me over the years.

Lastly, but possibly most important. This research would not have been possible without the financial support of the NASA grant NNX10AU44G. This was funded through the Hurricane and Severe Storm Sentinel (HS3) program. This program also provided me the invaluable experience of forecasting Atlantic tropical cyclones during 2012-2014.

CONTENTS

1. Introduction

Most tropical storms in the North Atlantic are in some way influenced by synoptic scale disturbances that propagate from tropical Africa westwards over the Atlantic (e.g. Erickson 1963; Carlson 1969b). These disturbances known as African easterly waves (AEWs) are linked to around 60% of cyclogenesis cases over the Atlantic main development region (MDR) and up to 80% of major hurricanes (e.g. Landsea 1993; Avila and Pasch 1995). However only a small fraction ($\leq$15%) of AEWs each year are associated with tropical cyclogenesis. Recent papers have highlighted the notable differences between the small number of AEWs that are linked to cyclogenesis and those that are not (e.g. Hopsch et al. 2010; Agudelo et al. 2011). However there still lacks a detailed understanding in whether a wave will lead to development, this is due to a large overlap in the characteristics of developing and non-developing waves.

Tropical cyclogenesis can be broadly categorised into two stages of development, a "large-scale formation" stage followed by a "core formation" stage (e.g. McBride 1995; Karyampudi and Pierce 2002; Tory and Frank 2010). To clarify semantics at the start, the focus of this thesis will be the large-scale formation stage and "genesis" will therefore reference this scale. This large-scale formation describes the development of a conducive environment and an enclosed incipient disturbance up-to "tropical storm" ($\geq$ 17.5 ms^{-1}) intensity. The second stage of development is then dominated by both dynamical and thermodynamic interactions across the mesoscale vortices embedded within the synoptic scale flow (e.g. Ritchie and Holland 1993; Montgomery et al. 2006). The temporal and spatial scale of these processes is such that high resolution observations or numerical modelling is necessary. The dynamics and thermodynamics involved in this 2nd stage will be a consideration throughout this work, however due to the scope of this research and the scale of the data included, results will be largely restricted to the larger scale formation stage.

There are well established climatological conditions associated with tropical cyclogen-

esis. These conditions generally consist of warm sea-surface temperatures ($\geq$26.5°C), a deep surface-based layer of conditional instability, cyclonic vorticity at low levels, deep convection with large-scale ascent and humidity, and weak vertical wind-shear (e.g. Gray 1968, 1988; Zehr 1992; Briegel and Frank 1997; Tory and Frank 2010). These characteristics vary on different time and spatial scales and have been used to produce genesis potential indicators and explain the inter-annual and seasonal variance of genesis across various basins (e.g. Gray et al. 1994; DeMaria and Kaplan 1994; Camargo et al. 2007). Over the tropical oceans during the summer months, SSTs are generally above 26.5°C with periodic weather patterns including easterly waves, equatorial waves mid-latitude intrusions influencing the remaining characteristics (e.g. Erickson 1963; Carlson 1969b; Frank and Roundy 2006).

Over the Atlantic MDR the strong link with cyclogenesis and AEWs has been well documented (e.g. Carlson 1969b; Reed et al. 1977; Landsea 1993; Thorncroft and Hodges 2001). These westward propagating waves can can provide both a favourable environment for tropical cyclogenesis and an associated incipient disturbance. The synoptic scale wave can usually be tracked back in time for numerous days preceding the genesis event. Analysis of the AEWs prior to cyclogenesis has shown significant correlation between seasonal AEW activity and Atlantic storm activity (Thorncroft and Hodges 2001). The characteristics of the individual AEW troughs over African coast has also been show to be significantly correlated with the likelihood of genesis occurring downstream (Hopsch et al. 2007, 2010; Agudelo et al. 2011). The following subsections will review in further detail the previous research on AEWs and influences on TC genesis over the eastern Atlantic.

1.1 African Easterly Waves

African easterly waves are synoptic scale waves that propagate along the African easterly jet (AEJ). They typically have wavelengths of 2000-3000km, a phase speed of around 8ms^{-1} and a frequency of approximately 3.5 days (e.g. Carlson 1969b,a; Burpee 1972, 1974; Reed et al. 1977). AEWs have been shown to be supported by the dry dynamics of the AEJ,

through barotropic and baroclinic energy conversion (Charney and Stern 1962; Thorncroft and Hoskins 1994a), with latent heating from moist convection also playing an important role in defining the observed structures (e.g. Norquist et al. 1977; Thorncroft and Hoskins 1994b; Berry and Thorncroft 2012).

On average AEWs exhibit a jet-level (700 hPa) maxima in vorticity, with the trough of the wave tilting against the vertical and horizontal shear around the AEJ core. At low levels, north of the AEJ, a dry vortex is usually located along the baroclinic zone to the northwest of the jet-level circulation (Fig. 1.1) (e.g. Reed et al. 1977; Pytharoulis and Thorncroft 1999; Janiga and Thorncroft 2012). At upper-levels anomalous flow depicts a weak divergent flow above the trough of the waves (e.g. Reed et al. 1977) consistent with convective profile. Typically AEWs are cold core at lower-levels, with vorticity maxima around 700 hPa and low-level temperature anomalies of around 1K. Figure 1.2 shows 3 stages of the reduction in the low-level cold core as the AEWs move from West Africa over the eastern Atlantic. Associated with this change in dynamics in the trough the precipitation associated with waves also transitions from ahead of the trough over Africa to symmetric around the trough axis over the ocean. Janiga and Thorncroft (2012) showed that the vertical structure vorticity aligned with the climatological generation of PV from diabatic heating.

The link between AEWs and TC genesis over the Atlantic was initially shown on a case by case example (e.g. Carlson 1969b). Later interannual variability of Atlantic tropical storm count was linked to the variability of rainfall over Africa and also AEW activity (Gray and Landsea 1992; Thorncroft and Hodges 2001). Thorncroft and Hodges (2001) showed that interannual tropical cyclone activity may be influenced by the number of AEWs with strong low-level vorticity as they left the West African coast, though later analysis questioned whether the number of waves was an important factor (Hopsch et al. 2007). The structure and characteristics of the waves as they leave the African coast has become the dominant focus of recent research instead.

Thorncroft and Hodges (2001) showed that the southern vortex track was more directly

linked to cyclogenesis events and that the northern tracks were rarely involved. However Chen et al. (2008) argued that while a greater number of southern tracks formed disturbances, the conversion ratio of northern tracks was higher due to being less frequent. The importance and roles played by the northern and southern vortices is still a somewhat open question with papers finding contrasting results. It is also important to consider the data source with model and reanalysis datasets influencing the representation of strength and location of the different tracks (Hodges et al. 2003).

The basic characteristics of the waves as they leave the coast have been shown to be an important factor for cyclogenesis (Hopsch et al. 2007). Hopsch et al. (2010) addressed this in further detail providing structural composites of developing and non-developing waves as they left the West African Coast. Developing waves were seen to have a stronger cold-core signature 2 days prior to reaching the coast, coincident with more intense convective activity. The waves then progressed towards a more warm core-like disturbance, with high values of low-level vorticity upon reaching the coast. Non-developing waves had much weaker low-level vorticity signatures and also tended to have a drier environment and mid-levels ahead of the trough, though the causality of this remains an open question.

Agudelo et al. (2011) showed that, once again, the structure of waves as they left the coast was an important predictor of the downstream genesis probability. The most useful predictors of developing in this large-scale statistical analysis were trough scale column integrated heating, vertical velocity and specific humidity. This statistical model therefore focused on the convective activity within the trough for a useful indicator of TC genesis downstream. While this study gives a statistical sense of a wave's likelihood of development, the processes involved were not included in the research. This paper, as well as Hopsch et al. (2010), both highlighted the variability in trough scale characteristics. Showing significant overlaps between the distributions of non-developing and developing waves across all variables, revealing numerous non-developing waves that had favourable characteristics for development.

The West African coast is characterised by a maxima in climatological rainfall during the summer months. As waves transition over this region they not only modulate rainfall but are also able to aggregate and develop low-level vorticity. Berry and Thorncroft (2005) suggested that the Guinea Highlands region of West Africa can play an important role in strengthening waves through potential vorticity generation and mergers. The convective influence on wave development in this region has also been shown in a number of case studies. Ross and Krishnamurti (2009, 2012) discussed the importance of intense deep convection with a scale of over 500 km and diabatic heating rates 3-6 times those typically observed. They suggested that over the coastal region, these sustained mesoscale convective systems (MCSs) would lead to an enhancement of the AEJ, which in turn would feed back to the synoptic scale wave through barotropic energy conversions. Leppert et al. (2013) presented a more direct link with the coverage of convection in the troughs of developing waves over the coast being a more important factor than the intensity. This widespread convection was argued to increase divergence aloft and convergence at low levels, with sustained increased diabatic heating leading to a warm core transformation of the disturbance.

Ventrice et al. (2012a) highlighted the relative scales of convection during a tropical cyclogenesis event, with a large scale eastward propagating convectively coupled Kelvin wave, coincidently passing the West African coast at the same time as an AEW with associated diurnally triggered convection. It was hypothesised that the large scale invigoration of convection aided in the intensification of the AEW trough and thus was an important role for cyclogenesis. The modulation of convection by equatorial waves has also been shown across other basins and other scales of equatorial waves. (e.g. Schreck and Molinari 2011). Kelvin waves also have a dynamical impact on the region potentially enhancing the available barotropic energy conversion (Aiyyer and Molinari 2008) or influencing the deep layer vertical shear (Ventrice et al. 2012b). The various scales and complicated interactions of convection in this region play an important role on AEWs which is still not fully understood.

The role of moisture of West African transitioning MCSs has also been shown to have

an influence on development over the eastern Atlantic. The relationship between horizontal flux of moist enthalpy and conversion of baroclinic energy was shown in a budget analysis to be important factors in a small sample of developing and non-developing cases (Arnault and Roux 2009, 2010). The modulation of the environment by downstream waves was shown to be important in the evolution of two consecutive waves, where the first wave increased southwesterly flow over the equatorial atlantic which provided a more conducive environment for the TC genesis associated with the following wave(Vizy and Cook 2009; Dieng et al. 2014).

1.2 Environmental Impacts on TC genesis

Moisture over the eastern Tropical Atlantic has a strong meridional gradient with frequent synoptic outbreaks of dry air from the Sahara during the late spring through to early fall (e.g. Carlson and Prospero 1972; Zhang and Pennington 2004). Typically about 28 outbreaks occur during July through September each year and can extend as far west as the Caribbean (Laken et al. 2014). As the Saharan air leaves the West African coast it rises over the oceanic boundary layer with a vertical layer typically between 800 and 500 hPa (Carlson and Prospero 1972; Dunion and Velden 2004).

It has been suggested that these Saharan air layer (SAL) outbreaks can have negative influences on tropical cyclones and cyclogenesis though this remains an open question (Braun 2010; Dunion and Velden 2004). Dunion and Velden (2004) suggested these outbreaks were potentially unfavourable for TCs with dry intrusions into convection enhancing evaporatively driven downdrafts cutting off the moist inflow for convection (Xu and Emanuel 1989; Powell 1990; Emanuel 1989). The thermal impacts of a mid-level warm anomaly have been argued to be both detrimental and favourable. Through an eastward extension of the AEJ, shear would be enhanced, limiting cyclogenesis however as storms are typically in the cyclonic shear of the mid-level AEJ this could be a favourable feedback through increasing vorticity (e.g. Karyampudi and Carlson 1988; Karyampudi and Pierce 2002). The impacts of the radiative effects on the basic state have been shown in numerical simulations however the

relationship with AEWs and cyclogenesis remains (Chen et al. 2010).

Observational studies have shown a significant correlation between the presence of dry air in the northwest quadrant and weakening tropical cyclone intensities (Shu and Wu 2009). Fritz and Wang (2013) however showed that while dry trajectories were able to penetrate near the vortex center of developing systems, transient dry air was moistened while being wrapped in and thus did not impact the deep convection. However, for systems embedded in a more persistently dry environment, upward moisture transport was reduced due to mid-level drying and enhanced by a lack of moisture supply from the boundary layer (Fritz and Wang 2013). Idealised numerical simulations have shown that mid-level dry air has to be within around 150 km of the vortex center for any impact to be felt, though these simulations were in an environment with no mean flow (Braun et al. 2012). When numerical simulations included vertical shear, the tropical systems were more sensitive to the environmental dry air, in better agreement with observational studies (Ge et al. 2013).

The ability for the surrounding environment to entrain and interact with a storm or incipient disturbance was addressed in Dunkerton et al. (2009). The authors hypothesised that there is a region within the trough of a wave, that depending on the wave relative flow, would recirculate air and protect the incipient disturbance from the potentially detrimental surrounding environment. Within this protected region, coined the "pouch", convective activity would progressively moisten the inner region of the trough increasing the chances of TC genesis (Wang et al. 2010b). An important factor in this paradigm is the 4-dimensional evolution of the "pouch". To benefit from such recirculation, the "pouch" region should have both temporal and vertical integrity. Changes in the background flow, phase speed or ascent through the region would potentially negate the benefit of such a recirculation. Riemer and Montgomery (2011) demonstrated with a simple kinematic model that depending on the background phase speed and the intensity of the vortex, the circulation could potentially be open to the environment in certain regions.

Using ensemble numerical simulations of SAL air has been shown to slow the develop-

ment of tropical storms over the eastern Atlantic. Sippel et al. (2011) showed that rate of development for a pre-depression system was sensitive to surrounding dry air over the eastern Atlantic. Once the system had developed however SSTs had the greatest impact and not the environmental dry air. Rios-Berrios et al. (2015) also showed, through ensemble Kalman filter simulations, that genesis forecasts were sensitive to the lower tropospheric moisture around a pre-depression.

1.3 Scientific Issues to be Addressed

The research on AEWs and TC genesis so far has mostly addressed all waves as equal prior to leaving the coast. Hopsch et al. (2010) briefly compared developing waves to non-developing waves with strong low-level vorticity and hypothesised that waves with very strong low-level vorticity may through dry advection lead to their own demise. Other research has shown that developing waves are very convectively active over the coastal region and are developing and aggregating vorticity as they leave the continent. Therefore defining waves on a single variable may not be a complete characterisation of a wave likely to develop and a combination of characteristics may provide a more complete objective measure of the waves with respect to TC genesis likelihood.

Recent TC genesis research has focussed on the relative flow around pre-disturbances and highlighted the utility of the Lagrangian framework (e.g. Dunkerton et al. 2009). This analysis requires a phase speed of the disturbance and therefore a tracking methodology for waves was developed. The tracking methodology was designed to focus on the coherent jet-level disturbance whereas previous research has used 850 hPa vorticity maxima this can follow the smaller scale disturbances within the AEW trough.

The Lagrangian reference frame provides a instantaneous view of the interaction between the environment and circulation as well as the time evolving structure of the AEW troughs. However trajectory analysis is required to fully detail the time evolving flow associated with AEWs. There is very little research on the relative flow around AEWs over

Africa and the eastern Atlantic, therefore this thesis will present an initial analysis of the large scale flow related to AEW troughs. This will also link changes in the kinematic flow to evolution of the AEW troughs.

This thesis will build on the research reviewed here, with the overall aim to improve the understanding of why a relatively small percentage of AEWs are associated with TC genesis over the eastern Atlantic. To address this aim, the research presented in this thesis will focus around the following questions:

1. What characteristics are associated with AEW troughs that are related to TC genesis and can these be linearly combined to produce a skilful diagnostic of genesis favourability?

2. What is the variability of AEW characteristics and how many troughs are diagnosed as favourable for TC genesis?

3. How does the environment influence the genesis or the non-genesis from favourable AEWs?

The data and methodologies used throughout this thesis will be detailed in chapter 2. Following this the research will be presented across four chapters. Each chapter will include a brief introduction with additional literature review and specific details about methodology where necessary. Each chapter will then close with a discussion and concluding remarks of the research presented therein. The chapters are organised as follows; Chapter 3 will introduce an objective measure for AEWs with respect to TC genesis and compare favourable developing and non-developing AEW troughs. Chapter 4 will analyse the large scale kinematic flow around AEWs and the associated regional differences. Based on the results of these chapters, Chapter 5 will present detailed case study of 2 developing and 2 non-developing waves. The composite analysis will provide the motivation to analyse how cases evolve in detail. This added detail will also provide further understanding of the processes involved. The final

chapter of the dissertation will discuss the overall results, final conclusions and ideas for future work.

1.4 Figures

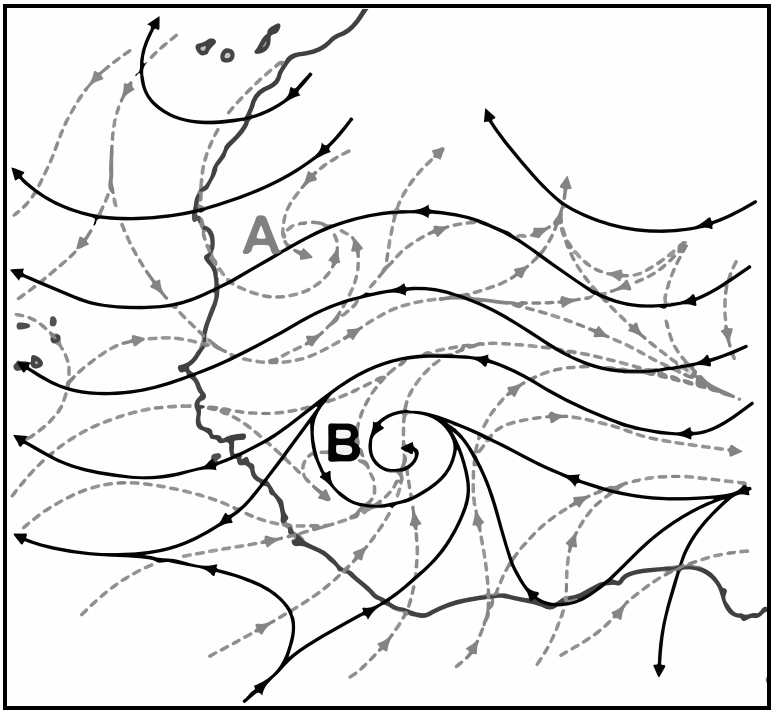

Figure 1.1: Streamlines at 700 hPa (black solid) and 925 hPa (dashed gray) associated with an African easterly wave over West Africa. A and B denote the northern low-level and southern mid-level circulations, respectively. Adapted by Janiga (2013) from Fig. 4a in (Carlson 1969a).

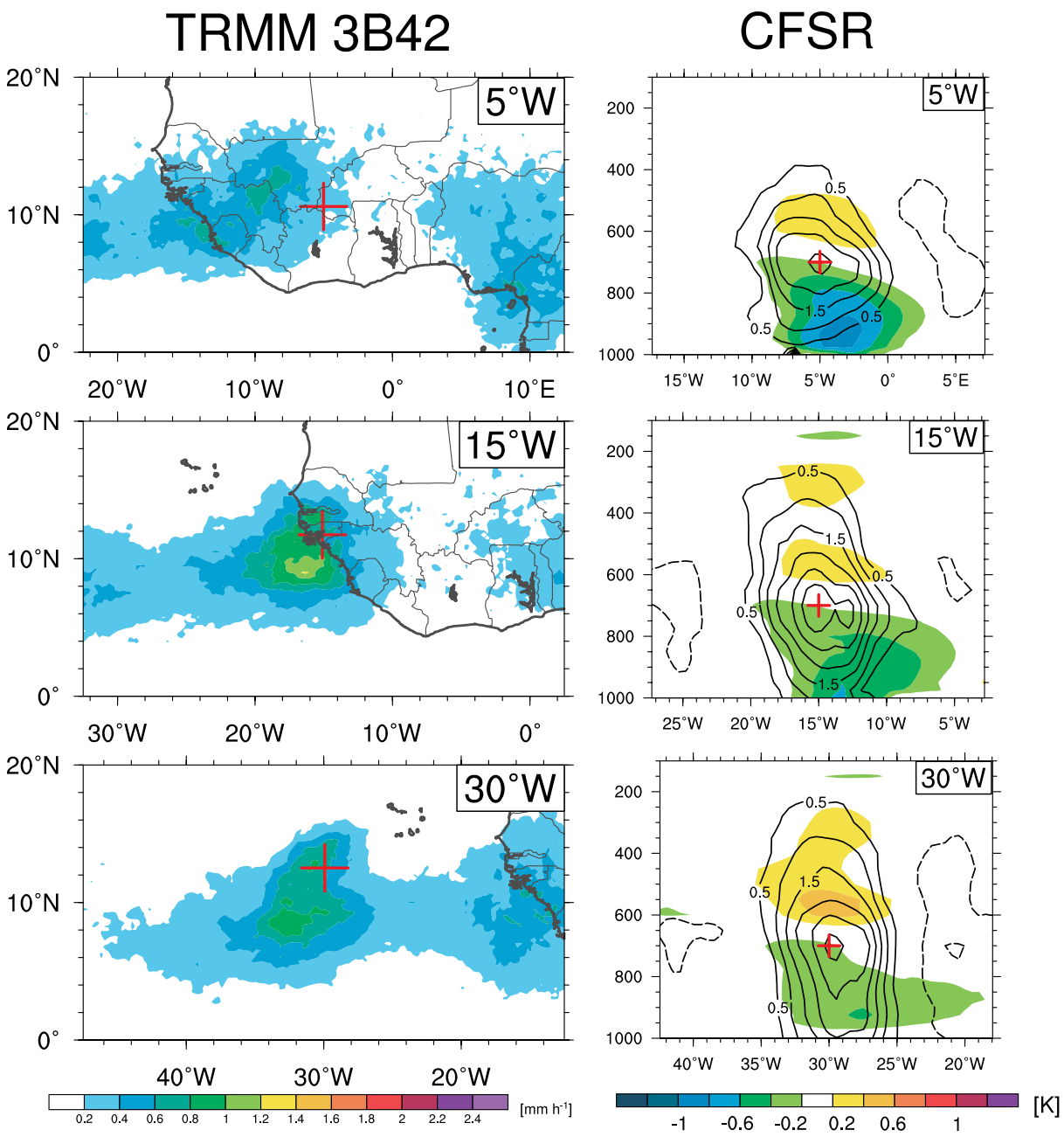

Figure 1.2: Left: Vorticity-maxima-centred composites of TRMM 3B42 rain rate (mm h^{-1}, shaded). Red crosses indicate the mean position of the composited 700 hPa vortex location. Right: Zonal cross-sections of 2-10 day band-pass filtered temperature (K, shaded) and relative vorticity (10^{-5} s^{-1}, contours). Cross-sections are centred on the latitude of the mean 700 hPa vortex position. From Figs 12 & 13 in Janiga and Thorncroft (2012).

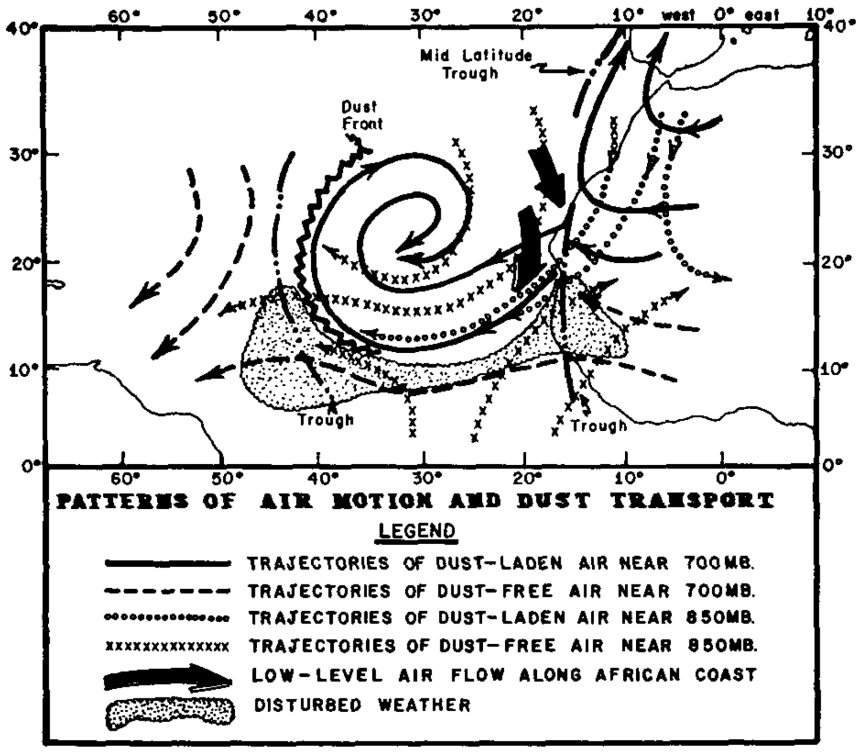

Figure 1.3: Schematic model of air motions accompanying the movement of African Disturbances and the associated dust pulses from Africa. Fig.20 from Carlson and Prospero (1972)

2. Data and Methodology

2.1 Data

2.1.1 Reanalysis

This research uses the most recent reanalysis data from the National Centers for Environmental Prediction (NCEP), the Climate Forecast System Reanalysis (CFSR Saha et al. 2010). This data spans 1979 - 2012 with a temporal resolution of 6-hours and horizontal resolution of 0.5°. The original CFSR was run for the time period 1979-2011. In 2011 the same dynamical core with only minor adjustment in model setup began running in realtime as CFSv2 (Saha et al. 2014). These two datasets provide a quasi-continuous analysis dataset from 1979 to present. Hereafter the combined datasets will be referred to as CFSR. Anomalies are calculated by subtracting a 32-year (1979-2011) climatology, calculated as the first four harmonics of the mean annual cycle, from every 6-hour period rather than daily means so that low-level anomalies were not aliased by the diurnal cycle.

2.1.2 Satellite Based Observations

Infrared brightness temperature is used throughout Chapter 3. This research uses the Gridded Satellite (GridSat-B1) data (Knapp et al. 2011; Knapp and NOAA CDR Program 2014). This dataset is available at a 0.07° horizontal resolution with a 3 hour temporal resolution. These data are available for 1980-2015. For the analysis in chapter 3, this meant that cases from 1979 were excluded from any analysis including the brightness temperature. Given the number of cases studied however this should not impact the results. These data are created through merging satellite observations in space and time to create a normalised continuous record over 30+ years. During the early 1980s satellite coverage over Africa was limited and there are periods where there remains missing data. Where possible data was averaged over a full diurnal cycle to both reduce the impact of the diurnal cycle on results and also reduce the impact of missing time periods. Given the almost 30 years of near

complete coverage, it is not expected that these deficiencies at the very start of the analysis impact the result in any meaningful way.

2.2 Methodology

2.2.1 AEW Tracking

As part of this research a tracking methodology was developed that is similar to that used by Agudelo et al. (2011) and Bain et al. (2014) utilising a hovmöller to determine the longitudinal track of the waves. AEWs are identified by analysing radially averaged curvature vorticity (with a radius of 500 km) close to the level of the AEJ (700 hPa). Curvature vorticity at 700 hPa was shown by Berry et al. (2007) to be a useful real-time diagnostic for distinguishing the trough of a wave from the background shear vorticity.

The tracking methodology is done in two steps: (1) a hovmöller is used to track waves in two dimensions (time and longitude, Fig. 2.1a), (2) the tracks are then refined into 3-dimensions using the hovmöller "guess" location and the previous latitude or starting at the center of the hovmöller. Both these steps use the same basic logic, using linear extrapolation of the track over the previous 24 hours. Maxima are connected using a cost function combining the expected location and the expected magnitude of the vortex. At times where multiple weak maxima are present, a magnitude weighted centroid is calculated to select the vorticity centroid at that time (Fig. 2.1b).

The hovmöller is used primarily for the waves when they are over Africa where the 3-dimensional vortex can be transient in nature. The temporally continuous synoptic scale wave is well captured by the hovmöller whereas a full 3-d vortex tracker would define multiple short-lived MCSs or small vortices. When the waves are over the ocean and are less latitudinally restricted, their projection onto the hovmöller can become separated from the center of the trough if they start to move out of the latitudinal bounds of the hovmöller . At this point, if the track is longer than 4 days and the vortex has been consistently strong, the hovmöller "guess" locations are dropped and the tracking relies on the extrapolation of

the system.

Wave tracks were then matched up with cyclone location data from the Atlantic HURDAT2 data (Landsea et al. 2014). A cyclone was deemed related to the wave if the tropical disturbance was first located within 500 km of the wave maxima. This allows for flexibility in the event of potential errors in both the tracking routine and in the location of disturbances in the reanalysis of dynamic fields (e.g. Schenkel and Hart 2012). Lastly, waves were only kept if they existed east of 5°W and west of 40°W. Therefore only well developed waves that fully transited the coastal region of West Africa and into the MDR are retained. For the developing subset here, only tropical cyclogenesis events east of 45°W were included. Systems that developed west of that longitude were excluded from both subsets. This threshold was chosen due to the reduced impact that the characteristics over West Africa will have as the waves move farther from the continent (Hopsch et al. 2010).

The track density of all waves is shown in Fig. 2.2. The density of tracks is comparable to other tracking papers with maxima over Western Africa and the MDR of the Atlantic (e.g. Thorncroft and Hodges 2001; Hodges et al. 2003; Chen et al. 2008). This tracking algorithm is able to detect systems that originate from the Ethiopian highlands, a potential source of AEW disturbances (Berry and Thorncroft 2005), and waves that transit the whole Atlantic ocean and cross over to the eastern Pacific. Some of these tracks may develop over the eastern Pacific but were not classified as developing; since only the Atlantic HURDAT data was used to match waves to named systems. This will not impact the results though, as the characteristics of the waves over West Africa and the eastern Atlantic will have very little influence that far downstream.

Waves are composited throughout the paper based on their time relative passage over the coastal region. Members in composites are shifted to the mean location at that time. All composites are therefore trough centric with location based on the number of hours from the West African coast. This passage over the coastal region (18°W) will be referred to as day 0 throughout.

2.2.2 Significance Testing

The statistical significance of composites was tested using a bootstrap method similar to Matthews and Kiladis (1999) and Schreck et al. (2013). This methodology uses the non-developing cases as the null cases for comparison with the developing cases. The null hypotheses for the composite analysis were that the developing and non-developing waves were comparable. The test generates 1000 randomly sampled equal sized composites for both subsets, and significance is found if 975 of the developing composites are either greater than or less than 975 of the non-developing composites. This two-tailed test returns significance at the 95% level for each grid cell and is not susceptible to differences in the sample sizes.

2.2.3 Trajectories

Kinematic trajectories were calculated from the 6-hourly 0.5° CFSR data using the HYSPLIT trajectory model (Draxler and Hess 1998). Trajectories were initialised between 10-20°N and 30-20°W at 1° horizontal spacing and vertically between 900 hPa and 600 hPa at 50 hPa intervals. These were initialised at the time the trough was closest to 18°W (i.e. over the coast) and run forward for 48 hours. Only trajectories initialised more than 350 km from the vortex centre were then analysed. If a trajectory came within 200 km of the vortex centre between 12 and 48 hours in the forward calculation it was deemed to have been ingested by the trough. While 200 km could be considered large for a mesoscale system, it is less than 10% of the typical AEW wavelength. Backward trajectories were calculated for those forward trajectories that were classified as ingested, with the backward trajectories calculated over the 96 hours prior to the wave leaving the coast. Kinematic trajectories from reanalysis data have limitations in their accuracy due to the interpolation methods used. For large scale flow, 0.5° and 6-hour trajectory calculations have been shown to be reasonably accurate outside of regions of strong ascent (Stohl et al. 1995). Hence, emphasis has been given to the flow prior to ingestion by the system as the convective nature of the disturbance is unlikely to be accurately represented by the reanalysis data.

2.2.4 Logistic Regression Model

A logistic linear regression model is utilised in section 3 to combine coastal characteristics of the AEWs. The model was developed through the selection and combination of variables, averaged over 500km around the trough vortex maxima. The selection method followed a forward step criteria (Wilks 2011) in which the model was developed iteratively increasing by one variable at a time. Variables were selected at each iterative step based on the lowest mean squared error from the verification set of waves and only coefficients that were significant at $\geq$95% were kept. The forward step development therefore had two stopping criteria; either mean squared error did not decrease with additional variables or the additional variables were no longer significant. While it would be possible to develop the model on a large number of predictors, this also has the likelihood to overfit the model to the training dataset, which will then perform poorly outside of the training data (e.g. Neumann et al. 1977). Predictors available to the selection process (Table 3.1) were chosen based on the results presented in section 3 and previous work, as well as variables that have been used in other statistical genesis and intensity models (e.g. DeMaria and Kaplan 1994; Dunion et al. 2013).

The development process trained the models on a random selection of 60% of waves and was tested on the other 40% to avoid over fitting the model to the training set. Once the variables were selected the final selection of variables was trained on the whole dataset.

2.3 Figures

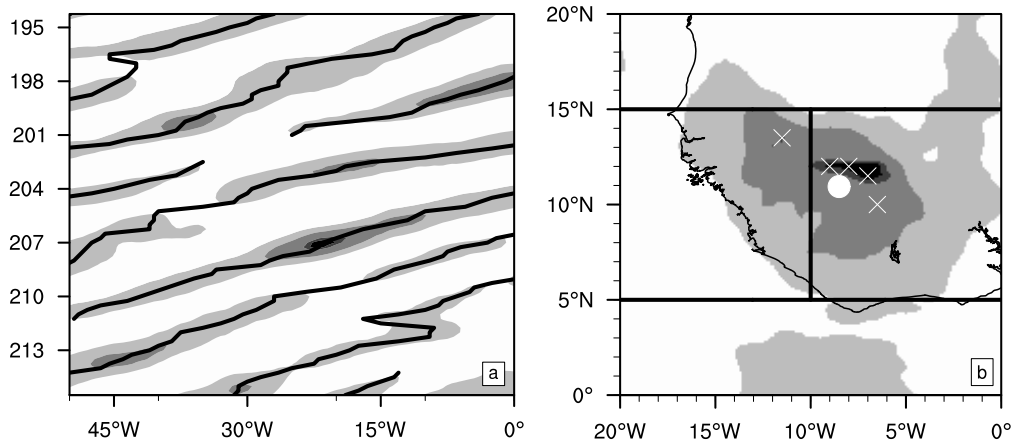

Figure 2.1: a) Hovmöller of Curvature Vorticity averaged 5:15°N. Black lines represent initial 2d track of waves on hovmöller. b) Example map of unfiltered curvature vorticity (700hPa), horizontal lines represent bounds of hovmöller, vertical line represents longitude of maxima taken from hovmöller. White crosses show local maxima, white dot shows final location of maxima determined through weighted mean of the local maxima.

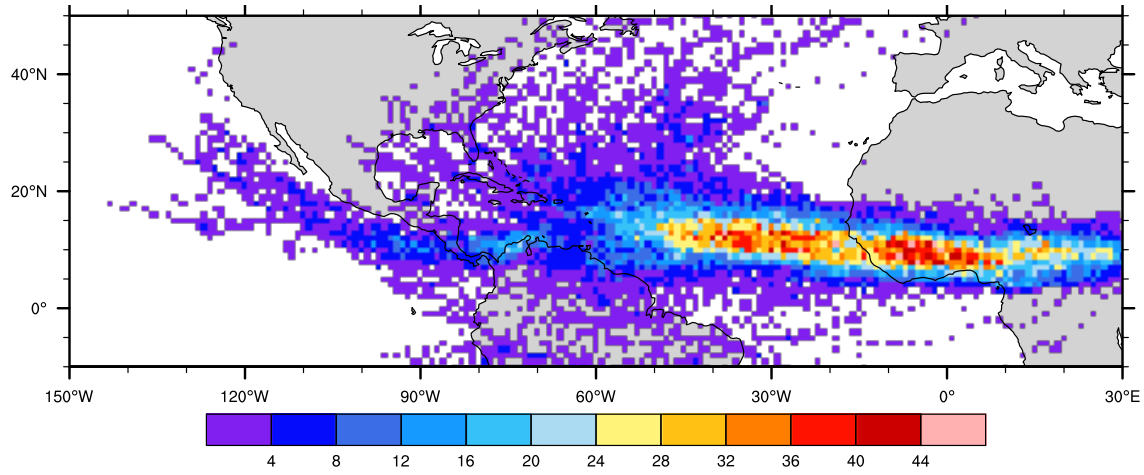

Figure 2.2: Count per 0.5° grid of all waves/storms originating from Africa tracked over 1979-2012.

3. Evolution and Variability of African Easterly Wave Structures

3.1 Introduction

The literature reviewed earlier in this thesis detailed the previous research on AEWs over West Africa and the relationships with tropical cyclogenesis. Analysis of AEWs in a Lagrangian framework, presented in this chapter, will document the evolution and variability of the vertical structure of developing and non-developing waves. These results will highlight that the variability in the differences between the means of the developing and non-developing subsets conceal a potential wealth of further detail. An objective characteristic of the AEW troughs will be developed to define waves favourable for TC genesis over the Eastern Atlantic. This will enable AEWs to be objectively defined based on a combination of characteristics as the trough leaves the coast. Composite analysis of waves favourable for TC genesis will therefore reveal further detail about developing and non-developing waves outside of the trough scale differences

3.2 AEW Characteristics and Evolution

This section will include analysis of the mean evolution of developing and non-developing AEWs across West Africa and the eastern Atlantic. This analysis will extend on the previous work which has shown composite structures at various locations (e.g. Reed et al. 1977; Janiga and Thorncroft 2012). Daily lagged composites or regressions based on a chosen point or region is a commonly used diagnostic tool to highlight the common evolution of AEWs (e.g. Kiladis et al. 2006). This tool is sufficient for waves with constant and consistent phase speeds but events with different phase speeds will deteriorate the analysis within a few days. Figures presented in this section are therefore all based on the location of the tracked AEW troughs and thus allow differing and variable phase speeds of the waves.

3.2.1 Evolution of Developing and Non-Developing Waves

The evolution of the vertical profile of trough-centric variables is presented in Fig. 3.1. These profiles show the longitudinal evolution of variables averaged over 500 km around the location of troughs' vorticity center. For every wave, azimuthally and radially averaged variables were taken around the center of the trough every 6 hours providing an evolution in space and time for each trough. These variables were then interpolated to a 0.5° grid and composited over all troughs. Therefore each vertical slice represents the profile of the composite trough at that longitude. The hatching on the developing composite shows the regions where there is no significant difference between the developing and non-developing composite.

Figure 3.1a,b shows the evolution of moisture within the trough of the non-developing and developing waves respectively. Non-developing waves are seen to have small positive moisture anomalies around the trough over land. As the waves leave the coast (around 18°W) the mean non-developing wave starts to moisten throughout the lower levels of the trough (700 hPa and below). In comparison, the developing waves have an increased amount of mid-level moisture over West Africa and rapidly moisten throughout the lower troposphere as they approach the coast, passing 20°W with >0.5 g/kg of anomalous moisture between 900 hPa to 400 hPa. As the developing waves leave the coast the entire column (<200 hPa) is significantly moister than the non-developing wave composite, with the mid-levels (300-800 hPa) being significantly different as far east as 0°.

The evolution of anomalous vertical motion, anomalous temperature and relative vorticity are also shown in Fig. 3.1. The developing composites are statistically significantly different from the non-developing composite west of around 0°, except temperature which becomes significantly different between 200-300 hPa west of 20°W. Anomalous vertical motion (Figs. 3.1c,d) shows that non-developing waves typically have a convective period over the West African coast, but this is localised to the coastal region. The developing waves show increasing vertical motion as they approach the coastal region, however the AEW composite

then maintains strong vertical motion over the eastern Atlantic. The thermal anomalies (Figs. 3.1e,f) associated with the AEW composites show that non-developing waves have a small positive temperature anomaly at the mid to upper levels consistent with convective activity. Developing waves however have a much stronger signal throughout the mid levels with a significantly warmer troposphere above 300 hPa from approximately 20°W. As the composite trough progresses westward, the significant differences gradually descend through the column. The bimodal peak of temperature in the developing waves, is interpreted as increased convective activity in general. The profile is generally consistent with both upper level heating from stratiform convection and mid-level heating from deep or shallow convection (e.g. Schumacher et al. 2004; Zhang and Hagos 2009; Ling and Zhang 2013).

The evolution of trough-based vorticity (Figs. 3.1g,h) is consistent with the previous figures. Developing waves exhibit a significantly stronger trough throughout the lower troposphere west of 0°, which extends up to 300 hPa upon reaching the coast. As the non-developing waves leave the coast a downward extension of the mid-level vorticity is seen between 20°W and 30°W. This result is consistent with the mean structures of all AEWs presented by Janiga and Thorncroft (2012) with a downward extension of vorticity occurring when the waves move over ocean. As before, developing waves exhibit stronger vorticity below 400 hPa over land and increase at a faster rate as they approach and leave the coast.

Figure 3.2a shows the evolution of mid-level humidity and vertical motion. Hovmöllers here are trough relative with the longitudinal distance from the trough center on the x-axis. The center vertical line therefore represents the westward propagating trough line. The mean longitude of the troughs for each time is also displayed on the ordinate. Contours of 500 hPa anomalous specific humidity of all non-developing waves show that the waves are typically moister than climatology around the trough and east of the trough axis. Ahead of the trough axis in the northerlies, negative anomalies are present in the non-developing troughs. This is consistent with the southerlies east of the trough bringing moisture poleward and northerlies drawing drier air equatorwards. The background shading shows the differences between the

developing and non-developing troughs. This reveals the significant differences in moisture are initially west of the trough axis. After leaving the coast the differences between the subsets colocates with the troughs axis with greater than 1 g/kg increased specific humidity around the trough axis 72 hours after leaving the coast.

The evolution of 500 hPa vertical motion relative to the mean trough line shows that vertical motion maximises around 3°W of the trough line. As the waves reach the coast the vertical motion also colocates around the trough axis. Over the continent there are no significant differences in the longitudinal distribution of vertical motion between the developing and non-developing subsets. Significant differences become apparent as the troughs reach the coast, with developing waves having increased vertical motion initially west of the trough axis. Similar to the moisture anomalies, these anomalies are centered around the trough axis within 72 hours of leaving the coast, as the troughs cross 40°W.

The thermodynamic profiles of the waves are consistent with previous studies concerned with the differences between developing and non-developing waves and the evolution of the composite troughs over West Africa and the transition to over the eastern Atlantic (e.g. Hopsch et al. 2010). The composite results here show that in general the mean of all developing waves is distinguishable from the mean of all non-developing waves as early as 0° to 5°W across a number of variables and are already evolving towards a developing tropical storm upon reaching the coast.

Figure 3.3 shows the differences in the evolution of convection between the developing and non-developing waves. The panels show the longitudinal and latitudinal distribution of convection relative to the wave troughs. The troughs are composited by a time lag relative to their passage over the West African coast. Figure 3.3a shows the difference in mean convection averaged 5°S to 5°N of the trough center. Significant differences between the subsets are apparent between 48 hrs and 60 hrs before the troughs reach the coast, when the waves are typically between 1°W and 4°W. The significant differences in convection at this time are ahead of the trough by around 300 km. As the troughs leave the African

continent the region of significant differences move east relatively towards the trough center. Janiga and Thorncroft (2012) showed that in general, convection in AEWs over the African continent occurred ahead of the trough and also moved towards the center of the trough as the waves moved over the eastern Atlantic. Figure 3.3b shows the convection now relative to the latitude of the trough center, focussing on the convection west of the trough axis, averaged 5°W to 0° of the trough line. Significantly colder brightness temperatures are evident north of the trough axis over West Africa. As the troughs approach the coast the differences in convection is spread evenly across the latitudes and doesn't show a substantial preference north or south of the circulation center.

The wave centric differences at -60,-36,0 and 36 hours relative to trough passage at the coast are shown in Fig. 3.4. These show in greater detail the spatial distribution of convection in the mean developing and mean non-developing waves. At 60 hours before the troughs reach the coast there is very little difference between the two subsets of waves. Generally convection is concentrated ahead of the trough with a reduced amount of convection in the southerlies and the ridge east of the composited trough. As the composite trough reaches the coastal region, convection increases over the Guinea Highlands near the coastline. Convection at this point is still predominantly west of the trough axis. At this time developing waves have significantly colder brightness temperatures over the Guinea highlands and along the coast. As the troughs move over the eastern Atlantic, convection is more focussed in the trough of the waves, as was shown in Fig. 3.3. Convection at this time is oriented almost SW to NE along the ITCZ with very little convection to the northwest of the trough. Developing waves however have significantly colder brightness temperatures along the trough axis of the AEW. After leaving the coast the mean non-developing waves lose most of their convection, only retaining a very weak signal to the south. Conversely, somewhat by their nature, developing waves have a large region of continued deep convection centered around the trough of the wave.

The intensity of convection is not necessarily well captured in the mean brightness tem-

perature plots, so the percentage of waves with brightness temperatures less than 240K are shown in Fig. 3.5. Leppert et al. (2013) noted that over the coastal region the areal coverage of brightness temperature less than 240K was a better indicator of an AEWs future genesis potential than the minimum of brightness temperature per wave. Figure 3.5 shows a similar evolution to the mean brightness temperatures. Northwest of the trough is a maximum in the occurence of moderate convection. At this time, developing waves do not exhibit any significant increase in the occurence of deep convection in any specific region of the wave (Fig. 3.5b). As the waves approach the coast the deep convection is also predominantly ahead of the troughs, in the region of northerly flow. At this time however the area of significant differences between the subsets is less than found when analysing the mean brightness temperature. Over the ocean, the occurence of brightness temperature less than 240K still has smaller regions of significant differences compared to the mean brightness temperature. Leppert et al. (2013) shows the coverage of intense convection was a good indicator of developing waves, this analysis has shown that spatially the occurence of deep convection doesn't have significant differences in specific regions. Due to the size and lifetime of deep convection associated with developing waves, however it is likely not that it is not spatially coherent enough for this analysis and percentage coverage over a broad area is more applicable.

The section has briefly shown the Lagrangian evolution of developing and non-developing waves across reanalysis variables and satellite based convection variables. The results here are in agreement with previous Eulerian views of the evolution of the waves over West Africa (e.g. Hopsch et al. 2010). The composite results here show that in general the mean of all developing waves is distinguishable from the mean of all non-developing waves as early as 0° to 5°W across a number of variables and are already evolving towards a low-level warm core depression upon reaching the coast. These figures, consistent with previous research, are however focussed on the composite means and therefore conceal the large variability that comprises both composites.

3.2.2 Variability of Developing and Non-Developing Waves

The variability of the developing and non-developing waves will be presented in this section. The overlap in the distributions of the subsets will reveal how frequently the characteristics associated with developing waves occur in the non-developing subset. Figure 3.6 presents the variability of specific humidity and relative vorticity as waves cross 20°W and 10°W. These plots highlight the variability contained within the mean structures which were presented in Fig. 3.1. While the means of both these variables are significantly different at both of these longitude bands, it is clear that there is a large overlap in the distribution of characteristics of both subsets of waves.

At 10°W both the variables show large overlaps in their distributions. Only the top 25% of developing waves at this point are distinguishable from the non-developing waves (i.e. do not overlap with the non-developing distribution). The largest separations in the characteristic distributions occur at mid-levels with around 25% of non-developing waves having lower humidity between 500-800 hPa than any of the developing waves and, conversely, 25% of the developing waves having higher humidity than any of the non-developing waves. Both sets of waves have a similar moist profile below the jet and a peak in vorticity around the jet-level.

At 20°W there is still a large overlap in the distributions of moisture. Above 900 hPa the moisture anomaly has increased across both subsets. However, differences in the relative vorticity distributions become more pronounced as the waves reach the coastal region. Between 50% and 75% of the developing waves have stronger vorticity than 75% of the non-developing waves below the AEJ at this location. The vertical extent of vorticity among the developing waves has increased with a maxima between 850 to 600 hPa, while the non-developing waves are still characterised by a pronounced jet-level maximum.

The distributions of the convective variables at multiple longitudes are shown in Fig. 3.7. Similar to the reannalysis based variables there is a large amount of overlap between the developing and non-developing subsets over the African continent. Fig 3.7a,b show the areal

coverage of IR brightness temperature less than 240 K and 220 K. In both plots it is clear that around 24-36 hours before the troughs reach the coast the mean of the distributions separate substantially. However there is a still a great amount of overlap in the tails of the distributions. After the troughs have left the coast, the distributions start to separate and there is much greater distinction between developing and non-developing subsets.

Figure 3.7c shows the minimum brightness temperature associated with each trough. Over land this appears to be a poor indicator for distinguishing between developing and non-developing waves. This has been shown before, with temporal and spatial coverage of convection suggested as a better indicator for developing AEWs rather than intense short lived convective bursts (e.g. Ross and Krishnamurti 2012; Leppert et al. 2013). Mean IR temperature west of the trough shows the greatest seperation between distributions prior to leaving the West African coast (Fig. 3.7d). Twelve hours before the waves leave the coast almost 75% of developing waves have lower mean IR temperatures than around 75% of the non-developing waves. This large seperation in the distributions is evident 48 hours before the waves reach the coast.

The distributions presented here are a very small example of the overlap in the subsets of these waves. The key point to note here is that, while the means of variables are different, there are potentially a comparable number of non-developing waves with characteristics similar to developing waves. These waves are effectively hidden in the composite analysis due to the large sample size of non-developing waves. Differences between developing and non-developing waves appear to begin as early as 48 hours before the troughs reach the West African coast, but there are many non-developing waves with comparable structure and convective signatures. It would therefore be difficult to objectively or subjectively identify waves as having the potential to develop from a single variable due to the overlap in the distributions. In the following section AEW troughs will be characterised through a logistic regression model using a combination of multiple variables.

3.3 Development of an AEW Genesis Diagnostic

The aim of this section is to define waves that are favourable for development based on a combination of trough characteristics prior to leaving the coast. Combining trough-centric variables through a logistic regression model provides a way to objectively define AEWs based on multiple characteristics with respect to downstream cyclogenesis probability. Table 3.1 displays all the initial variables considered in the model development. These are comprised of basic attributes derived from the track of the troughs (referred to as statistical predictors), variables extracted from the reanalysis dataset (synoptic predictors) and variables extracted from the GridSat-B1 dataset (IR predictors). These variables were chosen based on previous research and results from analysis presented in this chapter. The selection process of the statistical model is detailed in section 2.2.4. The satellite based observations suffer from some periods of missing data earlier in the study period, therefore models included these data are using a slightly reduced number of waves. Based on this limitation, the logistic regression model was trained using three different combinations of the available observations. Initially the model was provided with all the listed variables in table 3.1, secondly only the statistical and reanalysis based variables were included, finally only IR and statistical variables were provided to the model.

The receiver operating characteristic (ROC) curves for the three models are presented in Fig. 3.8a with the area under the curve (AUC) parameter included inset. A model of random guesses would fall along the y=x dashed line with an AUC of 0.5; a perfect model would have an AUC of 1.0. All three variations of the logistic model have very similar ROC curves. The models are excelling in part due to the large number of non-developing waves with very low values from the genesis diagnostic. The predictors chosen in each model are labelled with the superscript numbers in table 3.1. The three curves show that the two models which include the dynamical structure of the waves are slightly better than the model which relies on the satellite measure of convection. It is somewhat surprising that the diagnostic which does not include the satellite observations has the highest AUC. This

is likely because of the slightly higher sample size as the cases with missing satellite data could be included. There is low (around 0.25-0.3) but significant cross correlation between the individual reanalysis based predictors and the satellite based predictors. Therefore the reanalysis seems to be capturing the dynamical impacts of large scale convection within the troughs.

The diagnostic utilised in the rest of this research includes the statistical and reanalysis synoptic predictors. This final model included 5 predictors which were all significant within the model at 95% or greater. The resulting combination of variables is physically intuitive and is consistent with the results in the previous section. The coefficients (not presented here) reveal that a combination of increased upper-level temperature anomalies (400:200 hPa), relative vorticity at 850 hPa, vertical motion throughout the column (800:300 hPa), upper-level divergence (300:200 hPa) as well as the absolute number of days from the peak in the AEW season all point to favourable conditions for development. The first four variables are interpreted to be indicative of convective activity and associated low-level vorticity spin-up. Vorticity and anomalous temperature indicate previous convective activity which has modified the trough structure, while vertical motion and upper-level divergence are representative of current convective activity. These variables do exhibit significant cross correlation between themselves, however each variable improves the skill of the model significantly. The inclusion of the number days from the peak in the AEW season is a crude metric for capturing the large scale seasonality in the region.

Figure 3.8b shows the frequency of diagnosed genesis probability. The lowest bin of the diagnosed probabilities contains 75% of the non-developing waves, which makes clear that the majority of waves leaving the coast do not possess the combined characteristics that would be associated with tropical cyclogenesis. Therefore the inclusion of these waves in the developing and non-developing composite studies is concealing a lot of detail in the 25% of nondeveloping waves which are more favourable for tropical cyclogenesis.

AEWs can therefore be objectively defined using a combination of 5 predictors, which

when combined, indicate favourability for genesis within the wave between the African coast and 45°W. The metric will therefore filter out waves that have been defined as unfavourable and thus reduce the obvious differences in the trough scale features of the waves. A threshold was selected where there were an equal number of developing and non-developing waves. This retained 51 favourable developing and non-developing waves out of the original sample sizes of 65 and 382 respectively.

The distribution of these favourable waves with respect to day of year and year is shown in Fig. 3.9. These figures show that there are no obvious interannual differences or seasonal differences between these two subsets of waves. Favourable waves are found to leave the West African coast between late July and late September, with just one early season developing wave in mid-July.

The interannual variability in favourable developing and favourable non-developing waves are also similar (Fig. 3.9b). Also notable in this time-series is an increase in the total number of favourable AEWs between 1991 and 2012 that may be related to known influences of the AMO (Atlantic Multi-decadal Oscillation) on AEW characteristics (Martin and Thorncroft 2013). The relative roles played by the AMO and climate change on favourable AEW structures is an interesting topic but is beyond the scope of this study.

3.4 Analysis of Favourable and Unfavourable AEWs

The genesis diagnostic developed in this chapter enables each wave to be objectively quantified with regard to the characteristics of the trough relative to the probability of tropical cyclogenesis over the eastern Atlantic. Fig. 3.10 shows the distributions of the the areal coverage of IR less than 240 K and the mean IR brightness temperature west of the trough line for favourable and unfavourable waves. This is comparable to Fig. 3.7 but now with respect solely to the waves characteristics at the coast.

At about 48-60 hours before the waves reach the coast, it is clear that the favourable waves in general have higher rates of convection around the trough. At 60 hours before

the waves reach the coast, around 70% of the favourable waves have lower mean brightness temperature and higher coverage of moderate convection than the means of the unfavourable waves. There is still substantial overlap between the distributions however.

Evolution of specific humidity and vertical velocity for favourable and unfavourable waves reveals that significant differences now extend for the full 120 hours included in the analysis for mid-level moisture (Fig. 3.11). Favourable waves have significantly stronger vertical motion west of the trough axis west of 0° or once within 72 hours of the coast. Further analysis into the origins of favourable waves will not be conducted here however it appears that these waves may be identifiable throughout their evolution over West Africa.

3.5 Evolution of Favourable Developing and Non-Developing AEWs

Figure 3.12 shows the evolution of the favourable developing and non-developing waves. The regions of hatching (non-significant differences) now extends west to the coast across the 4 variables consistent with all the AEWs being favourable for genesis. The differences between these favourable composites, towards the left side of the figure, are expected as the developing waves will possess the characteristics of a tropical depression before 45°W. After leaving the coastal region, the two composites quickly exhibit significant differences in moisture, vertical motion and vorticity throughout the column. Non-developing waves exhibit strong vertical motion over the coastal region but rapidly weakens once over the ocean (Fig. 3.12c). Moisture, vorticity and temperature all increase in the favourable non-developing wave composite more than was shown in the composite of all non-developing waves (Fig. 3.1). Developing waves, however, have continued vertical motion after leaving the coast and increases in moisture, vorticity and upper-level temperature are significantly greater.

Trough-relative hovmöllers of 500 hPa specific humidity and 700 hPa vertical velocity are shown in Fig. 3.13. Here it is clear that favourable developing waves have significantly increased mid-level moisture between 200 and 600 km west of the trough-axis around 48 hours

before the troughs reach the coastal region. This significant difference is on the western edge of the gradient of moisture assocaited with the trough. This suggests that the moisture in the favourable developing waves covers a greater area and that the northerlies ahead of the trough are not as dry as in the favourable non-developing waves. At this same time there are no significant differences in vertical velocities between the two subsets. The mean non-developing waves do show maximised vertical motion west of the trough-axis, as shown previously but the developing waves are not significantly different until after leaving the coast. After crossing the coast the favourable developing waves have significantly increased vertical motion within 200 km of the trough-axis and the significant differences in moisture become more symmetric around the trough-axis.

Similar analysis of the trough relative brightness temperature shows that the observed convection also has no significant differences between the subsets prior to leaving the West African coast (Fig. 3.14). Upon reaching the coast, convection to the west and south of the trough center exhibits significant differences first but this quickly spreads to encompassing most of the trough region. These figures have shown that the trough scale characteristics of both the favourable developing and favourable non-developing waves are similar over West Africa. On crossing the coast convection evolves differently and significant differences are apparent very soon after the coastal transition.

The next section will analyse the large scale differences at the time when the waves cross the coast and the environmental influences on the waves that may lead to the differences in convection over the eastern Atlantic.

3.6 Environmental Differences Between Favourable AEWs

The large-scale differences between the favourable mean developing and non-developing waves at the time of coastal passage are presented in Fig. 3.15. Two pronounced regions with significantly different total precipitable water (TPW) are shown to the west of the composite trough (Fig. 3.15a). Developing waves therefore have a region with significantly

more moisture throughout the column to the northwest of the trough, while to the southwest the developing waves have significantly less moisture. These differences are located in a region of strong meridional moisture gradient. The north-south dipole structure of the anomalies suggests either a poleward shift of moisture in the developing composites or an equatorward shift of drier air in the non-developing composites. The mean developing wave contours show that the increase to the northwest is a separate region of anomalously increased moisture, likely the trough of a downstream AEW trough, with a reduced ridge between the two troughs. To the south, non-developing waves have horizontal axes with a greater southwest to northeast tilt such that the troughs extend farther to the southwest. Since moisture is greater along the trough axis, the developing waves have less moisture in this region.

Figure 3.15b shows increased upper-level (300 hPa) geopotential heights representative of a weaker mid-latitude trough to the north for the developing waves. This upper-level feature is displaced around 1000 km north of the composite troughs however. This difference is maximised at the level presented here, with significant differences extending down to around 600 hPa over the same geographical region. Associated with the differences in geopotential height are regions of significantly different wind (not shown here). Significantly increased northwesterly flow is present in the subsiding region on the western side of the mid-latitude trough. The developing wave composite (contour lines) shows that the difference between developing and non-developing composites is comparable to the difference between the developing composite and climatology. Therefore the non-developing waves have a more climatological structure with a mid-latitude trough in this region. The developing waves however exhibit a weakened mid-latitude trough and an associated region of increased upper-level temperature anomalies.

Vertical cross sections along 30°W and 20°W (depicted on Fig. 3.15b) showing the differences in moisture and geopotential height are presented in Fig. 3.16. Ahead of the trough (30°W; Fig. 3.16a) the differences in moisture are concentrated in the lower mid-

troposphere with the maxima at 850 hPa whereas the mid-latitude trough at this longitude has only a small area of significant difference. While the moist anomaly around 20°N is concentrated at low levels, along 5°N the region of decreased moisture extends from the boundary layer up to 400 hPa. Along the approximate longitude of the composite trough (20°W; Fig. 3.16b) there are effectively no significant differences in moisture. Around 30°N however, the developing waves exhibit increased heights with significant differences extending from 600 hPa up to around 200 hPa.

These figures reveal large regions of significantly different environmental conditions between developing and non-developing waves. Low-level moisture ahead of the waves is hypothesised to have a thermodynamical impact on the convection in the developing AEW trough through entrainment into and below the mid-level vortex of the trough. The upper-level flow north the of AEW however may have a less direct impact. While there are differences in the deep layer shear and upper-level temperature associated with the change in mid-latitude flow, these are restricted north of 20°N. It is hypothesised that the presence of a trough in this region, for the non-developing waves, will increase subsiding equatorward flow over the eastern Atlantic and may influence the environmental humidity ahead of the AEW trough.

The time-longitude evolution of these differences is presented in Fig. 3.17. The latitude bands used in the hovmöllers vary for each panel and are situated around the maximum differences in Fig. 3.15. The difference in moisture between the composite waves propagates westwards west of the composite trough, with significant differences extending back 120 hours when the troughs were over land (Fig. 3.17a). This difference in moisture is ahead (west) of the composited troughs over West Africa and the eastern Atlantic. Analysis of lagged maps reveals this represents a downstream AEW trough for the developing waves which has brought moisture anomalously far north on its eastern edge. Although this difference in moisture is present over West Africa based on the logistic regression output it appears to not influence the structure of the waves prior to the coastal region. Analysis of this northwest

region could however provide earlier information in determining the outcome of the waves after they leave the coast.

The geopotential height differences north of the composite troughs (between 20° and 30°N) is mostly a stationary feature across the latitude bands used (Fig. 3.17b). Significant differences appear in both fields at around 4 days prior to the trough passage at the coast. Analysis of the total fields at these times reveals that a more zonal flow is present in the developing composite, while the non-developing composite features a weak positively tilted mid-latitude trough and associated meridional flow. The influence the mid-latitude trough has on the eastern Atlantic is therefore present for around 4 days before the composited AEW troughs reach the coast.

Figure 3.18 displays wave-relative streamlines and anomalous specific humidity at 850 hPa from 96 hours before reaching the coast to 24 hours after at 24 hour intervals. At 96 hours before the composite troughs reach the coast, the mean longitude of the both composites is around 8°E. A clear difference is evident in the moisture over the western and southern edges of the Sahara, with developing waves having a large region of increased moisture. Around 72 hours before the troughs reach the coast the composite trough axis in both the developing and non-developing waves are evident at 0°. Both composites have a weak signal of a downstream trough which has just left the West African coast. The moisture to the north-west of the developing troughs seems to be associated with this downstream trough, which has greatly increased moisture northeast of the trough axis compared to the downstream trough in the non-developing composite.

As the downstream trough in the developing composite transitions over the eastern Atlantic it retains a strong positive moisture anomaly. The wave relative streamlines show that the 850 hPa flow is predominantly westerly, therefore the developing trough appears to be influenced by moisture advection from the downstream trough. At 48 hours and 24 hours before the composited troughs reach the coast, the relative flow west of the troughs, has a slight northerly component to it. At this time, the developing waves still have a large source

of moisture to the northwest associated with the downstream trough. The non-developing waves however have a slight negative moisture anomaly compared to climatology.

After the composite troughs have left the coast, the non-developing waves exhibit strong positive moisture anomalies however these are focussed to the north-east of the trough. On the western side of the trough line the non-developing waves exhibit negative moisture anomalies. Conversely, the developing waves possess strong positive moisture anomalies centered around the trough line and have no negative moisture anomalies to the west.

Wave relative streamlines at two levels in the lower troposphere (850, 700 hPa) for non-developing and developing waves are shown in Fig. 3.19. The wave relative flow is calculated by subtracting the phase speed of each wave from the wind components prior to compositing. When the troughs are over Africa, three days prior to reaching the coast (Figs. 3.19a,b), both composites exhibit almost zonal westerly relative flow below the AEJ (blue streamlines; 850 hPa). This is due in part to the monsoonal inflow which has a slight westerly component over this region in addition to the westward phase speed of the waves. At the jet-level (red streamlines; 700 hPa), the circulation associated with the composite trough is more evident; however, a region of recirculation is not evident in the streamline analysis at this time.

By the time the waves have left the coast (Fig. 3.19c,d), a closed circulation has become apparent at the level of the jet. Both waves exhibit recirculation in the streamlines where the vortex is strongest and the meridional shear of the jet allows for a moderate vortex on the southern gradient of the jet to recirculate. The relative inflow below the jet (850 hPa) has changed from westerly to northwesterly. Therefore, while at the jet-level air is recirculating in a 2-d sense, the vertical motion through the layer is being sourced from outside of the trough region. Over the eastern Atlantic, 72 hours after leaving the coast, both composites (Fig. 3.19e,f) have developed low-level recirculation regions. The non-developing waves are much weaker at this time, but in a quiescent background flow still have closed circulation at low levels.

From this analysis it is clear that as waves leave the coastal region, the wave relative streamlines below the jet are temporarily open to environmental air from the north and northwest of the trough. The streamlines suggest that the air that flows under the mid-level trough appears to have an origin from north and northwest of the trough. This region had significant differences in low-level moisture between the two composites, with developing waves having significantly increased moisture to the northwest in the lower troposphere. We hypothesise that waves are sensitive to the environment northwest of the trough in the 2-3 days after crossing the West African coast. The relative advection of either moist or dry air into the the lower levels of the vortex would likely influence the intensity and sustainability of deep convection, either helping or hindering the development process of favourable waves.

3.7 Trajectory Inflow for Developing and Non-Developing Waves.

The composite analysis highlighted large scale differences between the composites of waves diagnosed to be favourable for development upon leaving the coast of West Africa. Streamline analysis showed a potential kinematic route for the lower tropospheric moisture difference to directly impact the fate of the troughs. This section will present a trajectory analysis of the relative flow in a Lagrangian frame for all favourable waves. Trajectories were analysed with respect to each trough's track, with those that came within 200 km of the vortex centre classified as having been ingested by the system.

The fraction of all trajectories from the northwest quadrant that were ingested by the system within 48 hours after the trough had left the coast is shown in Fig. 3.20. Consistent with the streamline analysis of the previous section, there is inflow from the northwest quadrant with around 10-25% of the trajectories being ingested. The non-developing waves (Fig. 3.20a) have a higher fraction of ingested trajectories at greater initial distances from the trough. The developing waves (Fig. 3.20b) have the highest fraction of ingested trajectories originating from west-northwest of the trough and closer than 500 km at the initial time. The streamlines represent the 48 hour mean flow of the trajectories ingested by the troughs. The

non-developing waves have westerly flow across the vortex, whereas the developing waves exhibit recirculation. As the trough strengthens, the associated cyclonic flow will become more dominant than the background environmental flow enabling the stronger vortices to develop recirculation earlier than weaker vortices. The differences between the streamlines in Fig. 3.20 suggest that the developing waves are experiencing this strengthening and hence are not as open to the environment at greater radial distances.

The northwest quadrant was targeted due to the significant differences in moisture shown in section 3.6. Figure 3.21 shows the distribution of relative humidity and pressure for the ingested trajectories at 6 hour intervals relative to the time of each trajectory's closest pass to the trough center. The trajectories for the non-developing waves have significantly lower humidity at all time periods, though the distribution does shift towards higher humidities over time. The pressure of the trajectories is also significantly different over the first 18 hours. Around 50% of trajectories ingested by the non-developing waves are being initialised higher than approximately 75% of those ingested by developing waves. This suggests that as the developing waves strengthen, the layer of relative inflow is reduced to lower levels. The non-developing waves however, stay open to the environment over a greater depth due to the lack of strengthening.

3.8 Discussion and Conclusions

The characteristics of AEWs over the West African continent have been shown to be significantly related to the probability of tropical cyclogenesis over the eastern Atlantic. A tracking methodology was developed and a Lagrangian evolution of developing and non-developing waves was presented. This confirmed significant differences between developing waves and non-developing waves consistent with previous studies (e.g. Hopsch et al. 2010; Agudelo et al. 2011). In agreement with Janiga and Thorncroft (2012), convection was observed west of the composite troughs over West Africa. Developing waves had significantly colder brightness temperatures west of the trough axis after passing 0°. In both developing

and non-developing waves, as the troughs move over the ocean convection transitioned to be located around the trough axis. After leaving the coast most non-developing waves lose their convective signature in the mean composite with only a weak ITCZ signature remaining. Areal coverage of moderate convection ($\leq$240K) showed very similar evolution to mean brightness temperature and did not appear to reveal a greater distinction between developing and non-developing waves.

The variability of trough based characteristics highlights that there are a large number of non-developing waves that are characteristically similar to developing waves. Due to the sample sizes in the subsets there are typically more non-developing waves based on a certain threshold of a variable. This highlights that a lot of detail between developing and non-developing waves has been lost due to the sample sizes of the non-developing waves.

A logistic regression model was used to objectively define AEWs based on a combination of trough-centric variables. The logistic regression model was developed over three streams, combined track and reanalysis variables, track and brightness temperature variables and finally a combination of track, reanalysis and brightness temperature variables. Surprisingly the addition of brightness temperature variables did not greatly improve the model. Possibly due to less consistent temporal coverage in 1979 and 1980, therefore less waves were available, the ROC AUC metric was marginally lower for the model based on all three types of variable. The model determined that a combination of upper level divergence and temperature, with mid-level vertical motion, low-level vorticity and the number of days from the peak in the AEW season are able to statistically predict the outcome of eastern Atlantic genesis from AEWs with high skill.

Based on the logistic regression model, approximately 75% of non-developing waves are very unfavourable for genesis over the eastern Atlantic. This result highlights that comparisons between the few developing waves and all non-developing waves are limited in their usefulness. The logistic regression model objectively defined waves that were used in a composite analysis of 51 developing and non-developing favourable waves at the West

African coast.

This chapter has presented differences between developing and non-developing waves which were selected based on their trough scale characteristics over the West African coast. The two subsets therefore had minimal differences around the composite trough as they transitioned over the coast. Composite analysis of the two subsets revealed large scale significant differences in the environment around the troughs. As the troughs are over the coastal region, the composite developing trough has significantly increased lower tropospheric moisture ahead of the troughs. To the north of the non-developing composite there is an stronger mid-latitude trough present over the north-eastern Atlantic.

Wave relative lag composites revealed that the developing waves have consistently increased moisture to the north-west of the trough axis during their evolution over West Africa. Low-level wave relative streamlines show that typically the troughs experience almost zonal westerly flow through the low levels of the trough over the continent. As the troughs reach the coast the low-level flow acquires a slight northerly component, eventually becoming a cyclonic region of recirculation within 72 hours after leaving the West African coast. At the level of the AEJ (700 hPa) the vortex of the waves is maximised and the waves develop recirculation much sooner, in part due to the cyclonic horizontal shear of the jet. The kinematic flow is remarkably similar across the developing and non-developing favourable waves. The key difference is that as the waves move over the ocean the developing waves have postive anomalous moisture flux from the northwest into the low levels of the trough, while non-developing waves have a negative anomalous moisture flux from the northwest into the trough.

Dunkerton et al. (2009) suggested that AEW and other westward propagating disturbances have a region of recirculation. This region effectively protects the inner environment from external intrusions, this allows the interior to continuously moisten through convection, provide an area for vorticity aggregation and later TC development. The composite analysis here suggests that while the AEW troughs exhibit recirculation at the jet-level they remain

open to the environment below the jet for around 3 days after leaving the coast. While the figures presented here have focussed on specific humidity the analysis looks very similar in moist static energy or equivalent potential temperature (θ_e). The negative influences of dry air or low equivalent potential temperature typically focus on how the mid-layer minimum in θ_e can impact the boundary layer through convective downdrafts (e.g Bister and Emanuel 1997). Tang and Emanuel (2010, 2012) diagnose the impact of mid-level dry air on the system using an entropy deficit framework to analyse the ventilation of the storm. The impact on AEWs can be more direct than more developed storms as the vortex is still open to the environment. Developing and non-developing AEWs therefore have the same direct pathway for the environment to influence the storm. Positive moisture flux will moisten the low-level vortex, aiding deep convection, reducing the negative impacts of downdrafts and increasing θ_e in the lower levels of the trough. Negative moisture flux however will increase impact of downdrafts, reduce convection and potentially dry in the inner core.

For TC genesis from AEWs the chapter here suggests that not only does the wave need to be convectively active over West Africa thus creating a favourable wave for development. The favourable waves also then need anomalous environmental conditions over the eastern Atlantic to help the development of the trough. Before the vortex has extended down to the boundary layer, the troughs are susceptible to the environment in the NW quadrant. Over the eastern Atlantic this can be very unfavourable for TC genesis.

3.9 Tables and Figures

Table 3.1: Predictors used in development of statistical model to diagnose AEW genesis favourability. Bold variables are those used in the final model, selected via a forward step criteria process. Synoptics predictors are extracted over a 500 km radius around the trough location. IR predictors were extracted over 5°S to 5°N and 5°W to 0° box relative to the trough location.

Statistical Predictors	Synoptic Predictors	IR predictors
| Julian day - 239 |[123]	850:700 hPa Specific Humidity	Mean IR Brightness Temp[1]
(Peak Day of AEW activity)		
Latitude of system	600 hPa Relative Humidity	Std. Dev. IR
Total Phase Speed of wave	**Relative Vorticity (RV) 850 hPa[12]**	Minimum IR
Meridional Phase Speed	RV 850:600 hPa layer average	Area less than 240 K[13]
Zonal Phase Speed	RV 600-850 hPa difference	Area less than 220 K
850RV 5° longitude tendency[3]	**400:200 hPa Temp Anom[12]**	Mean IR 24 to 0 hours before coast[3]
	200 hPa Divergence	Mininum IR -24:0 hr
	300:200 hPa Divergence[2]	Area less than 240 K -24:0 hr
	Vertical Velocity 800:300 hPa[12]	Area less than 220 K -24:0 hr
	Deep Vertical Shear 200-850 hPa	
	Mid. Vertical Shear 500-850 hPa	

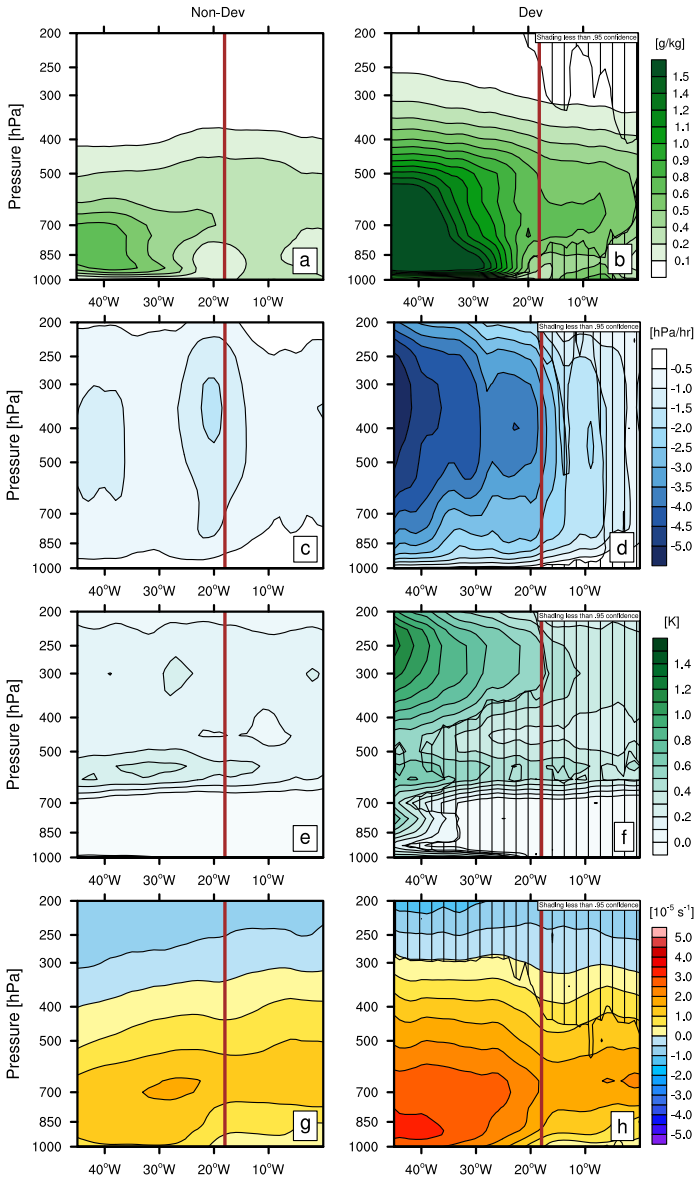

Figure 3.1: Vertical evolution of trough centred variables averaged over 500 km radius. Mean non-developing waves (a,c,e,g; n=382) and mean developing waves (b,d,f,h; n=65). Hatched region denotes areas which are not significantly different to non-developing composite at 95%. a,b) Anomalous Specific Humidity [g/kg]. c,d) Anomalous Vertical Motion [hPa/hr]. e,f). Anomalous Temperature [K]. g,h) Relative Vorticity [$10^{-5}s^{-1}$]. Approximate longitude of coast denoted by vertical brown line.

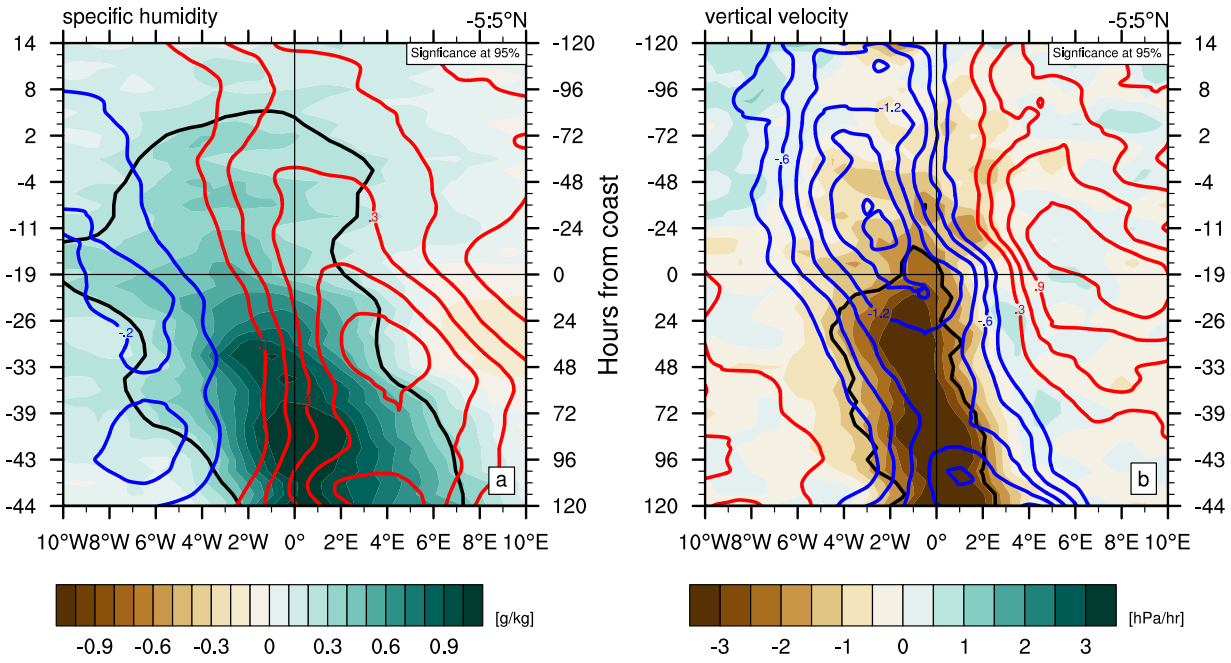

Figure 3.2: Trough relative hovmöllers of specific humidity (a) and vertical velocity (b). Contours depict non-developing composite. Shading shows developing composite - non-developing composite. Variables are averaged over 5°S to 5°N relative to each troughs latitude. a) Anomalous Specific Humidity (500 hPa) [g/kg]. b) Anomalous vertical motion [hPa/hr]. Bold black contours encompass regions of significance greater than 95%.

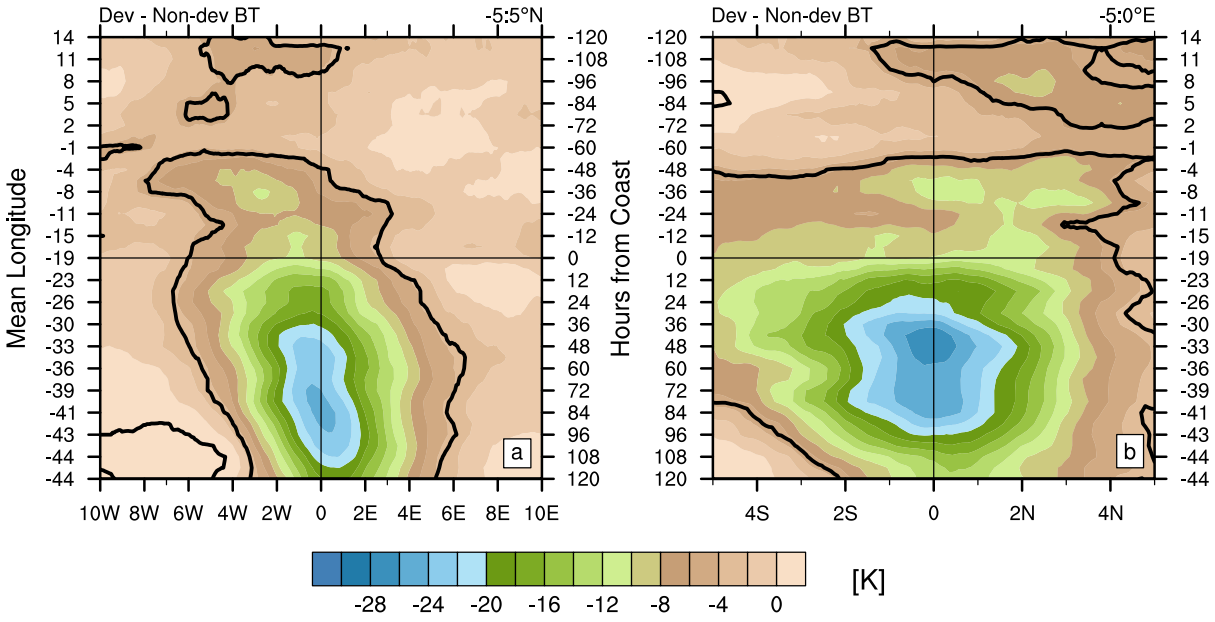

Figure 3.3: Trough relative hovmöllers of differences in infrared brightness temperature between developing and non-developing waves. Shading denotes developing - non-developing of mean IR brightness temperature [K]. Bold black contours oultines regions of significance at 95%. The x-axis of each trough is relative to the trough center. Mean longitude of the troughs per time is displayed along the y-axis. a) Differences relative to the longitude of the trough, averaged ±5° latitude around the center. b). Differences relative to the latitude of the trough, averaged -5 to 0° longitude of the trough axis.

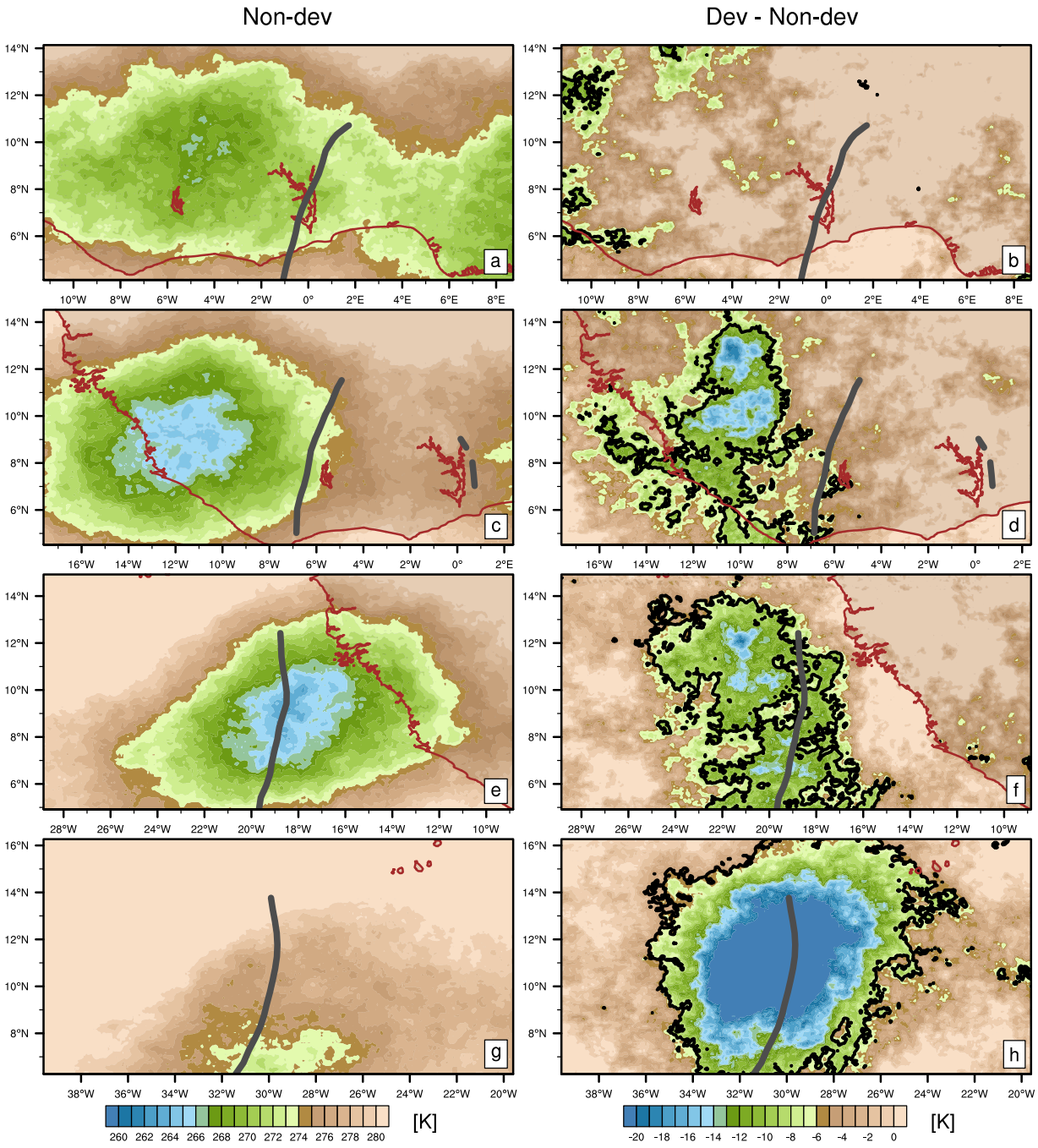

Figure 3.4: Trough relative composites of mean IR brightness temperature of non-developing waves (a,c,e,g) and difference between developing and non-developing (b,d,f,h). Areas of significance outlined by bold black contour. Rows show waves relative to the coast at -48,-24,0,+24 hours. Grey contour depicts mean trough axis of all waves.

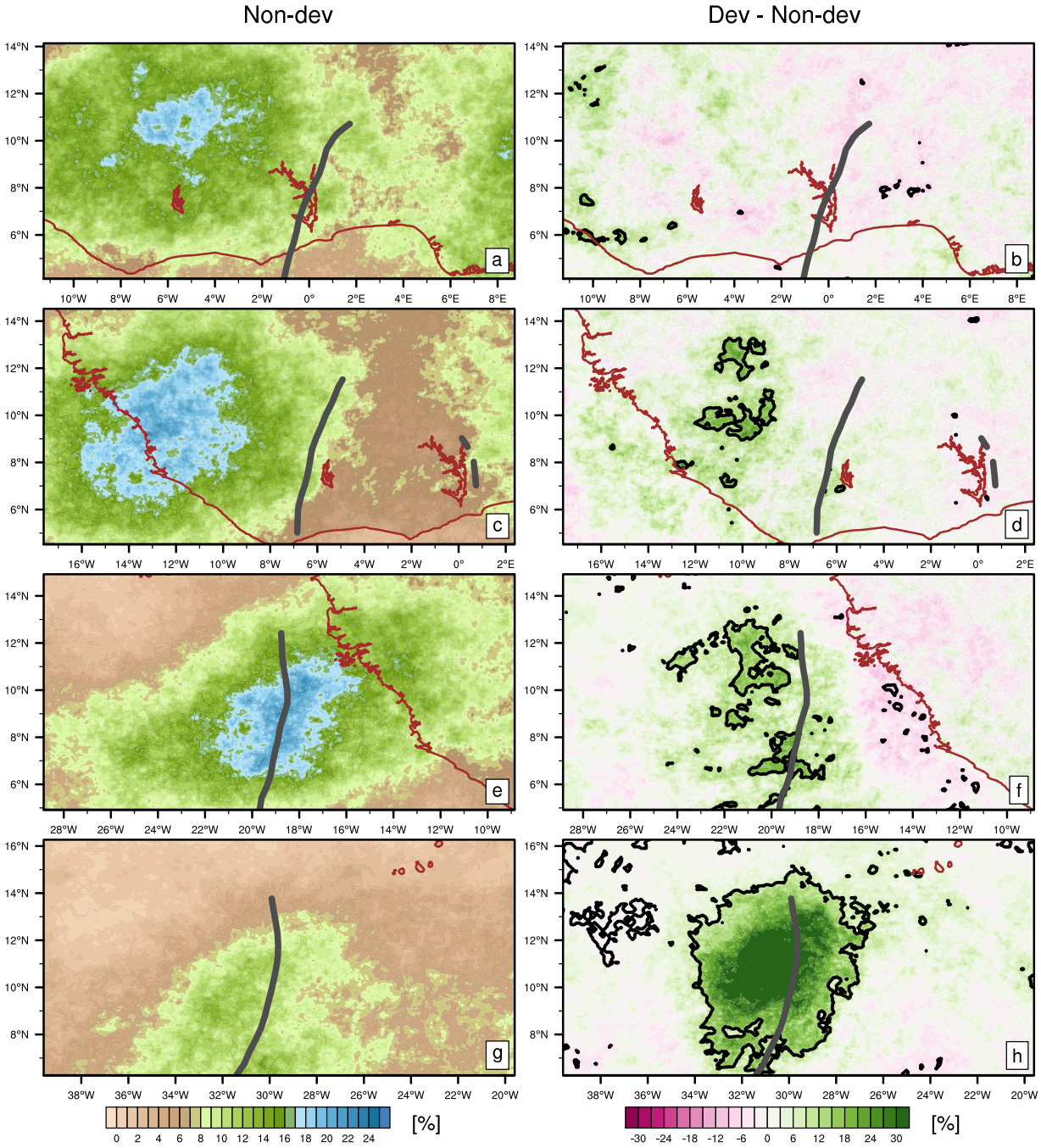

Figure 3.5: Trough relative composites of percent of waves with IR brightness temperature less than 240K per grid cell of non-developing waves (a,c,e,g) and difference between developing and non-developing (b,d,f,h). Areas of significance outlined by bold black contour. Rows show waves relative to the coast at -48,-24,0,+24 hours. Grey contour depicts mean trough axis of all waves.

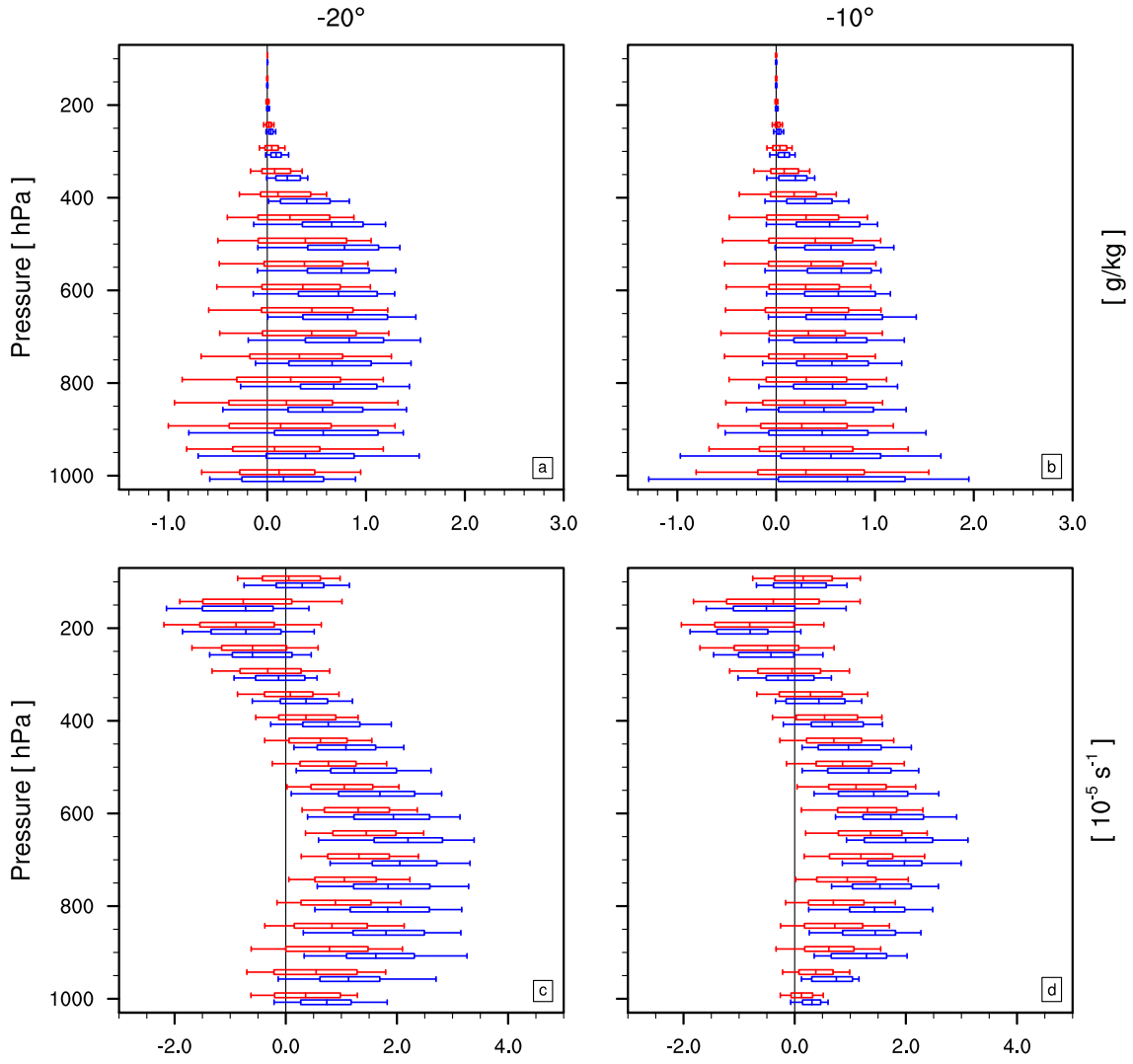

Figure 3.6: Distribution of variables with height (y-axis) and longitude (columns) of developing (Blue) and non-developing (Red) waves. Ends of whisker represent min/max, box displays the quartile range, and vertical line shows mean. Columns show variability at 20°W and 10°W (a,c & b,d respectively). Rows shows specific humidity [g/kg] and relative vorticity [$10^{-5}s^{-1}$] (a,b & c,d respectively).

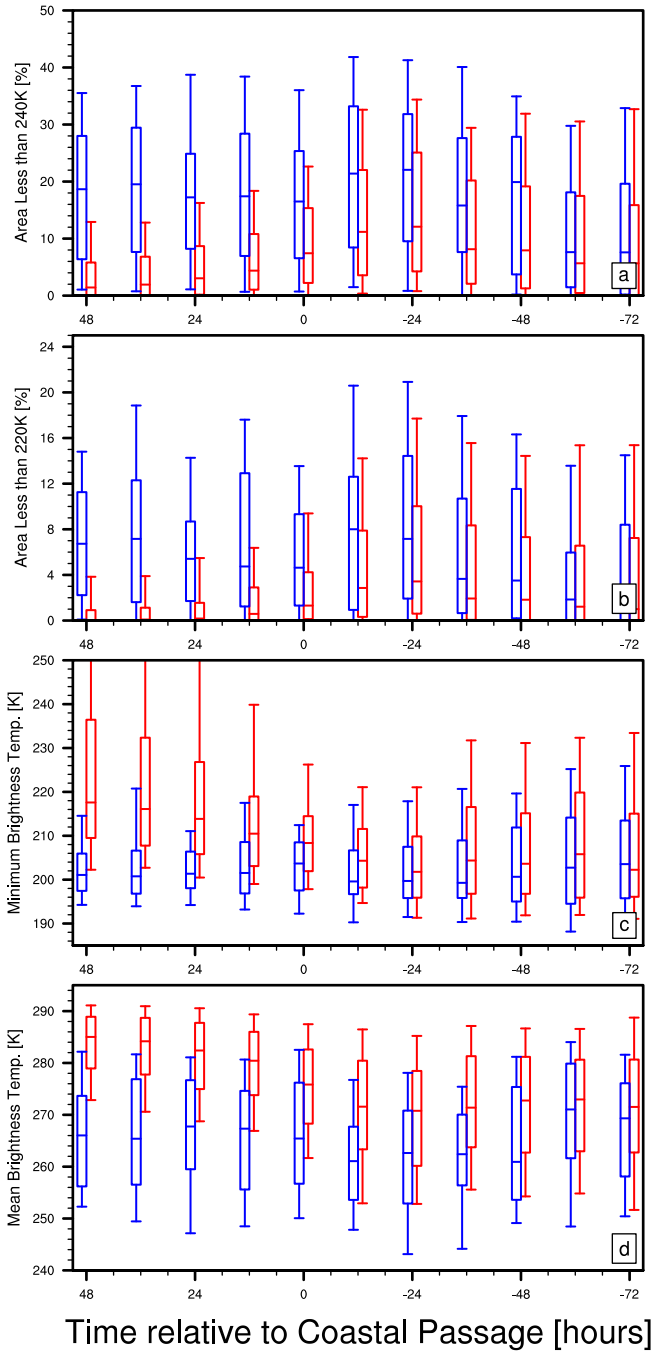

Figure 3.7: Distribution of variables with time (x-axis) of developing (Blue) and non-developing (Red) waves. Ends of whisker represent min/max, box displays the quartile range, and horizontal line shows mean. All variables were analysed over 5°S:5°N and 5°W:0° relative to the trough location. a) Percent area of IR grid cells less than 240K. [%] b) Percent area of IR grid cells less than 220K. [%] c) Minimum IR temperature. [K] d) Mean IR Temperature. [K]

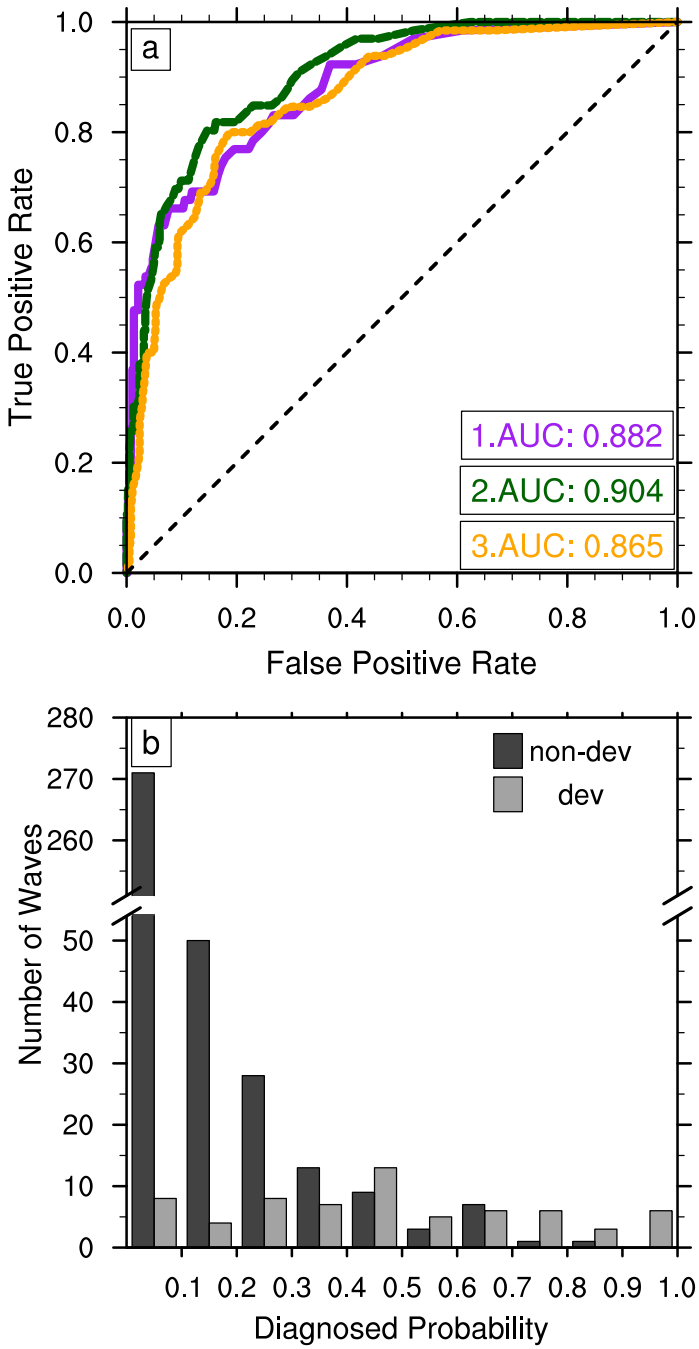

Figure 3.8: a) ROC curves for three AEW genesis diagnostics with the ROC area under curve included. The dashed line would represent a model of random guesses. 1. All predictors, 2.Statistical and Model predictors, 3.Statistical and IR predictors. b) Frequency of waves binned to 0.1 probability bins derived from the statistical and model based diagnostic. Note the ordinate is broken from 55-255. Non-developing and developing adjacent bars represent the same bin along the x-axis.

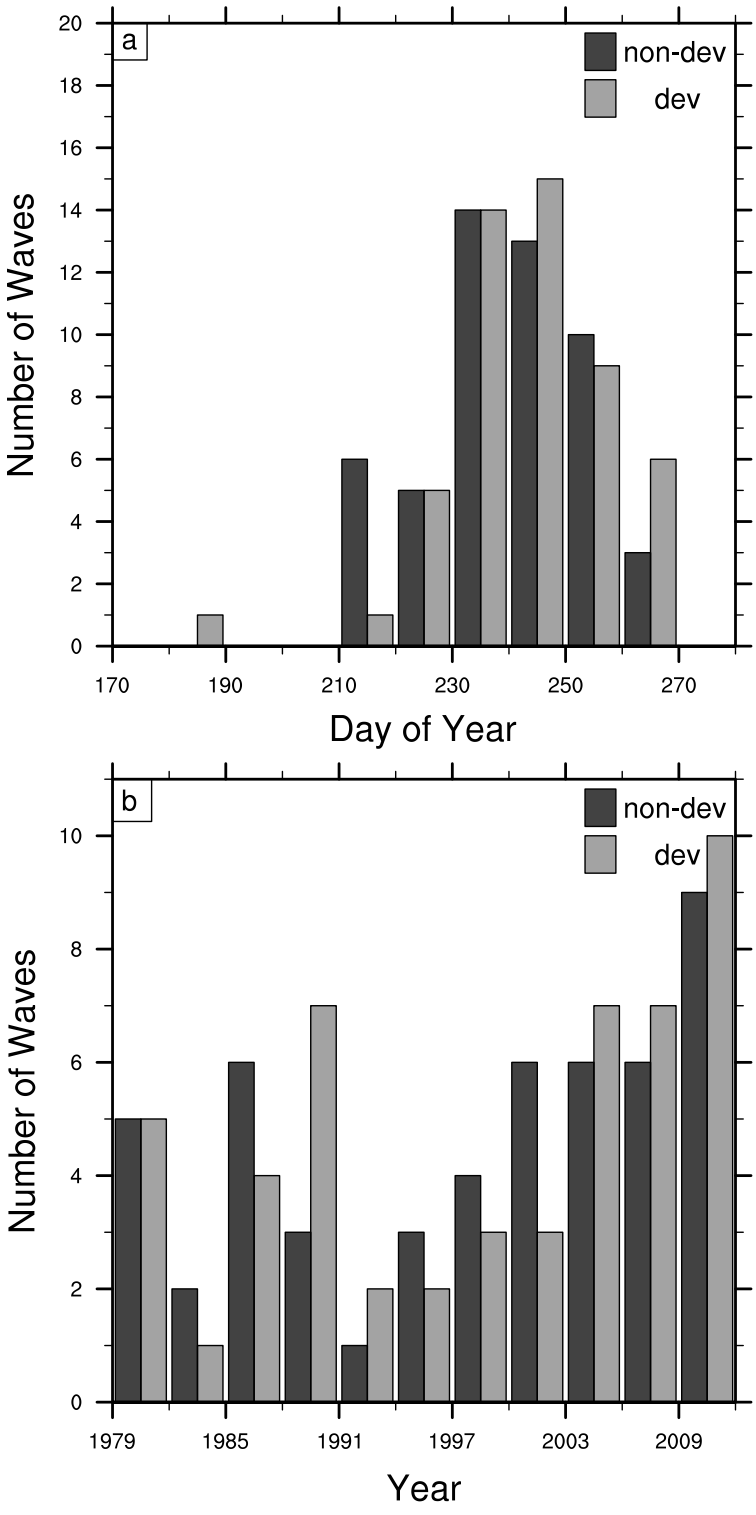

Figure 3.9: Frequency of favourable developing and non-developing waves. a) Day of year at 10-day intervals. b) Year at 3-year intervals

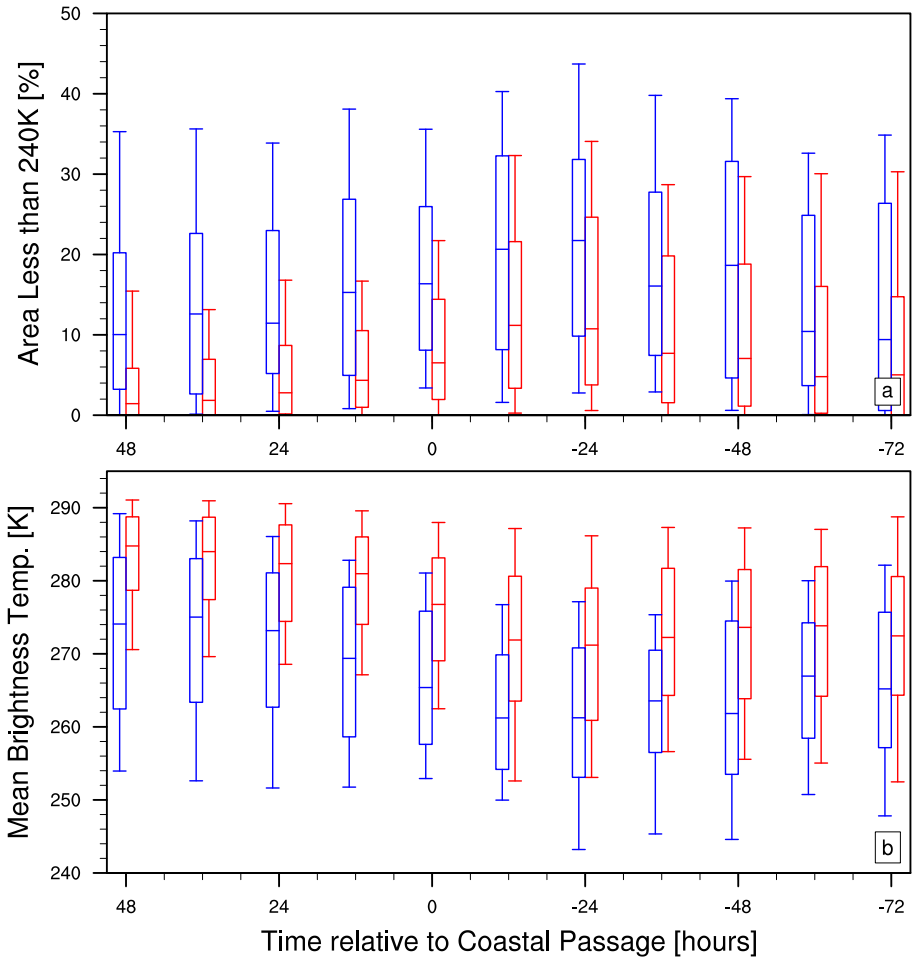

Figure 3.10: Distribution of variables with time (x-axis) of favourable (Blue) and unfavourable (Red) waves defined by logisitc regression model. Ends of whisker represent min/max, box displays the quartile range, and horizontal line shows mean. All variables were analysed over 5°S:5°N and 5°W:0° relative to the trough location. a) Percent area of IR grid cells less than 240K. [%] b) Mean IR Temperature. [K]

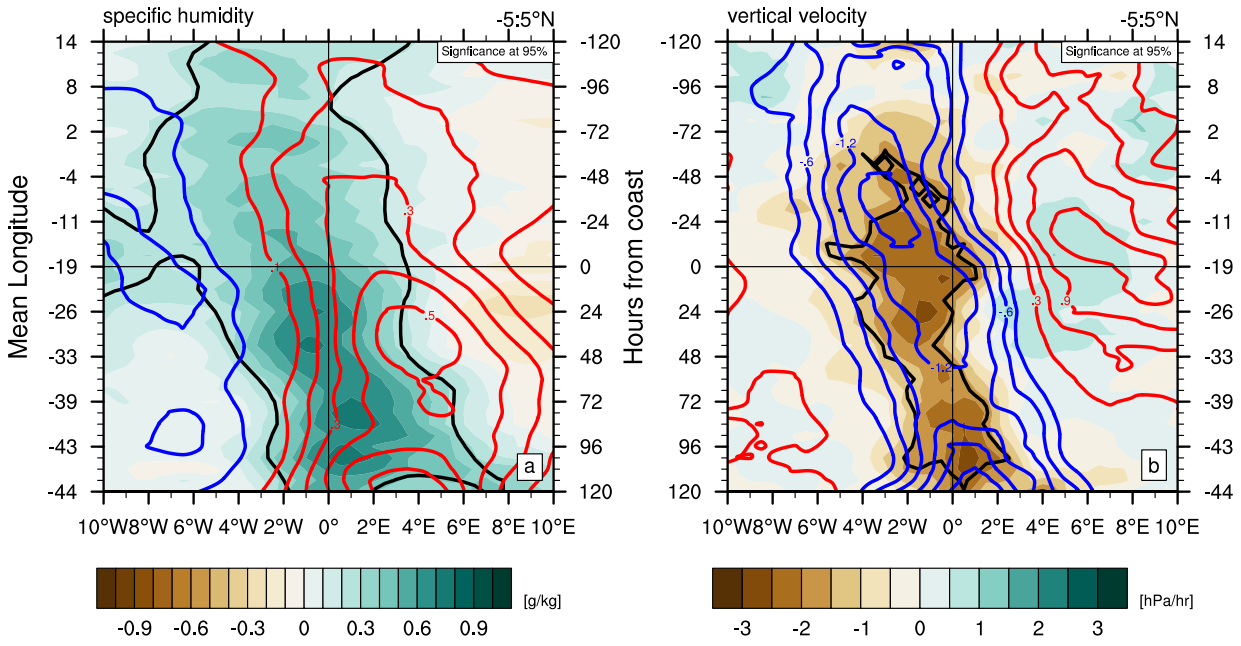

Figure 3.11: Trough relative hovmöllers of specific humidity (a) and vertical velocity (b). Contours depict composite of unfavourable troughs. Shading shows favourable composite - unfavourable composite. Variables are averaged over 5°S to 5°N relative to each troughs latitude. a) Anomalous Specific Humidity (500 hPa) [g/kg]. b) Anomalous vertical motion [hPa/hr]. Bold black contours encompass regions of significance greater than 95%.

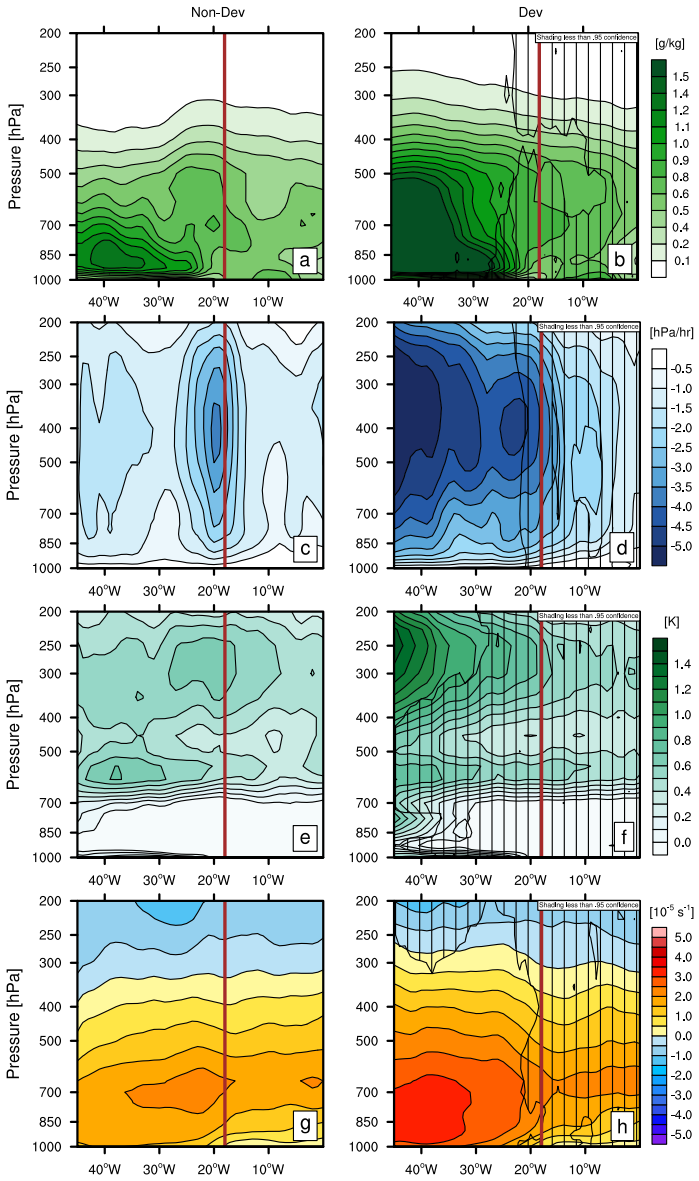

Figure 3.12: Vertical evolution of trough centred variables averaged over 500 km radius. Mean favourable non-developing waves (a,c,e,g; n=51) and mean favourable developing Waves (b,d,f,h; n=51). Hatched region denotes area not significantly different to non-developing composite at 95%. a,b) Anomalous Specific Humidity [g/kg]. c,d) Anomalous Vertical Motion [hPa/hr]. e,f). Anomalous Temperature [K]. g,h) Relative Vorticity [$10^{-5}s^{-1}$]. Approximate longitude of coast denoted by vertical brown line.

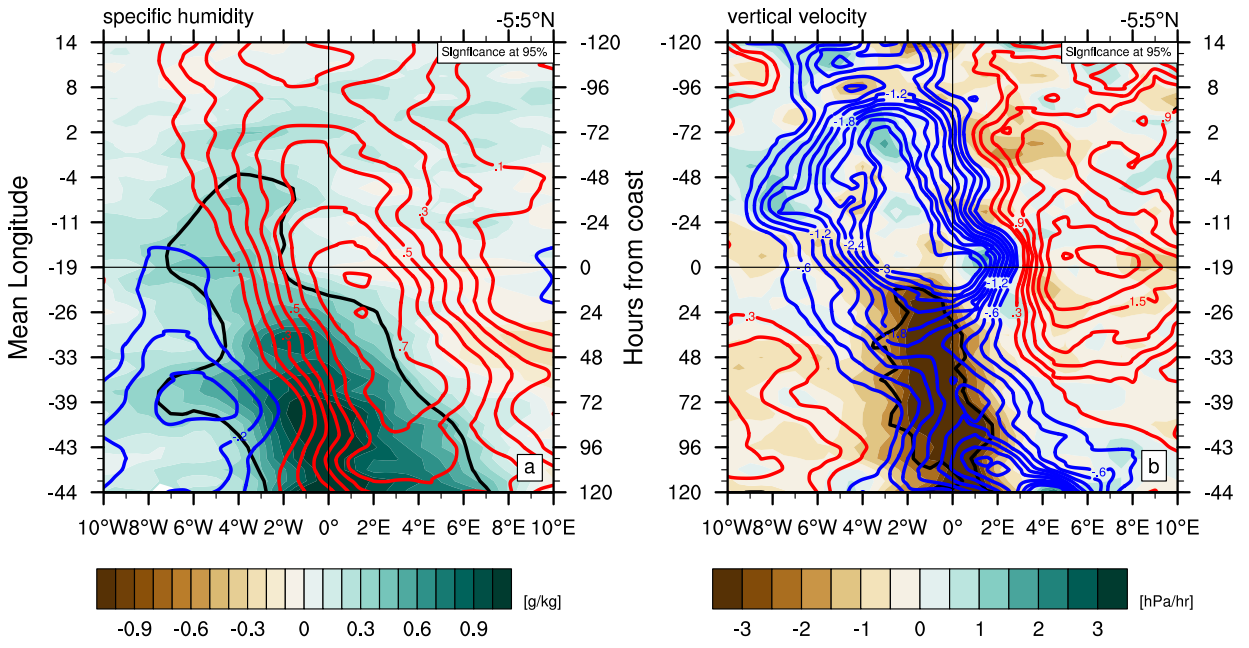

Figure 3.13: Trough relative hovmöllers of specific humidity (a) and vertical velocity (b). Contours depict composite of favourable non-developing troughs. Shading shows favourable developing composite - favourable non-developing composite. Variables are averaged over 5°S to 5°N relative to each troughs latitude. a) Anomalous Specific Humidity (500 hPa) [g/kg]. b) Anomalous vertical motion [hPa/hr]. Bold black contours encompass regions of significance greater than 95%.

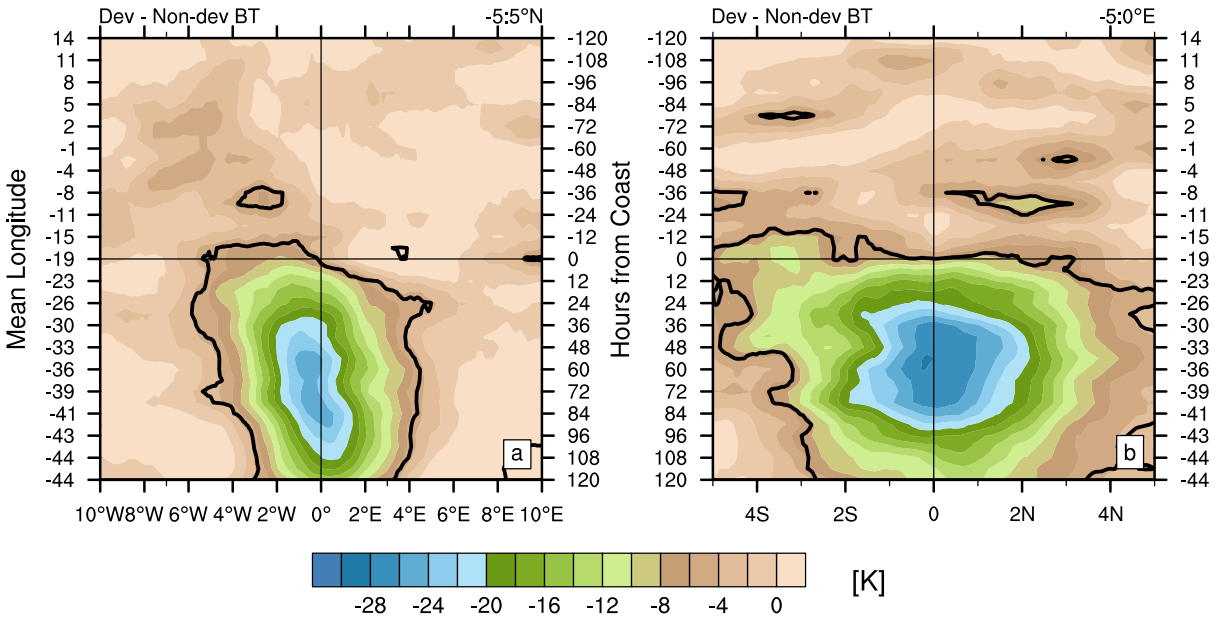

Figure 3.14: Trough relative hovmöllers of differences in infrared brightness temperature between favourable developing and favourable non-developing waves. Bold black contours oultines regions of significance at 95%. The x-axis of each trough is relative to the trough center. Mean longitude of the troughs per time is displayed along the y-axis. a) Differences relative to the longitude of the trough, averaged ±5° latitude around the center. b). Differences relative to the latitude of the trough, averaged -5 to 0° longitude of the trough axis.

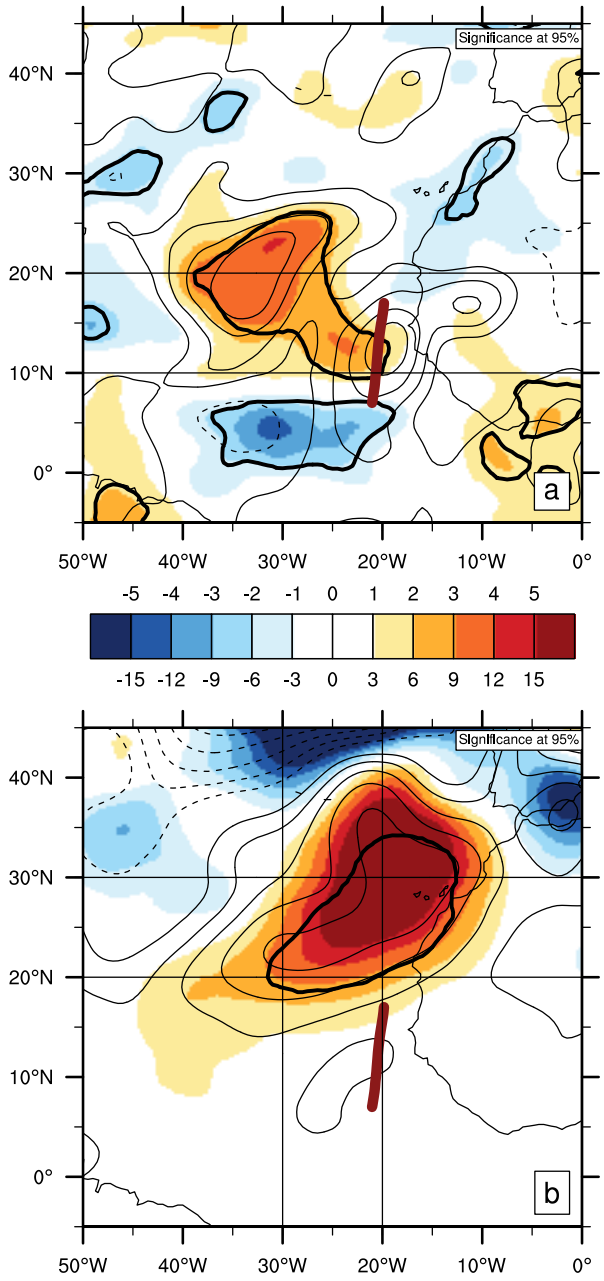

Figure 3.15: Mean composite differences for favourable developing waves - favourable non-developing waves (shading). Contours represent the composite favourable developing waves. The shading and contour intervals are equivalent. Colorbar applies to the plot above and below with labels on the respective side of the colorbar. Thick red line depicts the mean trough line of all included waves. Thick black contour encompasses the regions which are statistically significant at greater than 95%. (a) TPW [mm], (b) 300 hPa Geopotential height [gpm]. Horizontal lines denote bounds of latitudes used in Fig. 3.17, vertical lines in b denote cross sections shown in Fig. 3.16.

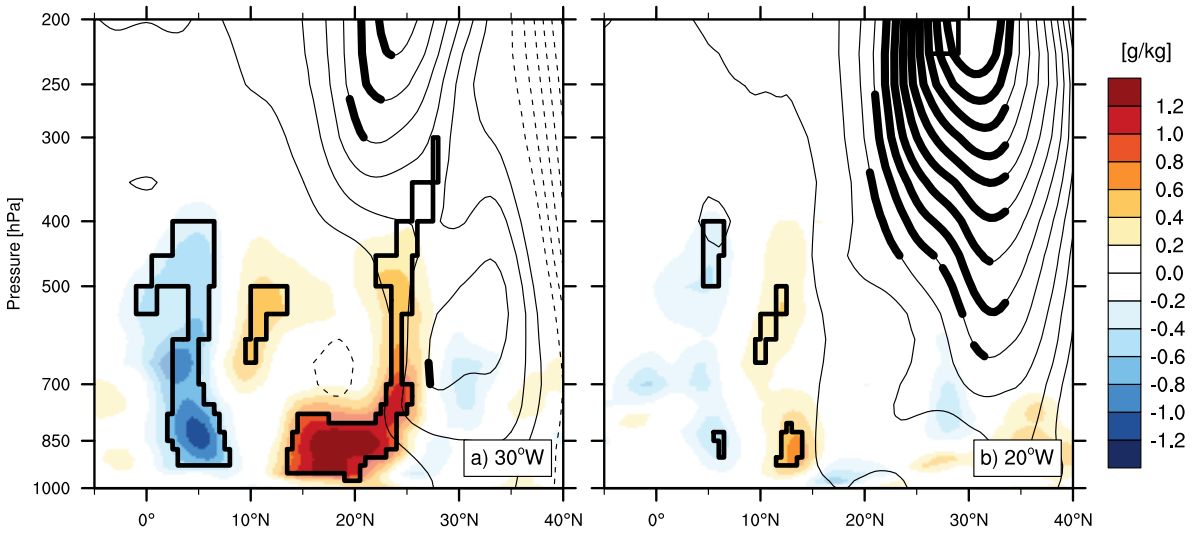

Figure 3.16: Latitude - height cross section showing favourable developing waves - favourable non-developing waves along 30°W (a) and 20°W (b) of specific humidity [g/kg] (shading) and Geopotential height every 2.5m (contours). Bold contours and shading (outlined) denote areas of statistical significance.

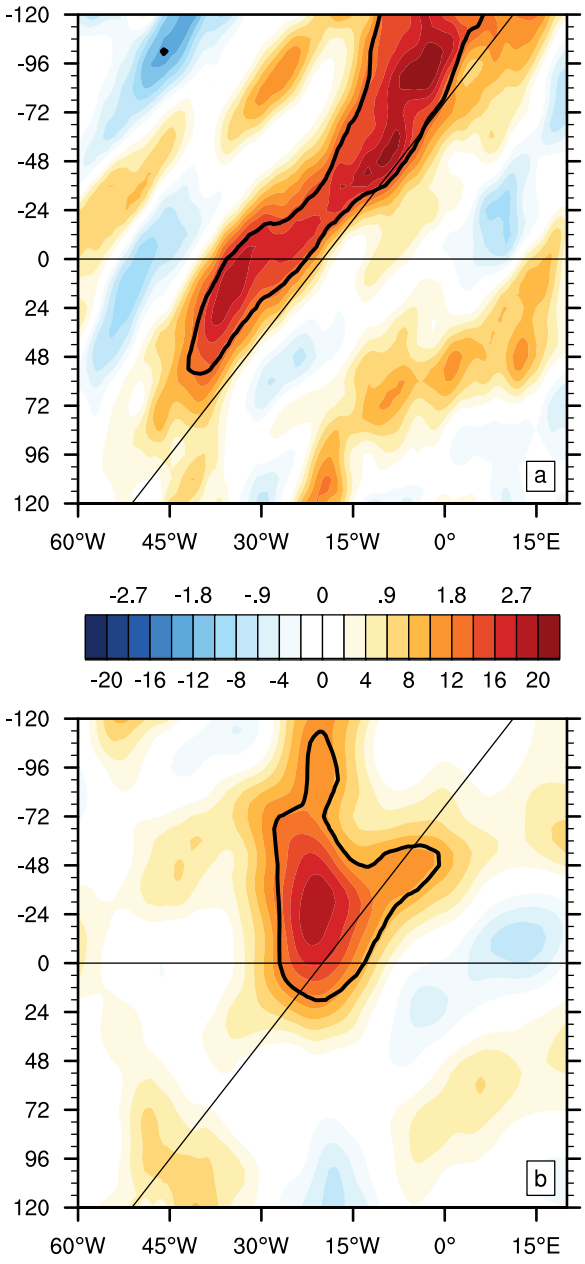

Figure 3.17: Mean composite differences for favourable developing waves - favourable non-developing waves for -120 to +120 hours of leaving the African Continent. Day 0 represented with horizontal black line. Mean track of composite trough depicted with diagonal black line. Black contours encompasses regions that are statistically significant greater than 95%. Colorbar represents plot above and below with labels on the respective side of the colorbar. Latitude bands for each hovmöller vary, these are shown in Fig. 3.15. (a) TPW [10:20°N; mm], (b) 300 hPa Geopotential height [20:30°N; gpm]

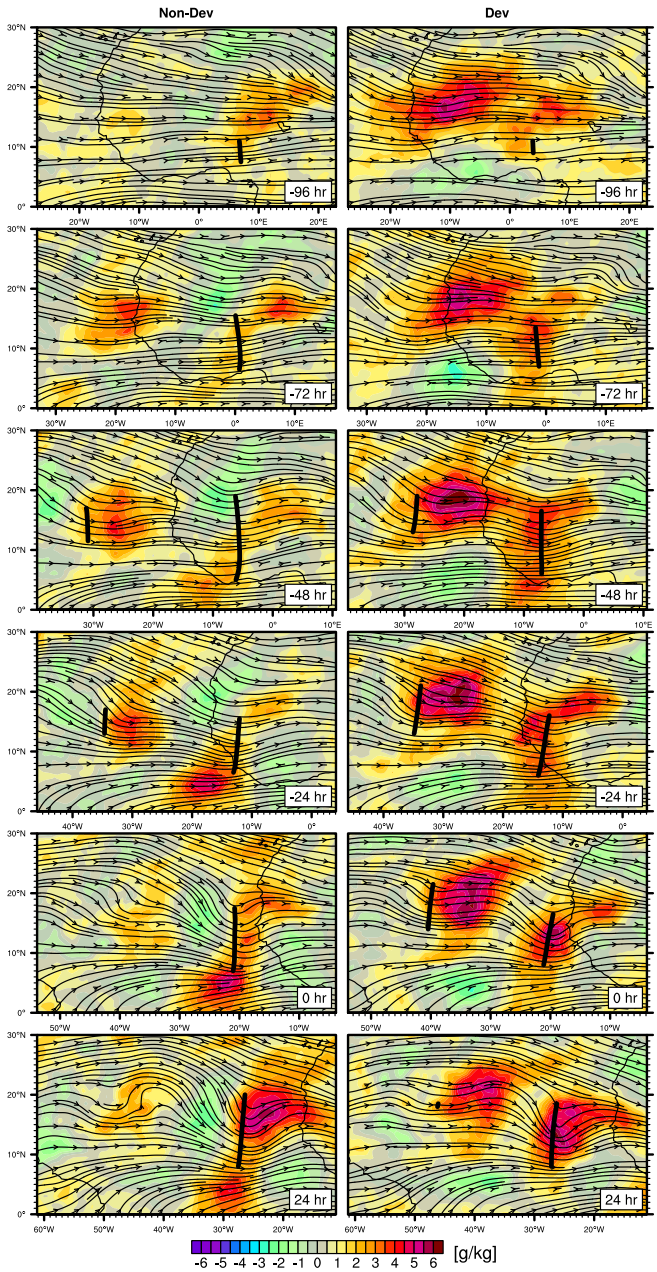

Figure 3.18: Composite anomalous specific humidity (850 hPa) and trough relative streamlines (850 hPa) for favourable developing and favourable non-developing waves. Rows span from -96 hours to +24 hours in 24 h intervals relative to the troughs passage over the coast. Maps are centered west of the composite trough to focus on the environment ahead of the troughs.

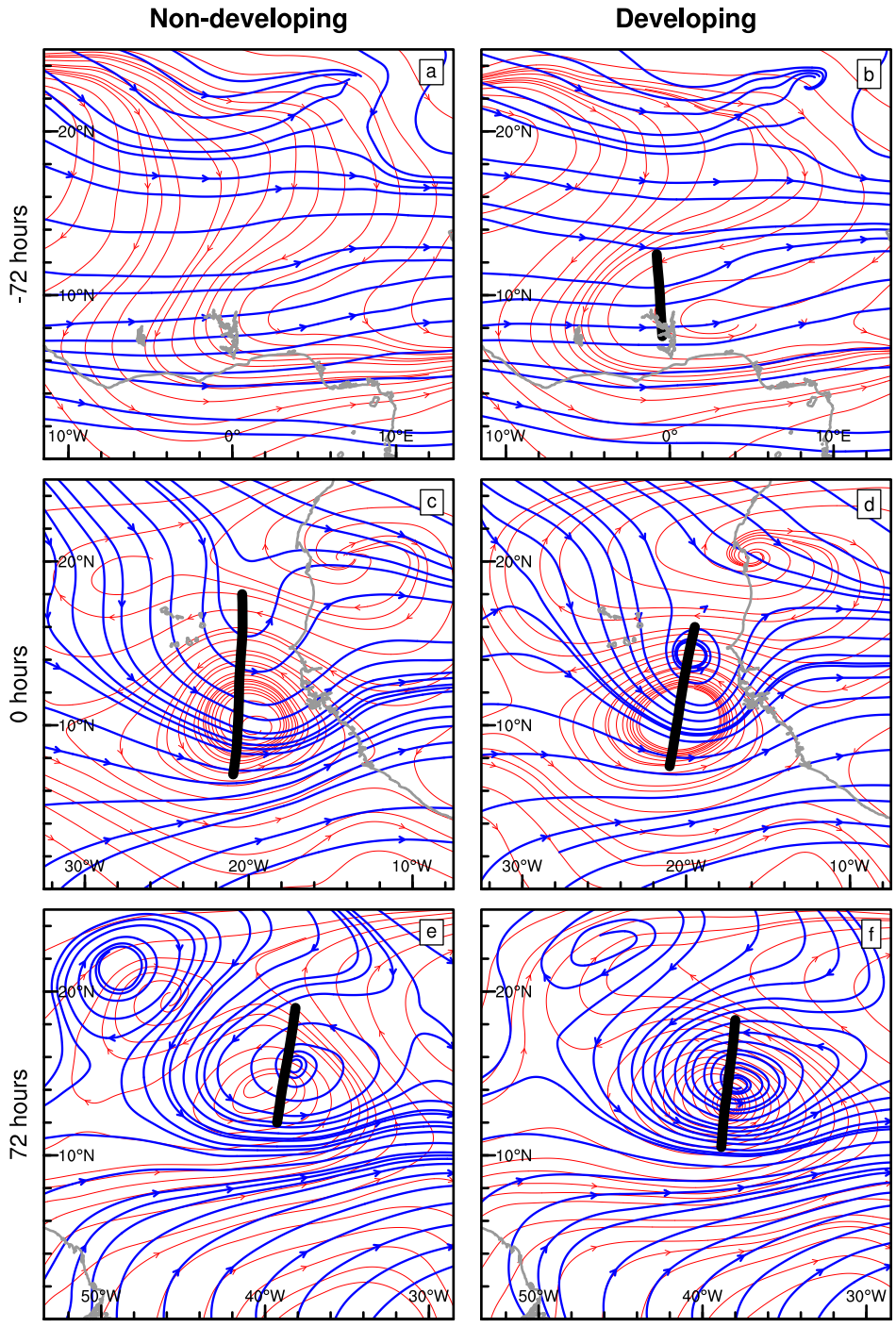

Figure 3.19: Composite wave relative streamlines at 2 levels for day -3 (a,b), day 0 (c,d) and day +3 (e,f) and favourable non-developing and developing waves (left, right respectively). Streamlines represent 700 hPa (Red), 850 hPa (Blue) wave relative flow. Thick black contour shows the 700 hPa trough line.

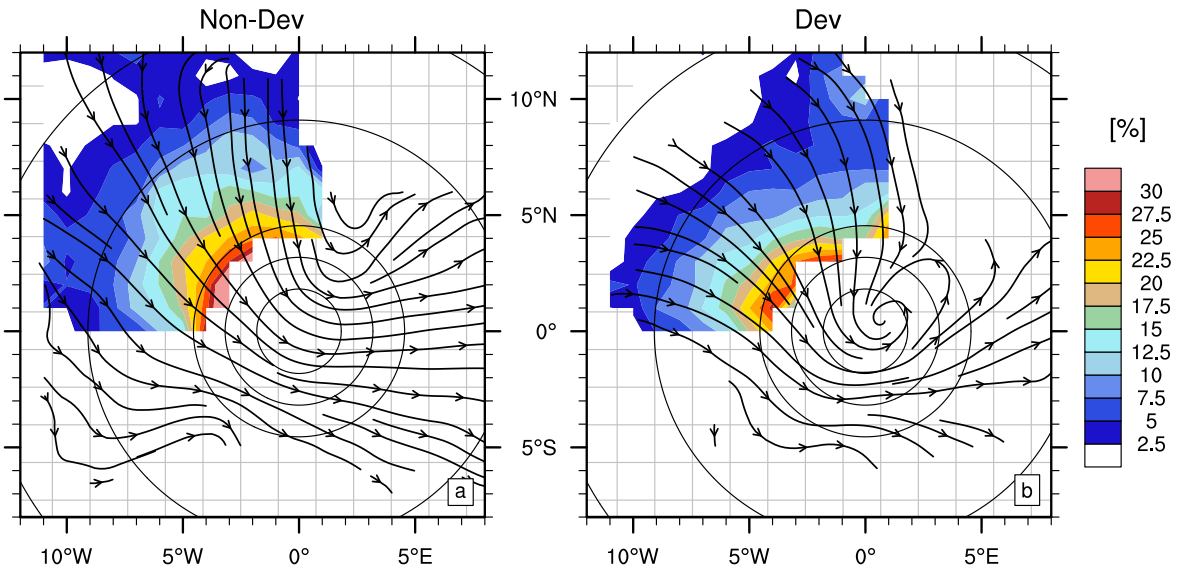

Figure 3.20: Fraction of trajectories that are ingested (come within 200 km of the vortex centre) by the trough. Percentage is relative to the total number of trajectories initialised at each relative grid point. Location is relative to trough centre at the time of initialisation. Range rings denote 200,350,500,1000,1500 km. Streamlines depict the 48 hour mean wave relative velocity of all ingested trajectories per grid point. Hatched background covers regions in which either no trajectories were initialised or were not included in the analysis due to their initial proximity to the vortex center.

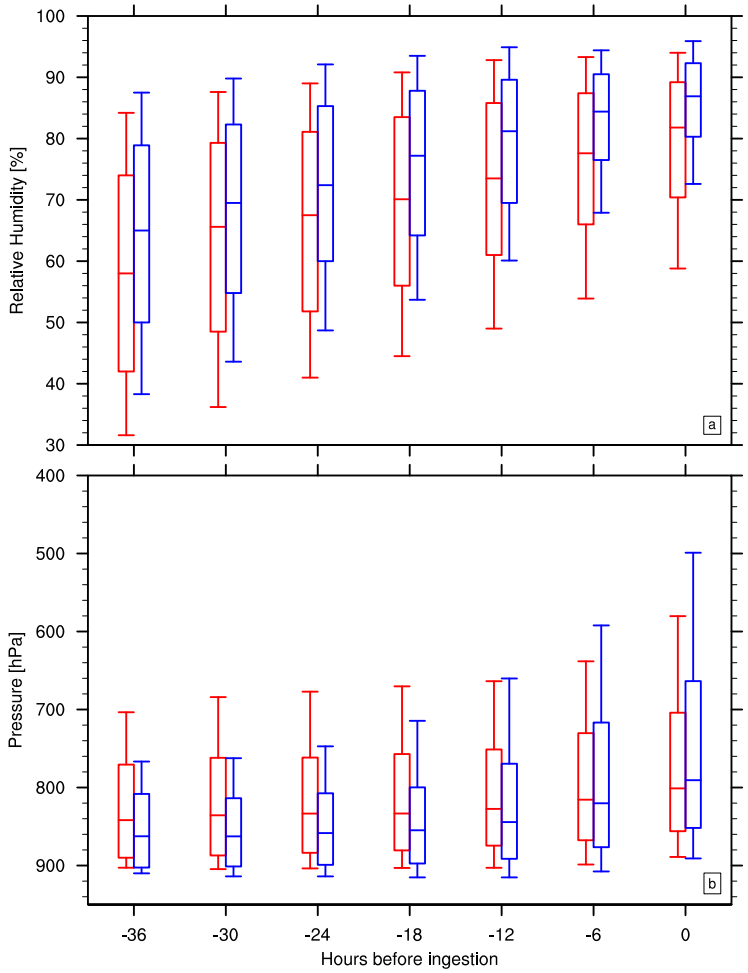

Figure 3.21: Distribution of ingested (within 200 km of the vortex centre) trajectory characteristics at 6 hour intervals relative to the time of ingestion for non-developing (red) and developing (blue) waves. a) Relative Humidity of trajectories [%]. b) Pressure of trajectories [hPa]

4. Environmental Inflow of AEW Troughs

4.1 Introduction

The structure and evolution of AEWs has been presented in many frameworks since the pioneering studies by Carlson (1969b), Frank (1969), Burpee (1972, 1974) and Reed et al. (1977) among many others. These early papers used in-situ radiosonde data from atolls or ships, as well as the extensive data collected during the Global Atmospheric Research Program Atlantic Tropical Experiment over Africa and the eastern Atlantic. Global models and long-term reanalysis products have enabled further research to reveal more details about AEW structures (e.g. Kiladis et al. 2006) as well as confirming the earlier results (e.g. Fink et al. 2004). Typically these papers have analysed the AEWs in the Eulerian framework. In recent years the use of the Lagrangian framework has become popular for understanding the early stages of tropical cyclogenesis (e.g. Dunkerton et al. 2009). Using the moving trough as a reference frame provides more detail about the relative inflow around the disturbance and how or whether the the environment above the boundary layer is ingested by the system. Despite this there is still a lack of research on the large-scale Lagrangian flow around AEWs.

Analysis of the relative flow around AEW troughs over West Africa is presented in this chapter. Initially the analysis of the degree recirculation in the 2-dimensional Lagrangian flow around the AEW troughs is presented. This framework while useful is somewhat limited due to the lack of consideration of both vertical ascent across pressure levels and evolution in time. Therefore kinematic back trajectories are utilised, these were initialised in the vicinity of AEW troughs.

The back trajectories reveal the large scale flow approaching the AEW troughs and the changes in the location sources as waves propagate westwards. Analysis of the sources of dry and moist air and the predominant trajectory routes towards the troughs is presented. Trajectory source regions are analysed with respect to convection in the trough as well as

differences in source regions and characteristics with respect to TC genesis over the eastern Atlantic.

The trajectories reveal the predominant regions that impact the AEW through advection of environmental air into the trough. The origin of trajectories with respect to the trough centre, shows how much the trough of a favourable AEW recirculates air. Analysis at different locations across West Africa also reveals how the source regions of trajectories change as the waves propagate westwards.

4.2 Methodology

4.2.1 Objectively Defining 2-Dimensional Recirculation

The recirculation for each trough was diagnosed for every time a tracked feature existed within 120 h of the West African coastline. The waves included here are the same sample used in the development of the logistic regression model in Chapter 3. At each time, the meridional and zonal phase speed of the wave at that time was subtracted from the wind components to reveal the trough relative flow. The detection of closed circulation is sensitive to the calculated phase speed of the wave. The use of a variable phase speed however makes no assumptions about the trough and thus allows the phase speed to vary in time or location.

Streamlines were calculated from each grid point within 250 km of either the 700 hPa vortex maximum or the nearest (within 500 km) minimum in windspeed less than 1.5m/s (i.e. center of recirculation). Closed streamlines were detected where there was overlap within 1 grid cell (0.5°) and 0.5 m/s velocity. For computational expense the first closed streamline found at each time and level was recorded, therefore in a system with no convergence within the recirculation it is possible that the largest area of recirculation was not identified. The frequency of this is expected to be very small and not influence the results in a significant manner.

4.2.2 Kinematic Back-trajectories

Trajectories were initialised at 6 locations, for the favourable troughs analysed in Chapter 3, as the waves propagate over West Africa and over the eastern Atlantic. Trajectories used in this chapter were all calculated using the Hybrid Single Particle Lagrangian Integrated Trajectory (HYSPLIT) Model (Draxler and Hess 1997, 1998). For each wave included in this analysis, trajectories were initialised around the troughs' centre at 6 locations across West Africa. These locations were determined relative to the number of hours each trough was from the coast (18°W), the times chosen were 24 hours after (west) the coast, over the coast (0 h), and 12, 24, 48 and 72 h before (east) the coastline. To avoid the confusion of having multiple time units, the locations will be referenced by the mean longitude of troughs hereafter (i.e. 24°W, 18°W, 15°W,12°W, 6°W,1°W respectively). At each time trajectories were initilised across a 3°x3° horizontal grid at 0.5° spacing centered on the trough location and at 11 vertical levels, spanning from approximately 900 hPa to 400 hPa at 50 hPa increments. This totalled 539 trajectories per trough per time.

The reanalysis fields from CFSR were used as input to the HYSPLIT model. As in the previous chapters this data has 6-hour temporal resolution with 0.5° horizontal resolution and 33 levels in the vertical; with 25 hPa vertical spacing between 1000 hPa and 750 hPa. The HYSPLIT model will continue to propagate trajectories, near the surface and at times below the interpolated terrain level. As this is a problem of the resolution of the data, once a trajectory came within 500 m of the terrain it was no longer followed. In total these surface interacting trajectories account for about 14% of all trajectories launched.

Trajectories were integrated backwards for a total of 120 h. In post-processing the trajectories were then also adjusted into a Lagrangian reference frame. This involved subtracting the location of the troughs which was interpolated to a 1 hour interval. If the track of the wave did not extend for the full 120 h, the mean phase speed of the wave was used to extrapolate the track backwards in time.

For the Eulerian compositing analysis, each trough was relocated to the mean location

of all troughs at that time. The trajectories were also subject to this small uniform shift over their entire integration. Geographical references are with respect to the mean trough location at that composited time. This trough relative adjustment is relatively minor though ($\leq 2.5^{\circ}$) so the general geographical references are still applicable. To clarify terminology, trajectories will be referred to in the chronological sense and therefore source/origin will refer to the trajectory 120 h before reaching the trough. Ingestion or initialisation location will refer to the locations within the trough where the back trajectories were initialised.

Trajectory compositing was performed to visualise the mean flow vector of the trajectories relative to a fixed grid. This involved calculating the 2 dimensional flow vector of the trajectories at each time and then compositing the horizontal components to a 0.5° grid. The streamlines are then computed on the resulting mean flow. The streamines therefore represent the mean flow of trajectories at a given location. This presents a unique representation of the flow around the AEW as the only data points are from trajectories that will reach the center of the trough.

4.3 Recirculation Within AEW Troughs

Recirculation was objectively identified at 12 levels within AEW troughs throughout 1979-2012. The frequency of identifiable regions of recirculation in the troughs relative to the West African coast is shown in Fig. 4.1. The three plots include all troughs, favourable developing waves and favourable non-developing waves. Recirculation is shown to typically occur over Africa around the level of the AEJ in each subset. The cyclonic horizontal shear on the south side of the AEJ means that even a relatively weak vortex can have a closed circulation. Across all waves and both subsets of favourable waves, closed circulation below 800 hPa is very rare over West Africa (-120:0 h). As the troughs leave the continent, occurrence of recirculation increases at the jet-level and also increases rapidly at low levels between 48 h after leaving the coast and 72 h (Fig. 4.1a).

The subsets of favourable developing and favourable non-developing waves show similar

occurrence of recirculation prior to leaving the coast of West Africa (Fig. 4.1b,c). As the troughs approach the coast the occurrence of closed streamlines increases from -72 h to -24 h. From 24 h before the coastline to 48 h after passage the evolution in developing and non-developing subsets is comparable to analysis of all waves. Developing waves however show much greater likelihood of recirculation and also a faster extension of closed circulation below the 700 hPa. The occurrence of closed circulation within the non-developing waves starts to decrease at all levels 48 h after leaving the coast. This signal is also present across all waves, suggesting that the waves typically lose the closed circulation after leaving the coast and moving away from the cyclonic shear of the AEJ.

The mean radius of the recirculation regions averaged over 100 hPa layers are presented in Fig. 4.2. The area encompassed by the closed streamline was converted to a radius for a circle of the same area for ease of interpretation. The radius of recirculation at different levels is fairly constant across level and time for all waves. If recirculation develops it is usually on a radial scale of about 250 km, with the levels closest to the AEJ (750:650 and 600:500 hPa) being slightly larger in area than above or below (Fig. 4.2a).

Developing waves experience a mean increase in area within the closed streamline around 48 h prior to reaching the coast (Fig. 4.2b). Low-level circulation (900:800 hPa) also shows a sharp increase in area as the troughs approach the coastline. By 24 hr after leaving the coast the low-level circulation covers an area only slightly smaller than the jet-level circulation. Non-developing waves have a very similar evolution in the area of recirculation to the all wave composite (Fig. 4.2c). While the developing waves had an increase in the area of the jet-level circulation, the non-developing waves do not exhibit such horizontal expansion. Therefore after leaving the coast the recirculation in non-developing waves is around 100 km smaller in radius than the developing waves.

The low-level circulation has been shown to lag behind the jet-level circulation in both occurrence and then also area encompassed. This shows that for at least 72 hours after leaving the West African coast, even developing waves are open to the environment at some

level. The temporal consistency of isobaric recirculation is also an important consideration, given an average radius of 250 km the outer circulation would have a circumference of around 1500 km in length. It would therefore take a moderate windspeed of 5 m/s over 3.5 days to recirculate. Therefore any changes in background flow or phase-speed would likely disrupt this isobaric recirculation within the troughs. Over this time frame ascent through the column will also flux environmental air from regions of open circulation through the closed circulation.

The vertical extent and also tilt of the closed circulation is therefore also worth consideration. If the levels of the vortex are closed in 2-dimensions but are tilted such that each level is open above and below it is expected that the potential benefits of recirculation would be negated. Figure 4.3 shows the mean vertical tilt for closed circulations for AEWs over the 72 h after leaving West Africa. In the first 24 h after leaving the coast (Fig. 4.3c) there is a distinct NE to SW tilt in the vertical with the low-level circulation around 200 km NE of the jet-level circulation. Above the jet, there is a further 200 km displacement of the circulation centers to the west. As the troughs get further from Africa the circulation above 700 hPa becomes more aligned in the vertical but the low-level circulation still remains offset to the NE (Fig. 4.3b). By 48-72 h after leaving the coast the low levels and mid-levels are more aligned and the centers of circulation are within 100 km of each other. The initial tilt of the circulation after leaving the coast is approximately equal to the radius of the recirculation. Therefore much of the jet-level circulation will be over a trough relative flow of environmental air from the west and northwest.

These figures show that over Africa the troughs are not commonly recirculating air in the simple 2-dimensional framework. As they leave the coast of Africa, closed circulation occurs near the level of the AEJ and extends vertically once over the ocean. Developing and non-developing troughs are both typically open to the environment below 800 hPa for up to 72 h after leaving the coast. During this time closed circulation at low-level also tends to be smaller than the jet-level counterpart and is also offset to the NE by almost the radius of

the recirculation.

This instantaneous isobaric view of the circulation is somewhat limited in its applicability for cases where the phase speed is liable to change or background flow varies. Analysis of full 4-dimensional kinematic trajectories will provide a more conclusive analysis of the relative flow around the AEW troughs and the sources of environmental air.

4.4 Composite Trajectory Analysis of Favourable AEWs

4.4.1 Eulerian Analysis of Trajectories

The density of all trajectories over the full backward integration of 120 h are visualised in Fig. 4.4. The boxes in each panel depict the initialisation region of the back trajectories and therefore the location of the troughs at that time. The approximate location of the troughs 120 h before is shown by the dashed line. In concert with the density of the trajectories, Fig. 4.5 visualises the integrated 120 hour flow towards the waves at each location with streamlines. The streamlines are coloured with respect to the mean pressure of the trajectories on the 0.5° grid. The mean relative humidity at each location is also represented in Fig. 4.6. The five day flow captured in these trajectories is largely representative of the large scale climatological flow over these regions revealing the transient nature of the AEWs on the background state.

The maxima in densities shown in Fig. 4.4 represent the dominant pathways of flow into the AEW troughs. When the troughs are over West Africa (Figs. 4.4a,b,c) there are two main pathways towards the trough; flow from the east and a secondary maximum from the southwest. Flow from the southwest is sourced at low levels below 800 hPa. This high relative humidity oceanic air is being advected northwards with the monsoonal inflow over the continent (Figs. 4.6a,b,c). Flow from the east is likely associated with the AEJ; the mean pressure of trajectories is between 700 and 600 hPa, the typical height of the AEJ. Along the northern edge of the jet, the trajectories represent the climatological distribution of relative humidity with a strong meridional gradient. To the northeast there are a combination of

trajectories from low levels (900 hPa) over Egypt and mid to upper levels from the central Mediterranean over Libya and Algeria. Both sources have mean humidity below 30% and approach the mid-level jet as they flow south towards the trough (Figs. 4.5,4.6).

As the troughs approach the coast, a third maximum in the flow density becomes evident representing flow from the north and northwest. The density of trajectories along this route increases as the troughs leave the coast. As the troughs cross 24°W (Fig. 4.4f) the flow from the northwest is slightly more dominant than the southwest source region. The trajectories from the north and northwest of the troughs, as they transition over the coastal region, are sourced from low levels between 800 and 900 hPa with mean humidities along this route between 30% and 60% (Figs. 4.5,4.6). Carlson and Prospero (1972) noted that flow along this route was generally dust-free air from northern latitudes, on the eastern edge of the subtropical ridge. There is also a suggestion of a few subsiding trajectories on the western periphery of the source region from the north; where trajectories have mean pressures less than 600 hPa with relative humidity below 40% 120 h before reaching the trough (Figs. 4.5e,f).

Figure 4.7 shows the geographical density of trajectories 120 h before reaching the troughs. This panel now focuses on only 3 of the trough locations (24,18,6°W). Trajectories have been grouped by initialisation level approximately relative to the AEJ. The top row shows inflow that reaches the trough above the AEJ (600-300 hPa), while the bottom row are trajectories initialised below the AEJ (900-600 hPa). Trajectories that end up within the trough above the AEJ are predominantly sourced from near the extrapolated location of the trough and farther east (Fig. 4.7a,b,c). Trajectories from the southwest increase in number slightly as the waves move west, but there isn't a substantial change in the source regions for trajectories initialised above the jet. Below the jet however the evolution is noticeably different. As the troughs transition over the coast there is a substantial increase in the number of trajectories from the northwest.

The low-level background flow over West Africa and the Sahel is predominantly south-

westerly monsoonal flow. The AEJ at 700-600 hPa imposes relatively strong shallow vertical shear with easterly winds around 12 m/s. Above the AEJ there is climatologically weakening easterly flow, except for the Tropical Easterly Jet to the south which imposes deep vertical shear over the Gulf of Guinea. When the phase speed of the waves is subtracted from this climatological flow there is wave relative flow of strong low-level westerlies across the Sahel, quiescent mid-level easterly flow around the AEJ, and a weak tropical easterly jet to the south. Over the eastern Atlantic there is also a contribution to the meridional flow by the subtropical ridge. This results in an enhanced convergence zone near the West African coast. The trajectories presented here therefore reveal the large scale contribution of the environment to the inflow of the AEWs. Variability along these routes is expected to influence the characteristics of the AEW troughs. This analysis highlights how changes in the tropical SSTs over the Gulf of Guinea and equatorial Atlantic could potentially impact AEWs over West Africa, or meridional flow over the Sahara or eastern Atlantic could impact the environment ingested by the troughs.

Figure 4.8 shows the joint probability distribution of source pressure and relative humidity of the trajectories shown in Fig. 4.7. Trajectories initialised above the jet are sourced across all levels of the troposphere up to around 300 hPa. When the troughs are near 6°W the trajectories are mostly sourced from very humid regions originating between 700 and 500 hPa (Fig. 4.8 c). This coincides with the high maximum in the location density coincident with the interpolated trough location. This suggests that jet-level air near the trough 7 days before the waves reach the coast is still near or within the circulation of the trough as they are reaching the coastal region. Low-level flow is also ingested by the troughs and rises to above 600 hPa. At this location (6°W; Fig. 4.8c) air from low levels is split between very low relative humidities and very high. As the troughs move west, the source of dry trajectories ending above the AEJ decreases. Instead trajectories initialised above the AEJ are predominantly from moist regions. Therefore the inner core of the troughs are generally moistening above the jet as the troughs approach the ocean and also, likely causally related,

mid-level dry air is either less prevalent near the troughs or isn't being ingested as easily by the troughs.

At low levels in the trough there are two main characteristics evident, which are almost exclusively from below 600 hPa, with either high or low relative humidity. At high humidities there are a small number of trajectories below 900 hPa. This source of trajectories is fairly constant across the three trough locations (Fig. 4.8d,e,f) and is likely associated with the cross equatorial flow from the southwest. Trajectories with dry origins that were initialised below the AEJ almost exclusively originate from pressures above 650 hPa, showing that over West Africa subsidence, within 120 h, is not a main route for dry air to influence the AEW troughs. However there is an increasing number of dry trajectories originating from 400-600 hPa as the waves propagate westwards, suggesting that over the Atlantic subsidence may be a more important route for dry air. The fraction of dry air at low levels also increases as the troughs transition over the coastal region.

Figure 4.9 shows the density of the sources for trajectories with relative humidity lower than 40%. The main source for trajectories initialised above the AEJ in the troughs is over the central and eastern Sahara, where deep isentropic mixing will lift low humidity air up to around 500 hPa (Karyampudi and Carlson 1988). Dry air that reaches the low levels of the troughs also originates from the eastern Sahara when the troughs are over the continent (Figs. 4.9f). As the troughs reach the coast, the eastern Atlantic becomes the primary source for dry air. These dry eastern Atlantic trajectories are from below 850 hPa therefore are likely not of SAL origin (Fig. 4.8d). Over the coast and eastern Atlantic the base of the SAL rises over the cooler maritime layer, forming an strong inversion at the lower boundary of the SAL. This strong inversion as well as cooler surface temperatures will not encourage ascent of the dry trajectories and therefore this region is reaching the low levels of the trough.

These figures show the large spatial extent that potentially influences the AEWs during their lifetime over West Africa and the eastern Atlantic. Three main pathways for inflow towards the trough have been shown. These are moist trajectories from the tropical Atlantic

at low levels, both moist and dry air from Africa at all levels as well as along the AEJ, and as the troughs approach the ocean the dry northerly sub-tropical flow over the eastern Atlantic. The trajectories also show that dry air within the trough is typically sourced (over the 120 h integration) at lower altitudes and ascends towards the trough. Over West Africa ascent through deep mixing over the Sahara lifts dry and warm air to mid-levels, where the AEJ, shallow monsoonal overturning circulation and the trough vortex advect the dry air west and south. Over the eastern Atlantic this deep mixing isn't generally present, therefore dry air is ingested at lower altitudes having subsided previously. The next section will analyse the evolution of the trajectories and troughs in a Lagrangian framework to provide more detail on the evolution and influence of the trajectories.

4.4.2 Lagrangian Analysis of Trajectories

The location or extrapolated phase speed of the waves was subtracted from the trajectories to provide a Lagrangian view of the inflow towards the troughs. Figure 4.10 shows the density of the trajectories now relative to the trough location throughout the integration time. At the levels around and above the AEJ, the background flow is easterly and therefore air is more likely to travel westwards with the trough due to the low wave-relative velocity. At lower levels however, the background flow over Africa consists of the monsoonal southwesterlies, resulting in a increased westerly wave-relative flow. This is represented by the extension of the trajectory densities to the west of the troughs beyond 3000 km. The meridional flow ahead of the waves therefore acts to channel environmental air into the path of the AEW troughs.

While the waves are over Africa the trajectories are mostly concentrated within 2000 km of the trough and extend out to 3000 km to the southwest (Fig. 4.10 c,f). As the waves transition over the coastal region the change from southwesterly dominated inflow to both southwesterly and northwesterly inflow is apparent. Trajectories ingested from the west are almost exclusively sourced from low levels, approaching the system between 800 and 900 hPa

(Fig. 4.11). There are a small number of subsiding trajectories however as the troughs move over the eastern Atlantic at 24°W. Though only a small percentage of trajectories, this shows a potential role of mid-level subsidence later being ingested from the northwest of the troughs over the ocean.

Figure 4.12 shows the median number of hours it takes the trajectories at each grid point to reach the trough center. At the three different trough locations presented here, the general picture is the same across the panels. Flow from the southwest enters the system relatively quickly, while the trajectories from the northeast at similar radial distances take much longer. The trajectories from the southwest have a much more direct route to the trough center, whereas as shown in Fig. 4.11 trajectories from the north initially move to the northeast of the trough and are then wrapped cyclonically around the trough center. Over land trajectories from the northwest quadrant take between 4-5 days to penetrate the trough. This route becomes faster over the ocean due to the increased background meridional flow. This shows that as the troughs reach the coast and eastern Atlantic, the influence of the northwest quadrant increases not only in the fraction of trajectories but the time it takes that environmental air to reach the center. A faster route to the center reduces the time for modification of the trajectories as they approach the center.

The trajectories have been categorised into 5 regions relative to the trough centers. These 5 regions are outlined by the bold lines in Fig. 4.12. The regions include 4 quadrants relative to the troughs location and an inner circle with a 500 km radius. Figure 4.13a shows the percentage of the total number of trajectories that were initialised in the trough above 600 hPa. For each region the box-plots show the evolution of the distribution of trajectories from that region as the troughs move westwards (presented right to left). The relative contribution from each region is fairly consistent as the waves propagate westwards. The southwest, northeast and northwest all contribute around 25% of trajectories to the trough. Only around 10% of trajectories remain within 500 km of the trough center over the 120 hour integration. Flow from the southeast shows a small increase as the waves move

westwards, referring to fig. 4.10 and fig. 4.11 these appear to be trajectories from either the east or southwest that are being ingested by the trough but are just outside of the 500 km threshold imposed here.

The percentage contribution from each for the trajectories reaching the lower-levels of the troughs (below 600 hPa) show a much greater evolution as the troughs move westwards (Fig. 4.13b). The number of trajectories from the southeast and northeast increase as the troughs move westwards, however the median number of trajectories from these regions is still less than 2% and 10% respectively as the troughs pass 24°W. The number of trajectories from the southwest exhibits a small increase in the distribution as the waves approach the coast but there is a sharp decline in the percentage of trajectories from the southwest by 24°W. After the troughs have left the coast, the air within 500 km of the trough over the previous 120 h is down to around 5%. This could be due to increased ascent through the column of the trough over the coastal region, or that the change in the background flow makes it less conducive for trajectories to recirculate around the trough during the convectively active coastal region.

Figure 4.14 displays the evolution of the distributions of relative humidity from each region. The distributions of relative humidity from each region don't have any notable changes as the waves move westwards. Even through the source regions move over the ocean, the NW quadrant retains very dry characteristics. Interestingly as shown in fig. 4.13 it is the northern and thus drier regions that show increasing contribution to the troughs as they propagate westwards. Relative humidity of the trajectories that remain near the trough appears to decrease slightly both above and below the jet as the waves move westwards, though there is a large overlap in the distributions though so this is unlikely to be a significant change within the troughs.

The analysis so far has shown how the synoptic scale flow around AEWs evolves as the waves propagate westwards over West Africa and the eastern Atlantic. This has not however shown any feedback due to the changes in source regions or differences between AEWs that

potentially have trajectories from different regions. The following sub-section will therefore compare the distributions of trajectories across 43 developing waves with 43 non-developing waves. Theses waves were those selected in Chapter 3, where composite analysis showed significant differences in the environmental ahead and to the northwest of the troughs.

4.4.3 Developing and Non-Developing Waves

The previous chapter found significant differences between favourable developing and favourable non-developing waves as they transitioned over the coast of West Africa. Streamline analysis suggested that there was wave relative inflow from the northwest quadrant coincident with where the greatest anomalies in environmental moisture were. This section will compare the distributions of the trajectories of the developing and non-developing waves.

Bean plots are used here to visualise two distributions together side by side. A kernel density estimate function is used to create a smooth distribution across the trajectories for each region, time and subset of waves. The area or horizontal extent of the distributions is representative of the number of trajectories in the distribution for that region and time. These plots therefore provide much greater level of detail about the distribution compared to standard box plots (e.g. Kampstra 2008). Figure 4.15 compares the distributions across 4 regions; the southeast was excluded as it includes very few trajectories. The columns separate the trajectories by the integration hours from the trough center. Trajectories included in this figure are those initialised when the troughs are are over the coast. The percentages in the bottom right corner indicate that the two distributions are significantly different at the indicated significance (at least 95%).

At this location, over the 120 h integration the only region with significantly different characteristics of trajectories is the NW quadrant. Over the 96 h before reaching the trough center, the trajectories in the NW quadrant have significantly lower relative humidity. The distribution of both subsets is similar in appearance with a somewhat bimodal distribution however the tail of dry trajectories in the non-developing cases is greater. Throughout the

120 h integration the non-developing waves also have slightly drier trajectories within the inner 500 km of the trough, however these distributions are not significantly different.

At 24 h after leaving the coast, trajectories from the northwest are still significantly drier throughout the full 120 h of backward integration (Fig. 4.16). Trajectories within the inner 500 km at integration hour 24 (when the troughs were over the coastline) are significantly drier than those in the developing waves.

Trajectories from the southwest quadrant have similar characteristics across both subsets and both locations. The non-developing waves have consistently fewer trajectories from this region but consistently more trajectories from the northwest quadrant. Figure 4.17 highlights these differences. Trajectory locations at 72 h from their initialisation in the trough, are binned by region relative to the trough location at that time. Trajectories that were initialised at -48,-24 and 0 h relative to the coast are included here. This shows that below the level of the AEJ developing waves are ingesting more trajectories from the southwest and fewer trajectories from the northwest. Above the AEJ developing waves have a greater percentage of trajectories that remain within 1000 km of the trough, while non-developing waves are ingesting more trajectories from the north and east.

4.5 Discussion and Conclusions

This chapter initially documented the occurrence of recirculation within AEW troughs over West Africa and the eastern Atlantic. Using an objective detection of a closed streamline at different times and levels this showed that troughs have closed circulation most frequently around the level of the AEJ over West Africa. As the troughs cross the coastline the recirculation slowly begins to occur more frequently at lower levels until around 72 h after leaving the continent recirculation is equally likely between 900 hPa and 600 hPa. Both subsets of favourable AEW troughs had increased frequency at the jet-level after leaving West Africa but non-developing waves did not develop a closed circulation at low levels and 48 h after leaving the coast the non-developing waves start to lose the closed circulations. Analysis of

the size of recirculation and also the vertical tilt of the circulation centres showed that as the troughs cross the coastline the low-level circulation expands slightly become more equivalent in size to the larger jet-level circulation. The vertical tilt of the circulation is however on average more than 200 km from NE to SW. The magnitude of the tilt is almost equivalent to the radius of the circulation. Therefore while the jet-level is closed on the isobaric surface, it is likely positioned over a large region of low-level environmental air outside of the low-level circulation.

To better analyse the relative and the time-evolving flow around the AEW troughs, kinematic trajectories were utilised for the remainder of the chapter. These trajectories were all initialised within the trough center and therefore represent the environmental air that will be ingested by the trough within the 120 h integration timeframe. Due to the large scale nature of the back trajectories though, the 120 h integrated flow is expected to be somewhat representative of climatology over the Sahel region. The analysis does however highlight the various sources and relative contribution of environmental air to the troughs. The waves studied here were selected through the logistic regression model methodology described in Chapter 3. These waves were selected as being "favourable" for development when leaving the coast of West Africa. This has effectively selected waves which have been convectively active in some way over West Africa. These waves therefore may have higher contributions of trajectories from the south and reduced contributions of dry trajectories from the north.

The trajectory analysis reveals the large spatial influence on the AEW troughs. At mid-levels the flow approaching the trough was relatively axisymmetric with large scale convergence from all directions. This includes ingestion of dry air from the north and moist air from the east and west. The flow towards the troughs above the jet did not show large regional changes as the troughs move across West Africa and over the eastern Atlantic. The background flow over this region has less zonal change over the coastal region with a mid-level high over the subtropical ocean and Sahara. At low levels the combination of monsoonal westerly inflow to the continent and the phase-speed of the waves means that environmental

air was sourced from regions extending west of the trough up to 3000+ km over the 120 h. Over the continent this low-level inflow is from the west and southwest, with an additional route from the northwest as the troughs approach the eastern Atlantic.

A 3-dimensional view of the flow into the AEW troughs is presented in Figure 4.18. This has been generated by creating 6 average trajectories initialised at each level. This combines the details presented earlier in the chapter and allows for a more complete view of the flow around the trough. At mid-levels the main trajectory shows low humidity trajectories from the east wrapping around the north and west of the trough. This mid-level air over cuts the low-level inflow from the west on the western side of the trough. The interaction between the high humidity at low levels with the mid-level (600 hPa) low humidity on the western periphery of the the trough is colocated with a region of increased low-level shear (925 to 600 hPa). Laing et al. (2008) showed that over West Africa deep convection was most generally aligned with the axis of this shallow layer shear. The equatorward transport of mid-level low humidity air is also likely to induce an increased generation of downdrafts from evaporational cooling (Emanuel 1989). Convection associated with AEWs over West Africa is typically located in this region of northwesterly flow ahead of the trough (e.g. Reed et al. 1977; Fink and Reiner 2003; Laing et al. 2008). Over Africa the low-level inflow into the troughs is therefore predominantly passing through the region of precipitation ahead of the troughs. This suggest that precipitation events ahead of the trough are influencing the low-level relative inflow. Moistening or heating occurring ahead of the trough is likely then ingested by the trough within a short period time. As the troughs approach the coast however the meridional extent of the inflow increases and the entrainment of low-level dry air from the north increases.

As the troughs approach the coast, trajectories approached the low levels of the AEW trough from both the high humidity maritime source to the south as well as colder, dry air over northwest Africa and the eastern Atlantic. The 3-dimensional view of the trajectories shows the convergence of dry and moist trajectories ahead of the trough. The moist cross

equatorial flow approaches from the southwest and ascends on the southern side of the trough circulation (Fig. 4.18). Approaching from the northwest are the low-level dry trajectories which although moistening on approach are still dry as they reach the trough center. The mean pressure of the trajectories from the north showed that the dry air over the eastern Atlantic was predominantly from the subtropical northeastern Atlantic at around 800 hPa. On the western edge of the trajectories though there was also a suggestion that tropical subsidence was a common route. Braun (2010) raised the importance of subsidence as a source of dry air over the tropical Atlantic and these trajectories highlight that both tropical subsidence and northerly flow of midlatitude subsidence can be major sources of dry air over the Atlantic.

Dry air approaching from the east of the trough typically reaches the system near the level of the AEJ. As suggested by the recirculation analysis, at these level the troughs are most likely to possess a closed circulation. Therefore entrainment of dry air from the east may have a reduced impact especially as the circulation within the trough strengthens. Fritz and Wang (2013) showed, through high resolution numerical simulation of developing case, that dry air was able encroach on a developing system from the east. However the trajectories were wrapped around the vortex in such manner that they were moistened enroute to the center and thus were not a significant detriment to the system.

Differences between developing and non-developing waves, revealed a similar result to Chapter 3. Developing waves ingested environmental air associated with low-level cross equatorial flow with high humidity. Non-developing waves conversely ingested more dry air from the north at low levels. Objective analysis of recirculation within the AEW troughs showed that this ingestion of environmental air at low levels may be reduced within 48-72 h after leaving West Africa, as the vortex and thus recirculation extend lower in the troposphere. Suggesting that the environmental impacts on the trough through low-level inflow may be reduced as the troughs move farther from West Africa.

This chapter has presented a large scale composite view of the 120 h flow towards the

AEW trough center. The spatial extent influencing the AEWs has shown to extend out over 3000 km to the west of the trough and 1500 km to the north, east and south. Three main routes for environmental air to approach the troughs was shown, these were mid-levels from the east, low levels from the southwest and when over the coast and east Atlantic low-level flow from the north. Continuing the analysis of Chapter 3 back trajectories originating from the northeastern Atlantic were shown to be significantly drier for non-developing favourable waves. Given the scale of the synoptic flow influencing AEWs it is suggested that analysis of the three main pathways into the trough may provide prognostic detail about the future of the trough over the coming days.

4.6 Figures

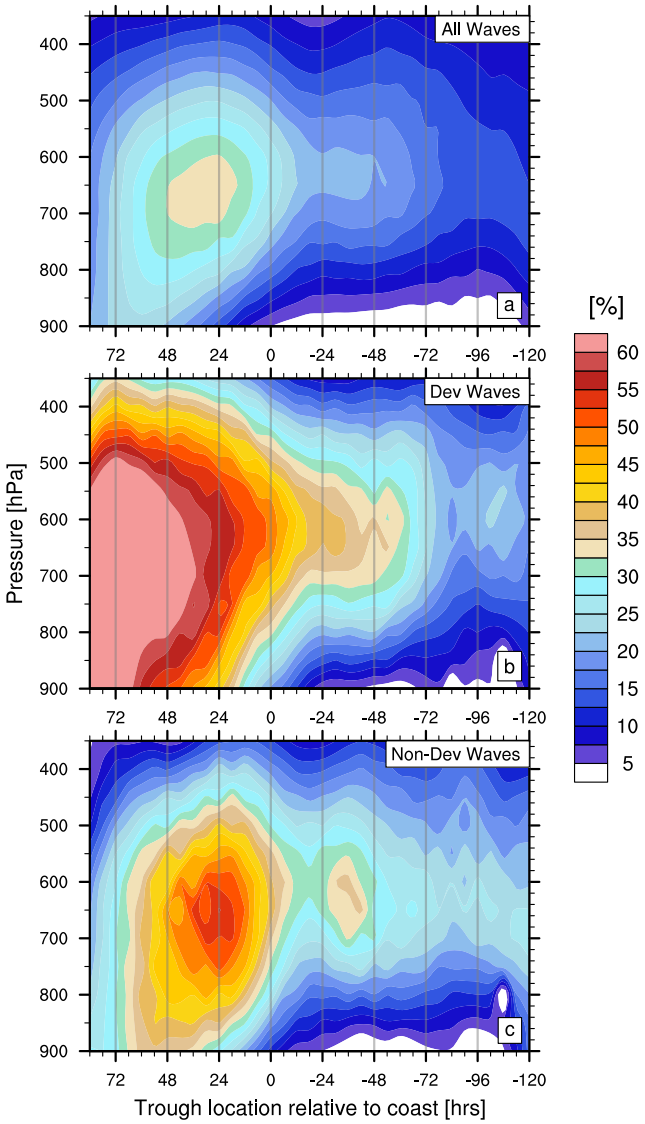

Figure 4.1: Frequency of objectively defined recirculation near trough center with respect to pressure level and trough location relative to passage over the West African coast. Negative hours represented troughs east of the coastline. a) Percentage of all waves analysed n=443. b) Percentage of favourable developing waves, n=43. c) Percentage of favourable non-developing waves n=43.

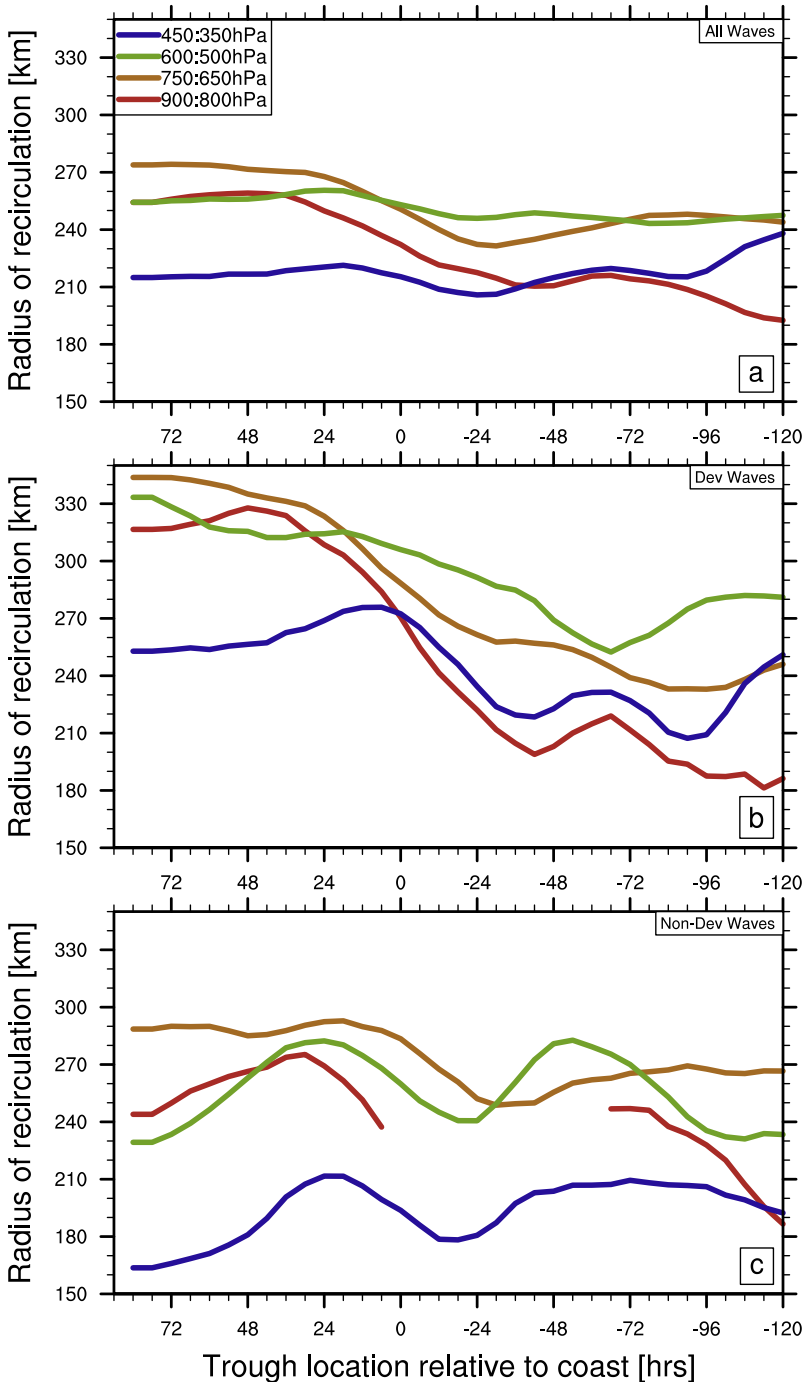

Figure 4.2: Mean radius of recirculation region averaged over a range of pressure levels. Abscissa represents the trough location relative to passage over West African coast. Negative hours represented troughs east of the coastline. a) All waves analysed; n=443. b) Favourable developing waves; n=43. c) Favourable non-developing waves; n=43. Legend for line colors are shown in panel a.

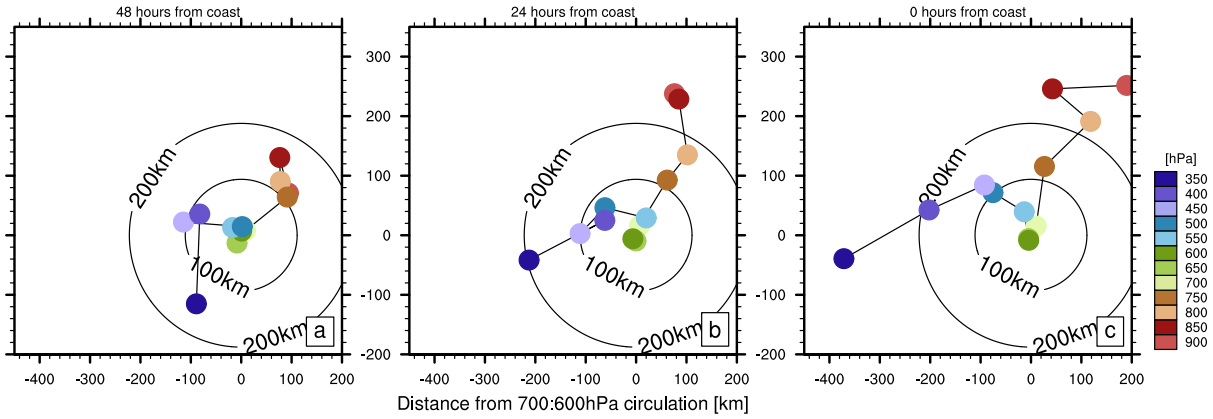

Figure 4.3: Relative distance of circulation centers at different pressure levels from the mean center of the 700-600 hPa levels. Distances are averaged over 24 h intervals starting at time displayed above plot. Times are relative to coastal passage. Plots are organised with respect to mean longitude center (east to west is portrayed right to left). a) 48-72 h from coast mean vertical offset of circulation centers. b) 24-48 h from coast, c)0-24 h from coast.

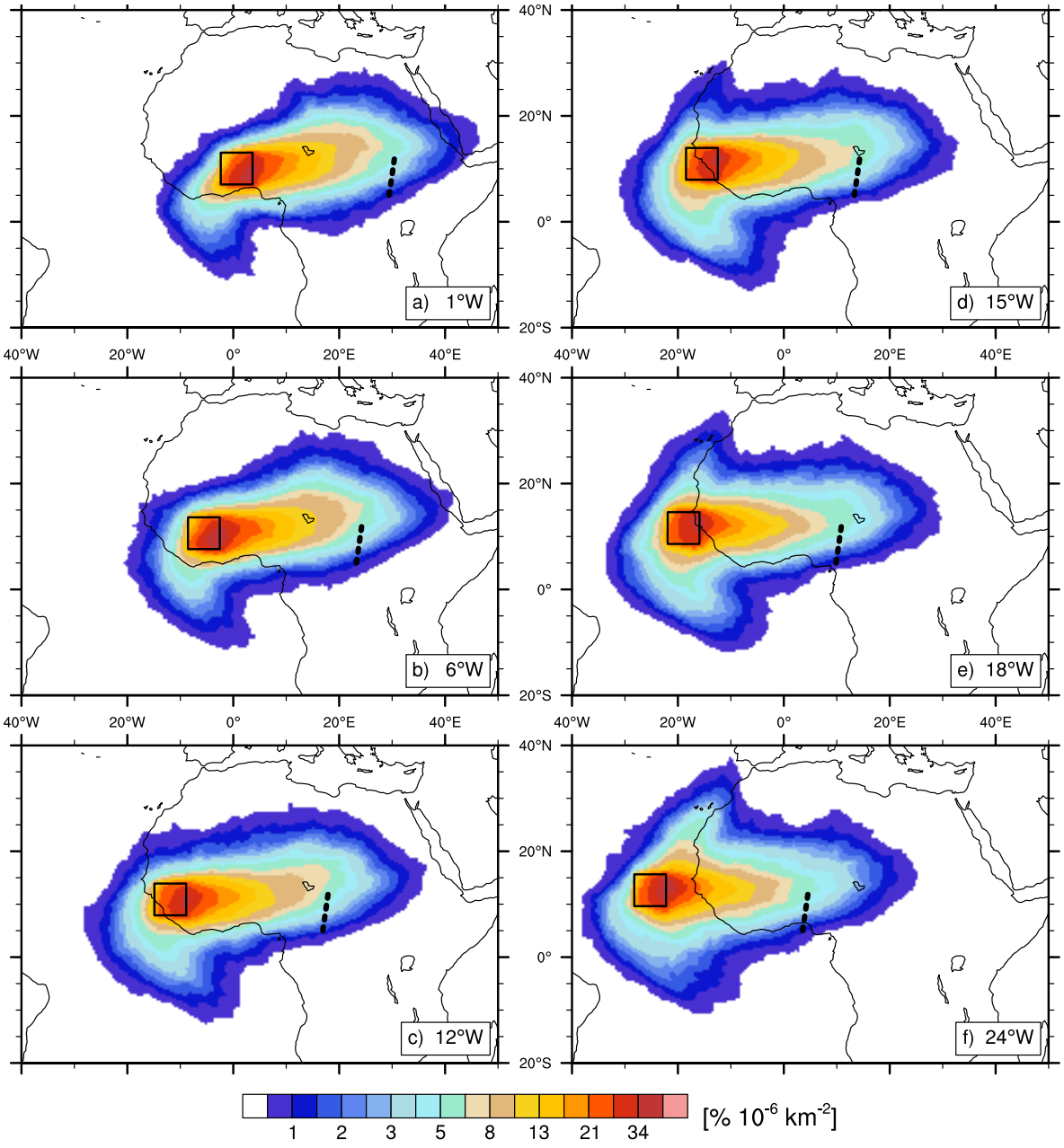

Figure 4.4: Density of total flow of trajectories released from 86 waves at 6 times relative to coastal passage for backwards integration of 120 h. Common flow routes towards the waves are visualised by maxima in the density field. Box contains the starting location of trajectories (location of trough at initialisation time). Dashed line shows mean location of AEW trough 120 h before the trajectories were initialised.

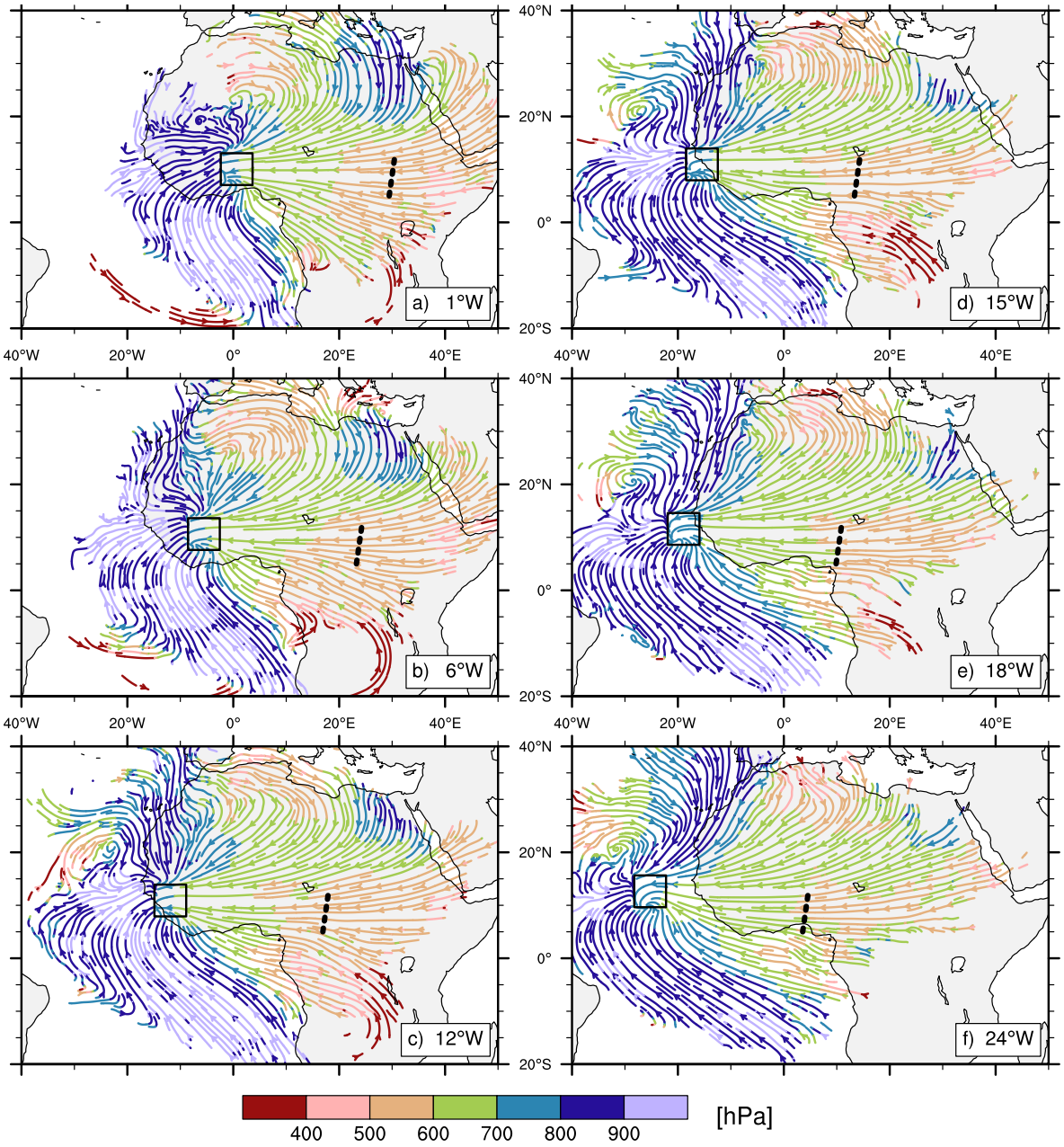

Figure 4.5: Composite total flow of 120 hour back trajectories for 86 waves. Initialised at 6 times relative to coastal passage. Streamlines depict the mean flow per grid point, coloured by the mean pressure of the trajectories at that point.

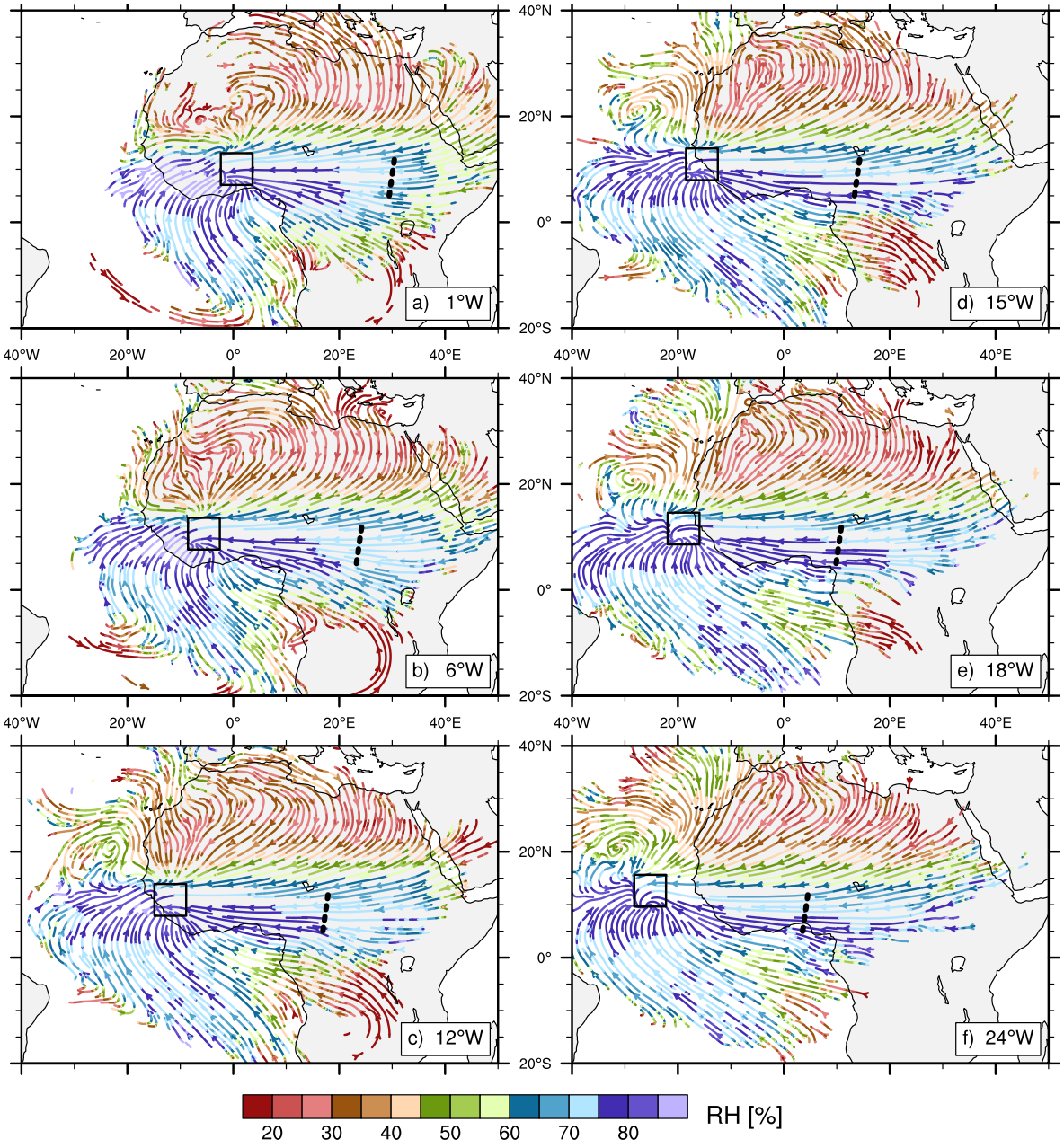

Figure 4.6: Composite total flow of 120 hour back trajectories for 86 waves. Initialised at 6 times relative to coastal passage. Streamlines depict the mean flow per grid point, coloured by the mean relative humidity of the trajectories at that point.

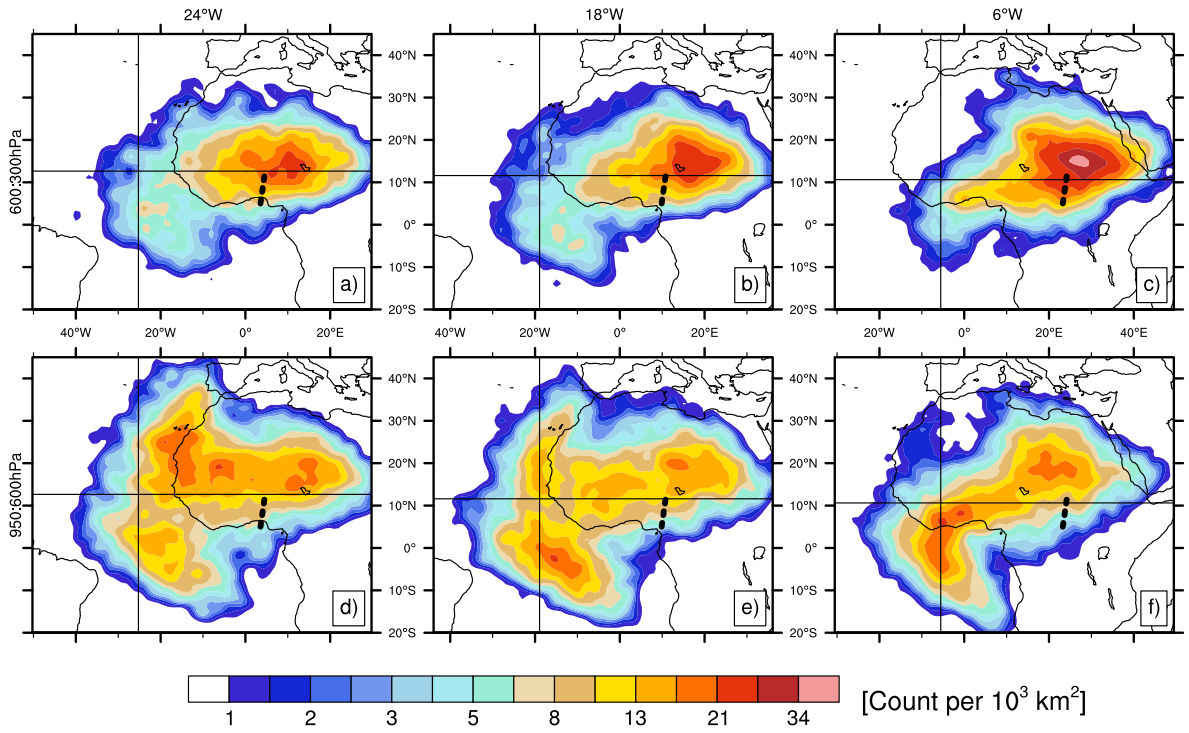

Figure 4.7: Density of source locations of trajectories released at 3 times relative to coastal passage for backwards integration of 120 h. Trajectories have been shifted to be trough relative throughout the integration. Columns contain plots with respect to time relative to coastal passage. Rows contain plots with respect to the initialisation level of trajectories.

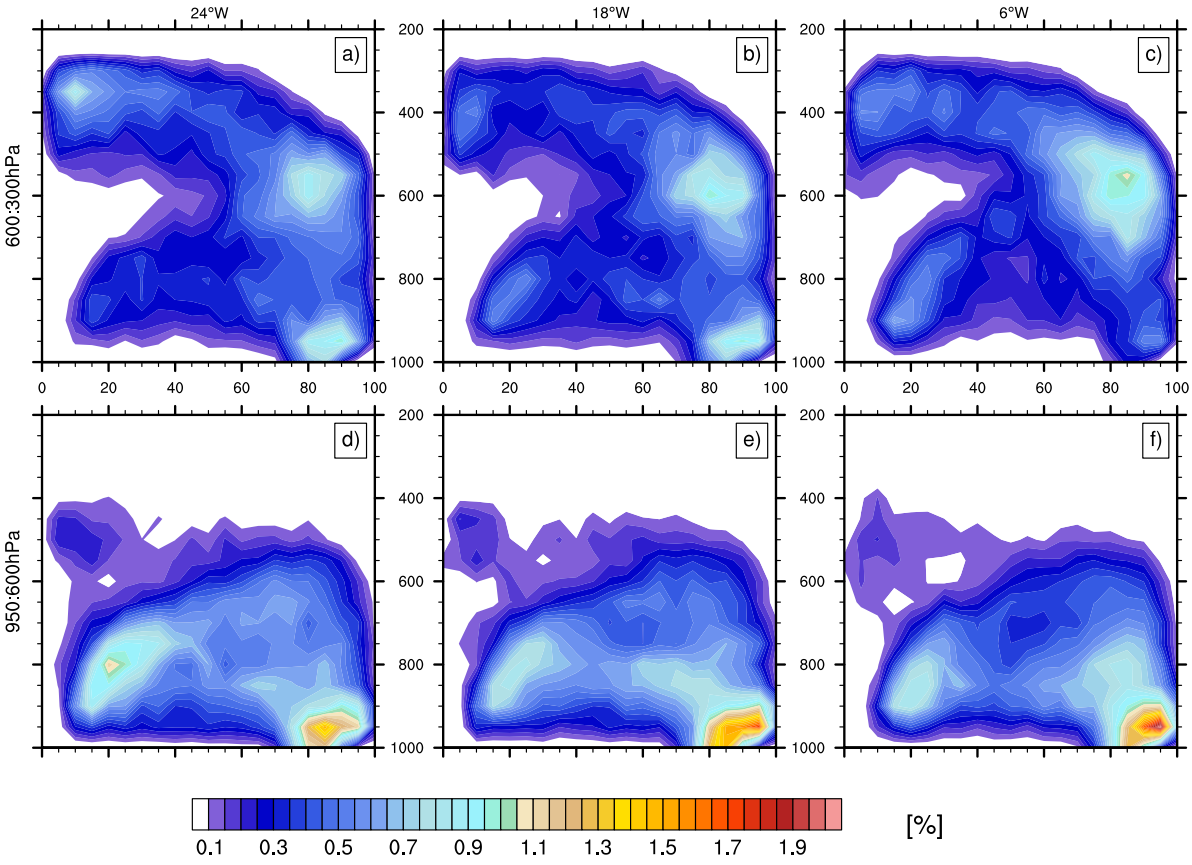

Figure 4.8: Characteristics of trajectories 120 h before initialisation from the AEW trough. Pressure (ordinate) by Relative Humidity (abscissa) density plot of trajectories for all 86 waves. Columns contain plots of the waves with respect to time relative to coastal passage. Rows contain plots with respect to the initialisation level of trajectories.

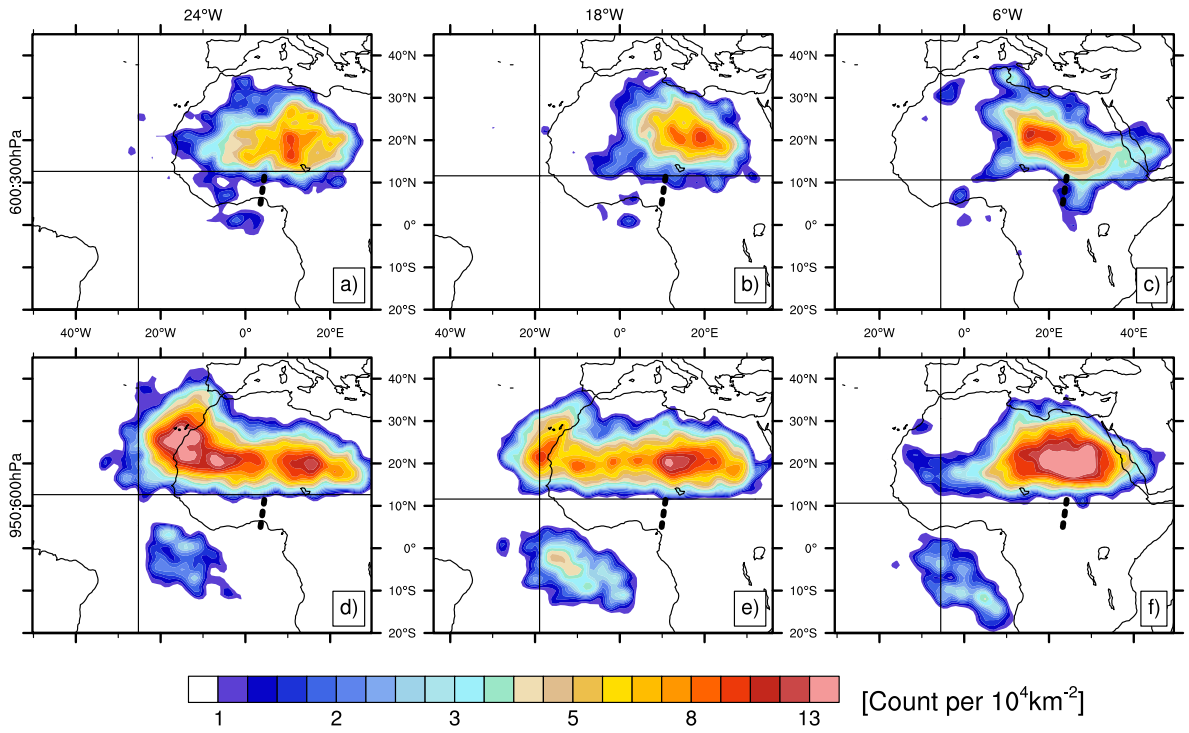

Figure 4.9: Density of trajectory sources with Relative humidity $\leq 40\%$. Columns contain plots of the waves with respect to time relative to coastal passage. Rows contain plots with respect to the source pressure of the dry air.

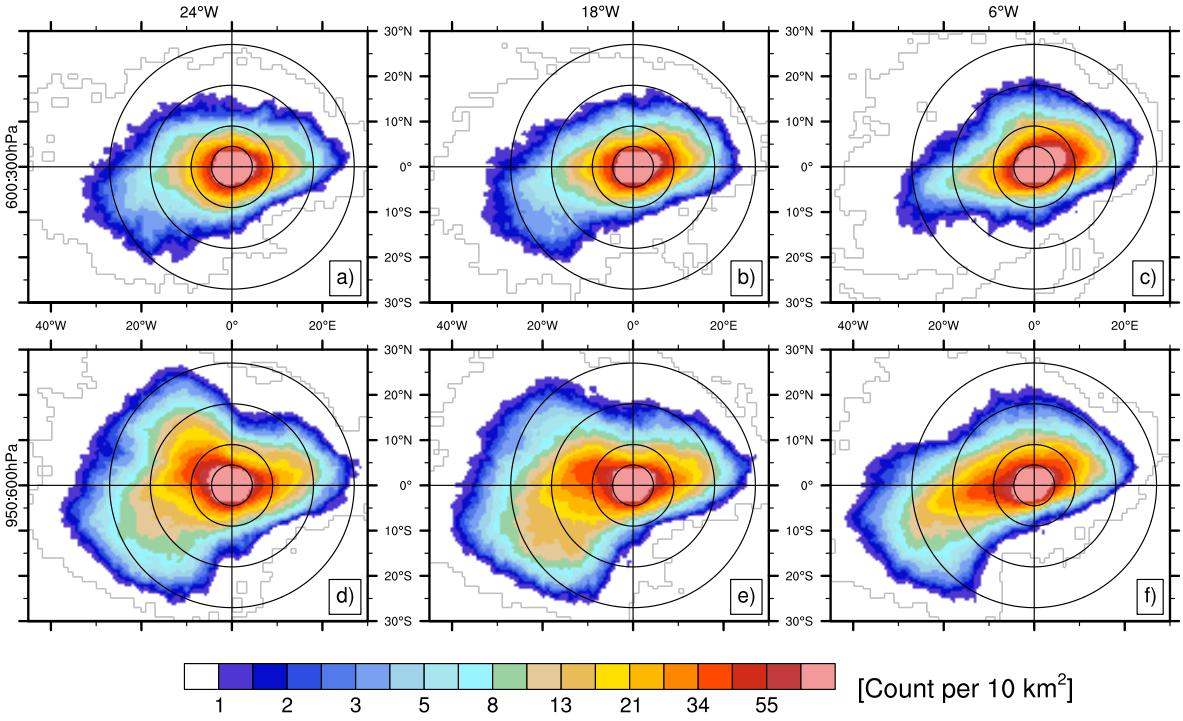

Figure 4.10: Density of total flow of trajectories released at 3 times relative to coastal passage for backwards integration of 120 h. Trajectories have been shifted to be trough relative throughout the integration. Columns contain plots with respect to time relative to coastal passage. Rows contain plots with respect to the initialisation level of trajectories. Range rings are shown at 500, 1000, 2000, 3000 km from center.

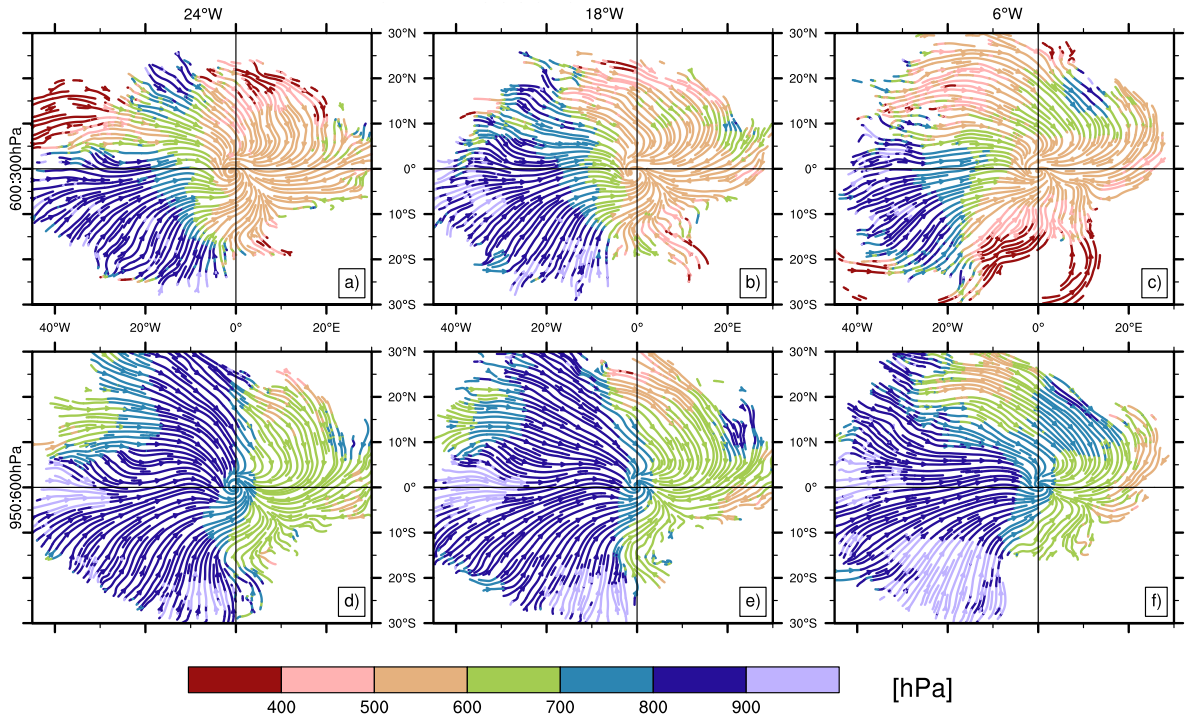

Figure 4.11: Density of total flow of trajectories released at 3 times relative to coastal passage for backwards integration of 120 h. Trajectories have been shifted to be trough relative throughout the integration. Columns contain plots of the waves with respect to time relative to coastal passage. Rows contain plots with respect to the initialisation level of trajectories.

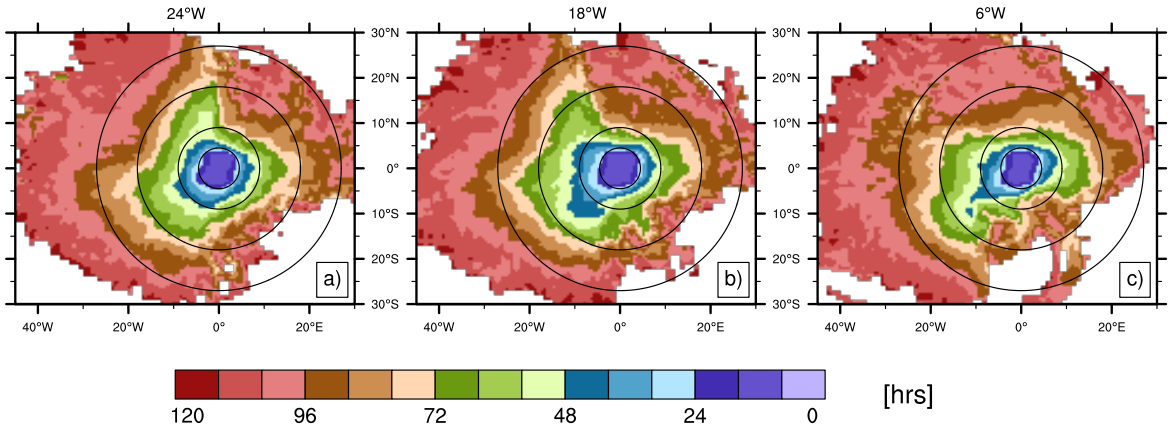

Figure 4.12: Median number of hours from trough center for all waves and levels. Panels are relative to trough passage at coast; 24 h after passage (a), Over the coastal region (b), and 48 h before coastal passage (c). Arranged west to east in mean trough location. Range rings are shown at 500, 1000, 2000, 3000 km from center.

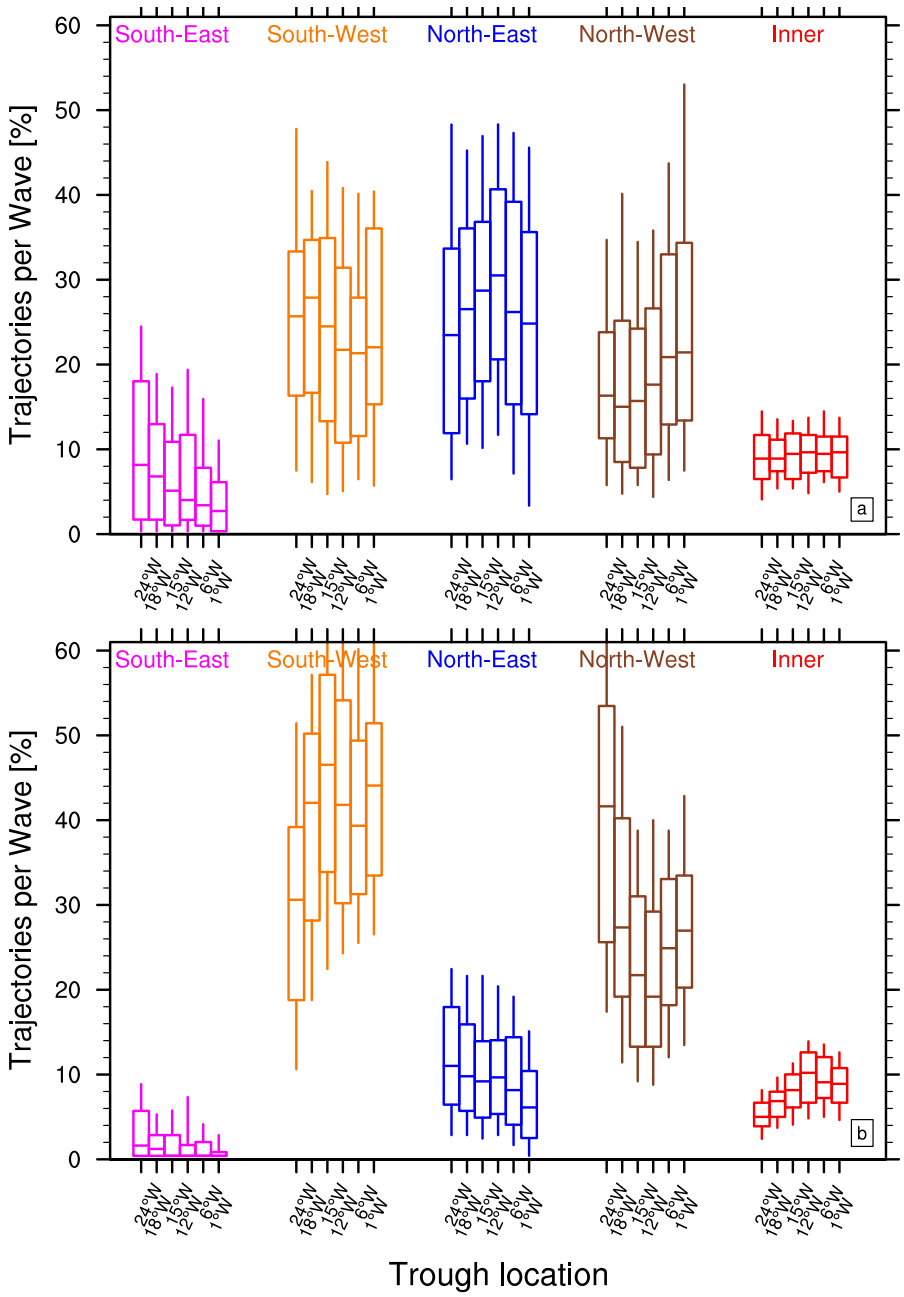

Figure 4.13: Distribution of percentage of trajectories sourced (-120 h) from each region, by wave location with respect to coast and grouped by region of trajectory source. a) Trajectories initialised above 600 hPa. b) Trajectories initialised below 600 hPa.

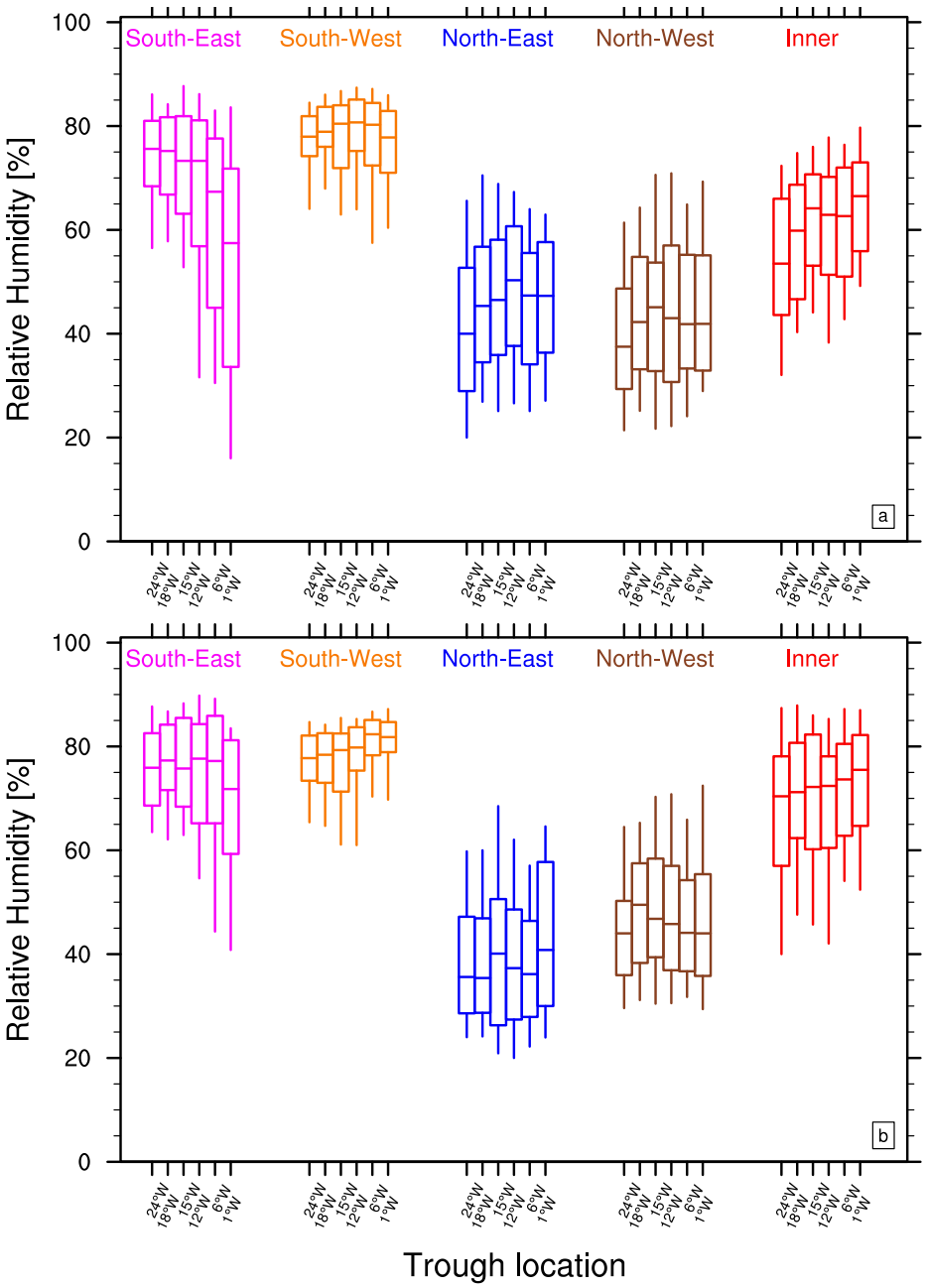

Figure 4.14: Distribution of relative humidity trajectories at -120 h, by wave location with respect to coast and grouped by region of trajectory source. a) Trajectories initialised above 600 hPa. b) Trajectories initialised below 600 hPa.

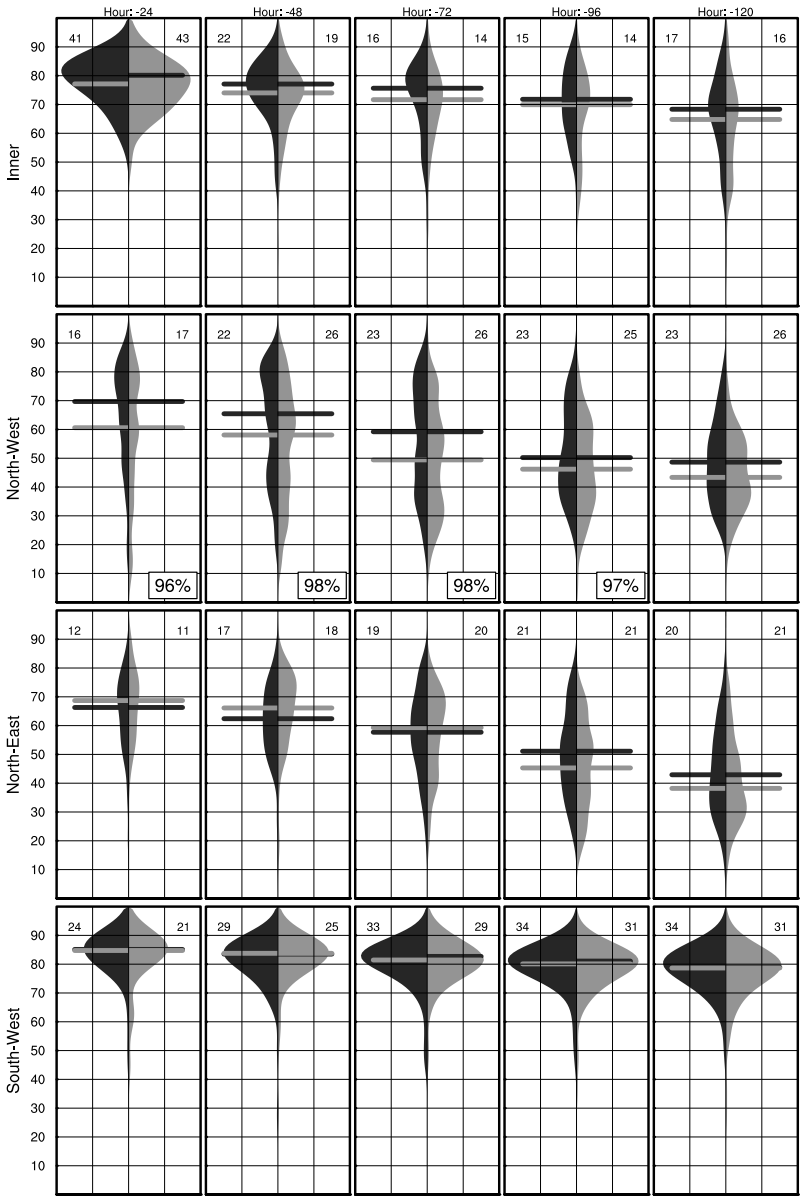

Figure 4.15: Bean plots showing the distributions of RH for trajectories of developing and non-developing AEWS. Columns display the distributions by hours from trough initialisation location (chronologically ordered right to left in 24 hour increments). Rows separate the distributions by the region that the trajectory is located in at that time. Black represents trajectories associated with developing AEWS, grey represents trajectories associated with non-developing AEWs. Horizontal bars represent the median of the distribution. Numbers in the top corners indicate the percentage of trajectories in that region at that time. Trajectories initialised in troughs over the coast.

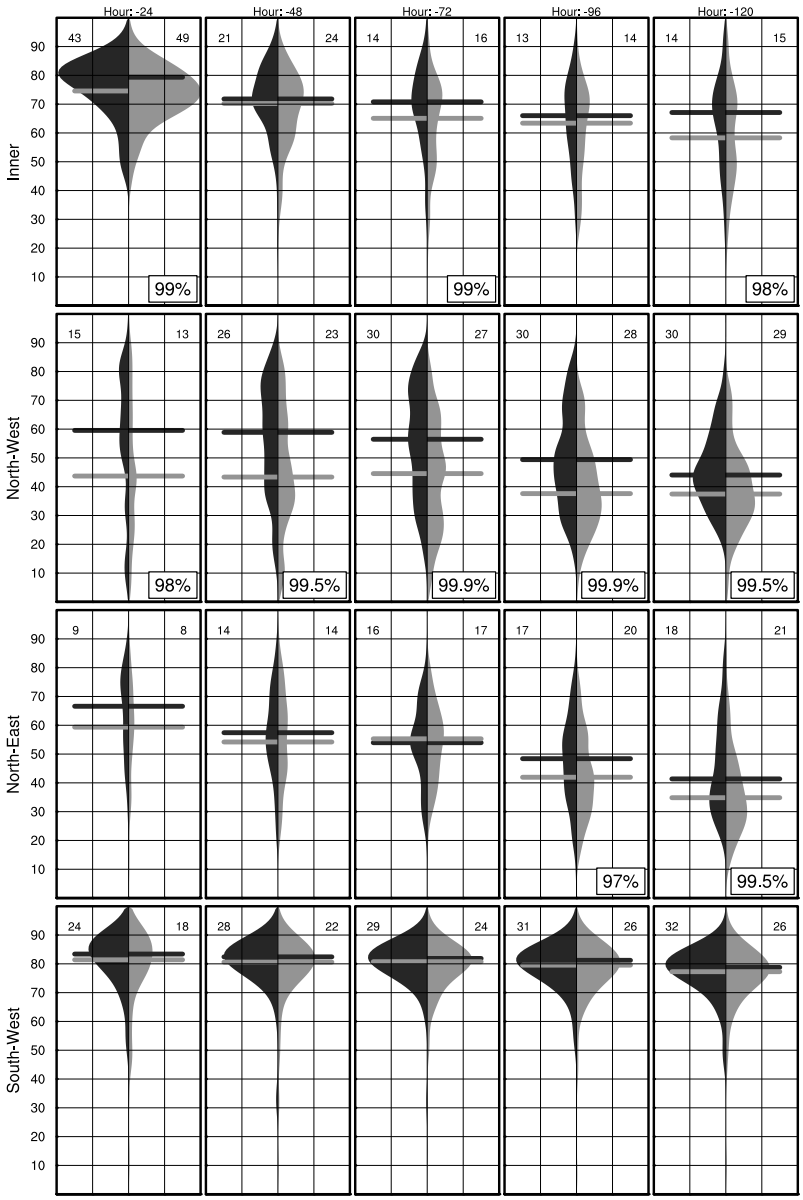

Figure 4.16: As Fig. 4.15. For trajectories initialised in troughs 24 h after passing over the coast.

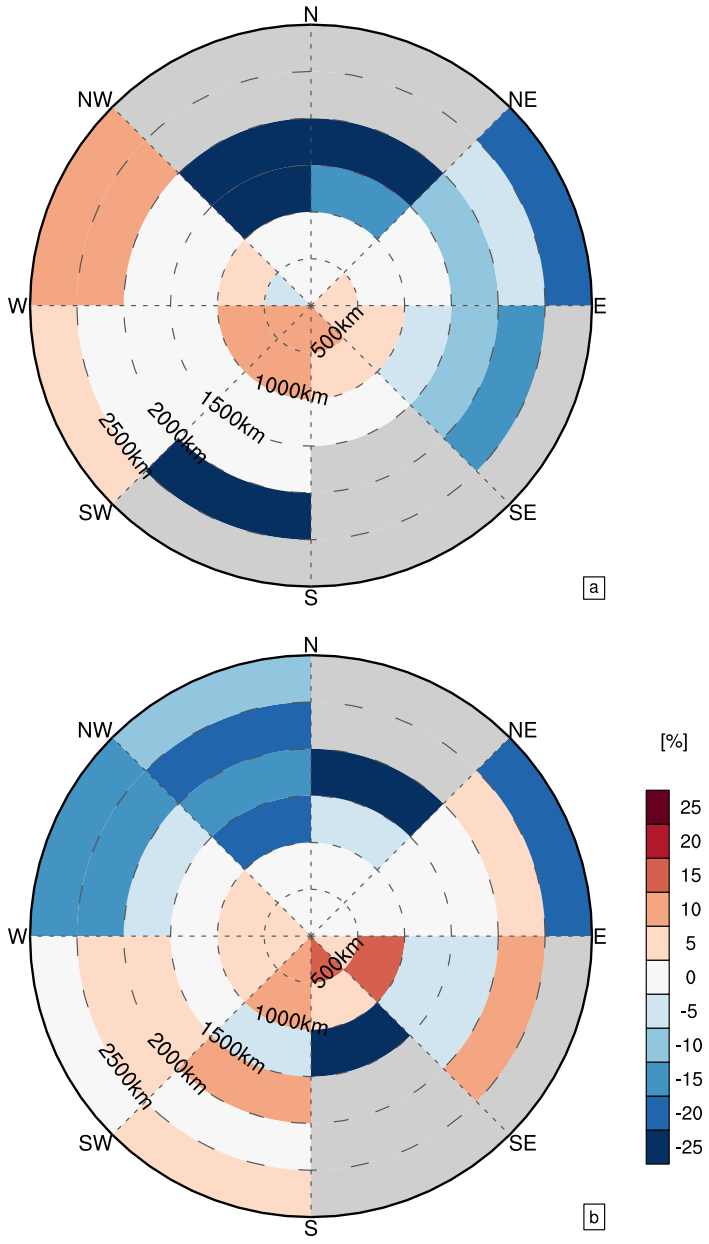

Figure 4.17: Difference in density of trajectory locations at 72 h from trough center, over three initialisation times (-48,-24,0 h), between developing and non-developing waves. Trajectories were shifted to trough relative locations. Values represent the percentage difference between developing and non-developing waves for that region. Positive values indicate more trajectories in developing waves, negative more trajectories in non-developing waves. Grey regions denote areas with less than 50 total trajectories. a) Trajectories initialised above 600 hPa. b) Trajectories initialised below 600 hPa.

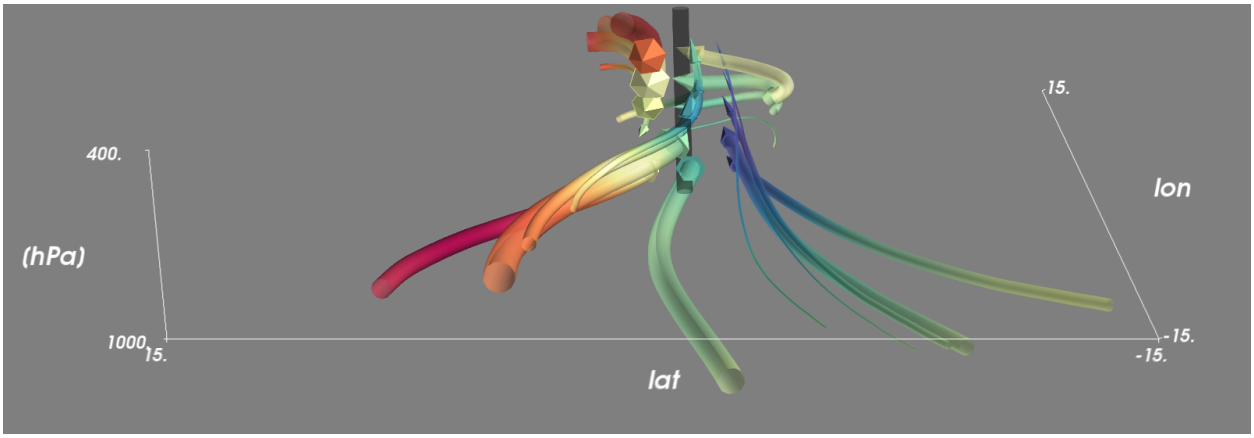

Figure 4.18: Mean trajectories approaching favourable trough located over the West African coast. Thickness of trajectory represents the frequency of trajectories along that route. Trajectories are shaded by the relative humidity along the route (Red = dry, blue = wet). Viewer is looking east towards AEW trough (vertical black cylinder).

5. Seasonal Review of AEWs during 2012, 2013 and 2014

5.1 Introduction

This chapter will briefly review AEWs and tropical cyclogenesis (TCG) over the seasons of 2012, 2013 and 2014. The first section of this chapter will provide a brief synopsis of the state of seasonal variability of AEWs during the three years focussing on waves during August and September. These are climatologically the most favourable months for TCG from AEWs over the Atlantic (McTaggart-Cowan et al. 2008). The brief overview of the three seasons will provide the basis to then analyse a select number of cases to detail the processes involved in both genesis from AEWs and non-genesis in favourable conditions.

The characteristics of AEW troughs leaving the coast has been associated with each trough's likelihood of providing the environment for TCG over the eastern Atlantic. Hopsch et al. (2010) showed significant differences between the structure of the troughs for developing and non-developing waves over West Africa. Brammer and Thorncroft (2015) and chapter 3 highlighted the environmental differences between AEWs that had been classified as favourable for TCG over the eastern Atlantic. Theses environmental differences revealed that differences in the moisture field to the west and northwest of the troughs were ingested at low levels in to the trough and potentially impacted the outcome of the waves.

Dunkerton et al. (2009) hypothesised that westward moving disturbances have a region of recirulcation in the Lagrangian flow. A critical latitude is defined at the center of this recirculation where the phase speed of the disturbance equals the surrounding environmental wind. This region of closed circulation should therefore protect the disturbance from lateral entrainment of the surrounding environment. Moistening of the column and aggregation of vorticity within this area can then facilitate the genesis process near the critical latitude without the negative impacts of the surroundings.

The vertical extent of the recirculating region however is critical for the trough to

provide a favourable environment in a hostile environment. Conversely, inflow of favourable environmental air into a less favourable trough may expedite the process of creating a region for TCG to occur. Montgomery et al. (2010) evaluated the vertical depth of positive Okubo-Weiss (as defined in Dunkerton et al. (2009) i.e. relative vorticity squared minus the squared stretching and shearing deformation terms) as a measure of recirculation for pre-Typhoon Nuri (2008). In a region of hostile environment the upper limit of positive OW decreased, suggesting that although protected, the depth of the recirculating region was influenced by the surrounding environment. The lower extent of the recirculation was not addressed in this study however. The vertical alignment and depth of the vortex was suggested to be essential for the development of Hurricane Karl and Tropical Storm Matthew in 2010 by Davis and Ahijevych (2012). Large displacements of the vortex in the vertical can impose relative flow below an otherwise recirculating level, making the vortex potentially sensitive to environmental air (e.g. Rappin et al. 2010; Raymond and Carrillo 2011). Davis and Ahijevych (2012) suggested that the misalignment of the vortex was an important factor in the weakening of Hurricane Gaston (2010).

AEWs are typically characterised by maxima in vorticity associated with AEJ at around 700 hPa, below which the trough typically exhibits a cold-core structure. Janiga and Thorncroft (2012) showed that once the waves are over the eastern Atlantic diabatic heating has a deeper profile throughout the troposphere contributing to low-level vorticity generation. At 30°W vorticity in the troughs had extended down towards the boundary layer and the cold-core had weakened. As suggested by Raymond and Sessions (2007) the reduction in the depth of this low-level cold-core will restrict the inflow layer associated with the vortex and as such would be a likely aid in the vertical development of a closed circulation. This however suggests that there may be a period of time where the mid-level vortex of an AEW is entraining environmental below the vortex. This was the period of time in the trough's evolution that Brammer and Thorncroft (2015) suggested, through composite analysis, was sensitive to the environment to the northwest of the trough. The results of chapter 4 suggested this

time was around 48-72 h after leaving the coast.

This chapter will review three seasons of AEWs and tropical cyclogenesis and then detail the evolution of 2 developing and 2 non-developing cases. Detailed analysis of the AEWs as they leave the West African coast will help in understanding how the environment interacts with the troughs and the ability for the troughs to recirculate; potentially providing a favourable environment for TC genesis.

5.2 Methodology and Data

5.2.1 AEW Tracking and Identification Numbering

AEWs are tracked according to the methodology described in Chapter 2. Troughs are given an identification number in each season. This number is defined at the genesis time of the trough. As a result of this identification system trough numbers crossing the West African coast are not necessarily sequential. However when troughs are non-sequential the length of the track can be inferred by the identification number.

5.2.2 Logistic Regression Model

AEW troughs that transition over the coastal region are objectively characterised using a logistic regression model. The details of the selection process are included in chapter 3. For this chapter, the anomalous total precipitable water over the eastern Atlantic the day each trough left the coast was also made available in the predictor selection. The forward step selection process found this to contribute significantly and replaced low-level vorticity from the model used in Chapter 3. This supports the analysis in chapter 3 showing that trough scale predictors and the moisture ahead of the troughs combine to produce a more skilful model, though further analysis of the significance and implications of this is needed but is not pertinent to this chapter. The logistic regression model will be reduced to three categories for simplification. These will be based on terciles of the waves tracked over 1979-2012. The terciles will be categorised as unfavourable, marginal and favourable for development.

5.2.3 Trajectories

Trajectories are calculated using the HYSPLIT model also used in Chapter 4. Trajectories are integrated backwards for 192 hours using the CFSR for input grids. Trajectories are placed west of the trough at grid cells with less than 50% relative humidity to analyse the origin of dry air present near the storms.

5.2.4 NASA HS3 Global Hawk Observations

Data from the Advanced vertical profiling system (AVAPS) dropsondes and cloud physics lidar (CPL; McGill and Hlavka 2015) will be used in the second half of this chapter. These instruments were used onboard the NASA global hawk aircraft in the Hurricane and Severe Storm Sentinel (HS3) field campaign during the three years reviewed here (Braun et al. 2015, *manuscript submitted to Bull. Amer. Meteor. Soc.*). The dropsondes measure pressure, dry-bulb temperature, relative humidity as well as wind-speed and direction. These data have been quality-controlled using established post-processing methodology (Wang et al. 2010a). The dropsondes used in this campaign use the same pressure-temperature-humidity sensor as the Vaisala RS92 radiosonde with documented high accuracy though with a diurnal bias due to solar heating of the sensor (e.g Intrieri et al. 2014; Wang et al. 2013).

CSFR data were interpolated in the horizontal using bicubic interpolation to the mean location of the dropsonde throughout the drop duration. Drops typically travel less than 20km in the horizontal. This is less than half of the reanalysis grid spacing, and therefore there is minimal impact of whether launch, splash, or locations along the drop are used. Some drops did not record to the surface, therefore the average recorded location is equivalent to median location of the sampled profile. The 6-hour data are then linearly interpolated to the time of the drop.

The CPL instrument measures cirrus and aerosol layers through multi-wavelength measurements from a back-scatter lidar. Post-processing of the data provides a classification of up to 8 layers in the atmosphere of three types at 1 second intervals (e.g. McGill et al. 2003;

Yorks et al. 2011). The data has a spatial resolution of 20m in the vertical and 200m in the horizontal.

5.2.5 Satellite Observed Precipitation

Precipitation is obtained from the Tropical Rainfall Measurement Mission (TRMM) dataset 3B42 version 7 (TRMM 2011). These data are produced by merging IR estimated precipitation rate with microwave and precipitation radar onboard the TRMM satellite. The 3 hour 3b42 product is the adjusted using an inverse-error-variance weighting based on the monthly accumulations from the Global Precipitation Climatology Centre (GPCC; Huffman et al. 2007). The produced data has a 0.25° horizontal resolution and 3 h temporal resolution spanning 1997-2014.

5.3 Overview of 2012, 2013 and 2014 Seasons

Discussion of the seasons will relate to the three hovmöllers presented in Figs. 5.2,5.4,5.6. Analysis of the 6 -hour CFSR fields was also conducted in analysing the evolution of the waves and consultation with the post-season reviews of the tropical storms performed by NHC (available at http://www.nhc.noaa.gov/data/tcr/). Notable cases will be presented in more detail in the following section.

5.3.1 AEWs During 2012

Tropical cyclone activity was above average in 2012 with a total of 19 tropical storms developing. Of these 19, 10 became hurricanes and 2 reached major hurricane strength. Through July to October 49 AEWs were tracked leaving the coast. 8 of the AEWs were associated with tropical cyclogensis occurring during August or early September. Figure 5.1 shows the tracks of all waves with the associated storm tracks included. With the exception of Gordon, the storms all developed initially east of 50°W and south of 16°N. It should be noted that while Helene initially attained Tropical Depression strength it subsequently weakened and later re-developed to Tropical Depression strength at 95°W. During 2012 AEWs were

involved in at least 42% of the tropical cyclogenesis events, 50% of the storms that reached hurricane strength, but were not obviously linked to either of the major hurricanes.

Alberto, Beryl, Chris and Debby developed early in the season over the north-west Atlantic or Gulf of Mexico, developing from either sub-tropical origins or complicated mergers of surface lows with tropical wave remnants.

During August and September 2012, 15 AEWs crossed the West African coast. Of these, 5 developed into tropical disturbances before reaching 45°W. Figure 5.2 shows the wave tracks and curvature vorticity overlaid with OLR anomalies filtered for Kelvin waves and the MJO.

Tropical cyclone activity during the August and September appears to be modulated by convective activity within the MJO filtered band. During late August (16th - 31st) Fig 5.2a shows a weak convective active MJO crossing over the Atlantic. During this time 4 AEW troughs left West Africa although only 2 were characterised as favourable all 4 developed. AEW33 was not objectively tracked to genesis, but analysis of 700 and 850 hPa relative vorticity shows that while the objective track followed a southern jet-level track, a weak vortex moved north was formed the precursor to Tropical Storm Kirk. Moisture associated with pre-Isaac and pre-Joyce (AEWs 29 and 32, respectively) was anomalously low at 600 hPa and close to climatology at low levels (Fig 5.2b). Both genesis events however do occur on the leading edge of a convectively active Kelvin wave (Fig 5.2a). The impact of Kelvin waves on genesis and AEWs has been shown in statistical and composite studies, therefore the combination of Kelvin wave and MJO activity may be an important reason for increased frequency of genesis events during this period.

During September a suppressed phase of the MJO filtered convection crossed the Atlantic. The genesis of Hurricane Nadine occurred in the days prior to the suppressed MJO convection. Following the genesis of Hurricane Nadine, 5 more AEW troughs crossed the coast however 3 of these did not cross 40°W. The short tracks align with the suppressed phase of the MJO and possibly suggest an influence on the AEW structure.

The case study analysis in the latter half of this chapter will focus on 2 of the developing cases from this year. AEW31 associated with the genesis of Leslie and AEW36 associated with the genesis of Nadine. The pre-cursosr trough to Hurricane Leslie, left the coast prior to the active MJO in late August. Over the coastal region a suppressed Kelvin wave intersected with the trough, which may be associated with the marginal genesis diagnostic. Moisture associated with AEW31 was anomalously moist at low levels with a small region of negative moisture anomalies at 600 hPa (Fig 5.2b). This case was therefore chosen to analyse the interaction between the low-level moisture and jet-level dry air, with a fast evolution to genesis with the TD declared east of 30°W.

The genesis of Hurricane Nadine from AEW36 will also be presented. Low-level moisture anomalies associated with AEW36 were very high with 5 g/kg positive moisture anomalies at 850 hPa to the west of the troughs track line. Superposed over this excessively moist low levels however is dry air to the east and west of the track after leaving the coast. This trough did take a longer time to reach tropical depression and the analysis will follow the evolution from the coast to the day before reaching TD status.

5.3.2 AEWs During 2013

Tropical cyclone activity in 2013 was historically quiet, with a total of 14 tropical storms, of which only 2 attained hurricane strength. Early in the season an AEW was tracked across the whole Atlantic basin and associated with the genesis of Barry in the west Caribbean. Dorian, Erin and Humberto all developed very quickly after leaving the West African coast. Chantal was tracked from the African coast with genesis occurring around 4 days after leaving the coast in the main development region (MDR; Fig. 5.3). While Jerry has an AEW source, the development was also through due to an interaction with a mid to upper level low. Genesis elsewhere was either from sub-tropical pathways or didn't have clear links to the African coast.

Fortynine AEWs were tracked leaving the West African coast between July and Oc-

tober (Figure 5.3). Seven AEWs were associated with the genesis of 50% of the tropical cyclogenesis events during the year. Of these genesis cases, 1 of the 2 hurricane strength systems during the year are included.

The frequency of waves and the number of favourable waves for 2013 is comparable to 2012 (Fig. 5.4). Although the season was historically quiet, having three developing systems east of 25°W is relatively rare. Preliminary research has attributed the quiet tropical cyclone season to combinations of increased subsidence over the Atlantic associated with drier than normal mid to upper level conditions, coupled with a reduced thermohaline circulation in the ocean in the Atlantic during the early months of the year (Klotzbach 2014). While this research can not address the reasons behind the lack of tropical cyclones during 2013, the tracks and diagnostics of the AEWs, suggest that it was not due to a lack of AEW activity or a lack of favourable AEW troughs. The anomalous moisture hovmöller during August and September the low levels around the coast experience anomalously moist conditions for extended periods of time (Fig. 5.4b). Conversely at 600 hPa there are a large number of negative moisture anomalies tracking west associated with AEW troughs. This season highlights that analysis of developing and non-developing systems is likely to include many different scales that can not all be controlled for. Controlling for favourable AEWs leaving West Africa may reveal more detailed results for iintraseasonal and interannual research.

During August and September, there were two developing eastern Atlantic cases. In mid-August tropical storm Erin developed in conditions close to climatology (Fig. 5.4b). The precursor wave was characterised as favourable on leaving the coast and appears to have merged with a short-lived track to its west prior to leaving the continent. This genesis event also occurred on the leading edge of a convectively couple Kelvin wave.

The case study analysis in the latter half will analyse the non-developing wave of AEW33 which left the coast in early September. This trough crossed the coastline after the intersection with a convectively active MJO and Kelvin wave (Fig. 5.4a). Ahead of the trough however was a large region of negative moisture anomalies at the jet-level and weak

negative anomalies at low levels as well (Fig. 5.4b). Roughly 10 days after AEW33 left the coast Hurricane Humberto also crossed the coast line and reached tropical depression status almost immediately on reaching the ocean. This suggests that the large scale conditions over the area were favourable for genesis during this time.

5.3.3 AEWs During 2014

Tropical cyclone activity during 2014 was below the historical average over the Atlantic. Only 8 tropical storms developed, though 6 of these became hurricanes and 2 attained major hurricane strength. The count of AEWs leaving the coast was mostly consistent with 2012 and 2013, with 51 waves departing the continent between July and October. Of the 51 waves, 4 were associated with tropical cyclogensis (Fig. 5.5). The only two eastern Atlantic genesis cases in the season, Bertha and Edouard, were tracked back to AEW origins. Further east both Cristobal and Dolly were also associated with AEWs which had tracked across the Atlantic. These cases however, are 50° and 70° west of Africa and the waves would have experienced significant evolution over that transit, making their characteristics over West Africa less important. AEWs again were associated with 50% of the total cyclogenesis events and also 50% of the storms that reached hurricane strength.

The equatorial wave activity during August and September 2014, was quieter than the previous 2 years (Fig. 5.6). A weak MJO convective signature is present over the eastern Atlantic during the first 10 days of August, this was coincident with the genesis of Hurricane Bertha on August 1st (not shown). Following this, convective activity on the MJO timescale shows little variability during the 2 months. Kelvin wave activity also appears quieter than the previous 2 years, with a single strong convectively active Kelvin wave in the last 5 days of August. During these two months the number of favourable waves leaving Africa is greatly reduced compared to 2012 and 2013. Although the total count of waves is comparable to previous years with 19 AEWs during the two months, only 5 of these were diagnosed as favourable for genesis.

Analysis of the individual predictors included in the diagnostic reveal that during early August, humidity over the eastern Atlantic was a consistent negative factor in the diagnostic of the waves (not shown). These negative anomalies in low-level humidity are evident between the 5th and the 21st of August over the eastern Atlantic (Fig. 5.6b). During this time 2 out of 7 waves are characterised as favourable. These troughs had higher values across the other predictors but still fail to develop once over the ocean in the anomalously dry environment. AEW33 although characterised as marginal due to the low-level humidity over the eastern Atlantic, after crossing the Atlantic the trough associated with the development of Hurricane Cristobal to the northwest of the Bahamas (Fig. 5.5).

During September there were no waves characterised as favourable for development. Low-level humidity over the eastern Atlantic had restored to climatology with occasional periods of positive anomalies (Fig. 5.6b). The predictors, however now indicate that vertical motion within the troughs was consistently weak over the coastal region. During this time of suppressed wave favourability, Hurricane Edouard developed from a marginal AEW over the eastern Atlantic. Using this genesis as indication that the large scale conditions weren't restricting genesis cases entirely the preceding trough was selected as a the second non-developing case study trough. AEW40 had a long track over West Africa and interacted with a strong convectively active Kelvin wave over Africa (Fig. 5.6a). After leaving the continent, the trough had slight negative moisture anomalies at low levels and a long track of negative moisture anomalies at 600 hPa (Fig. 5.6b). The case study will analyse the interaction of the trough with this region of dry air to the west of the trough.

5.4 Contrasting developing and non-developing AEWs

The work in the earlier chapters presented composite views of developing and non-developing waves. These composite results suggested the importance of the trough relative flow, closed circulation within the trough and vertical tilt of the vortex as the wave leaves the West African coast. Related to these factors the low-level moisture to the northwest

of the trough was shown to be a significant factor between developing and non-developing waves. The evolution of four waves from 2012 - 2014 will be presented in this section. Two developing waves from 2012, and a non-developing wave from 2013 and 2014. While the 2013 and 2014 seasons were less active than 2012 for tropical cyclogenesis the troughs are defined as characteristically similar and the results presented here may be a contributing factor for the lack of development during these seasons. The three waves from 2012 and 2013 were defined in the upper third of the genesis probability from the logistic regression model whereas the 2014 case was defined in the middle tercile. For the 2014 wave the trough scale characteristics were favourable, but the dry low-level environment ahead of the wave contributed to the lower score.

Each wave is analysed with respect to the evolution of the precipitation and vortex within the trough, and the trough relative flux of environmental moisture in the lower troposphere. Case study analysis therefore provides detailed information about how each trough interacts with the environment at and below the level of the AEJ (650 hPa).

5.4.1 2012 Hurricane Leslie

Hurricane Leslie developed from a moderately favourable trough that left the West African coast on August 26th 2012. The tropical disturbance was officially recorded at 0000UTC on August 30th and intensified to tropical storm strength within 12 h. The accumulated precipitation along the AEW track is plotted in Fig. 5.7. In the days before the trough reached the coast continuous precipitation fell within the vicinity of the trough. After leaving the coast, the vortex track shifted slightly south with the accumulated precipitation showing continuous coverage of convection around the trough. The background TPW in Fig. 5.7 shows that when the trough left the coast on August 26th, to the immediate NW of the trough there were TPW values of around 40 mm. Further to the west there was an enhanced region of 55+ mm of TPW associated with the downstream AEW trough. Geopotential height at this time shows a weak upper level ridge extending across the sub-

tropics with the southern extent of a mid-latitude trough just visible at the top of the figure (30°W). This upper level zonal flow pattern matches the composite result present chapter 3. Zonal flow over the region was expected to reduce subsidence and northerly advection of dry mid-latitude air over the eastern Atlantic, in comparison to the presence of a upper-level trough over the region.

The evolution of the vertical profile of vorticity and moisture anomalies within 300 km of the trough center is shown in Fig. 5.8. Over West Africa the vorticity associated with trough is maximised around the level of the AEJ with an anomalously moist low-level center. The trough relative wind vectors reveal that while the trough is over the continent there remains relative westerly flow below 800 hPa. As the trough reaches the coast the low levels become more dominant though the magnitude of the vortex is still weak at this point. In the 2 days after leaving the coast (27th - 29th) the trough accumulates or develops low-level vorticity and positive moisture anomalies in the column extend upwards from 700 hPa to above 400 hPa. Following the increase in moisture throughout the lower-troposphere vorticity in the column increases and the system is recorded as a TD near 40 °W on the 30th.

Three east west cross sections are shown in Fig. 5.9 highlight the evolution in the vortex in the 36 hours after the trough leaves the coast as the vorticity and moisture begin to increase in the trough. At 1200UTC on the 27th (Fig. 5.9a) the trough shows a large westward zonal tilt with height in the cross-section, with a region of 600 hPa anomalously dry air on the western edge of the vortex. The wind vectors reveal that at this level the trough relative flow is mainly easterly and thus eastward advection of the dry anomalies is faster than the troughs phase speed. At lower levels on the western side of the trough, below 700 hPa there are positive moisture anomalies of +2 g/kg with relative westerly flow towards the vortex core. To the east of the vortex in the trough is a secondary narrow vortex column. This remains east of the developing trough and does not appear to be involved in the evolution of the pre-Leslie trough. At 0600UTC on the 28th (Fig. 5.9b), the mid-level

dry anomaly has moved away from the vortex as expected and the zonal tilt of the column has also reduced in the lower levels. The layer of inflow had now deepened slightly with relative inflow of anomalously moist air from the west extending up to around 750 hPa. The vorticity has aggregated into a warm core vortex in the low levels by 0000UTC on the 29th (Fig. 5.9c). Relative inflow through the center of the vortex is now reduced at low levels though positive moisture fluxes remain on the western edge of the trough.

Trough relative streamlines at 850 hPa and 600 hPa detail the initial 48 hours after the trough leaves the coast (Fig. 5.10). The cross sections discussed previously coincide with Figs. 5.10a,d,g. After initially leaving the coast the low-level vorticity is meridionally elongated along the trough axis and both the jet-level and low levels show no sense of closed circulation (Fig. 5.10a). Over the following 24 h, (Fig. 5.10b-d) a new low-level circulation develops east of the trough axis, but then becomes open to the environment again by 0600UTC on the 28th (Fig. 5.10d). At the jet-level, the circulation extends zonally over a large region but is located over the northwesterlies of the low-level circulation. During this time, the meridionally elongated low-level vorticity is consolidating below the jet-level circulation. Between 0600UTC and 1200UTC on the 28th (Fig. 5.10e) the low-level centers align vertically, although the low-level circulation still remains smaller than its jet-level counter part. As such much of the jet-level circulation remains above the low-level northwesterly flow. Once the circulation aligned vertically the vorticity increases and both both levels develop overlapping closed circulation (Fig. 5.10f-h).

The trough relative moisture advection is shown in Fig. 5.11 for the three time intervals shown in Fig. 5.9 (note panels are organised right to left with respect to time). The negative mid-level moisture anomaly evident in the cross-section (Fig. 5.9a) shows up in panels a-c. At 1200UTC on the 27th (Fig. 5.11c) the weak closed circulation over the southern half of the trough axis is evident. The negative moisture anomalies to the east are outside of the closed circulation and are thus in the region of relative north-northeasterly flow. As the troughs propagate westwards the negative moisture anomaly is advected to the south-west

further from the circulation center. During this time the jet-level closed circulation expands although negative anomalies are present to the NE of the circulation by 0000UTC on the 29th (Fig. 5.11a) it is outside of the closed circulation. At low levels most of the domain plotted is anomalously moist with the trough also associated with a region of positive moisture anomalies to the north (Fig. 5.11f). As the closed circulation develops at low-level some of this moisture in encompassed by the circulation. As shown previously, by 0000UTC on the 29th the circulation centers are aligned vertically with positive moisture anomalies throughout the lower troposphere (Fig. 5.11a,d).

The analysis here has shown how the AEW associated with the genesis of Hurricane Leslie transformed from a weak cold-core AEW to a warm core vortex capable of continuing to intensify and develop in a tropical storm. After leaving the West Africa the trough encountered negative moisture anomalies at 600 hPa, but these were outside the closed circulation at this level. At low levels relative advection of positive moisture anomalies towards the trough were present throughout the evolution. The trough also had continuous precipitation along the whole evolution from West Africa. The low-level positive moisture flux into the trough is expected to have been beneficial during this time. The presence of consistent convection is likely to help the vortex diabatically generate vorticity through the column and aid in aligning the vortex against the initial vertical tilt. The tilt of the vortex positioned the jet-level center over the relative northwesterlies of the low-level center. In these favourable conditions this meant increased flux of positive moisture anomalies below the jet-level circulation. This is expected to have reduced the negative impacts of downdrafts resulting from the mid-level dry air. Therefore although there were negative impacts on the trough, it is hypothesised that the persistent convection aided the resiliency of the system and the moist low levels were a beneficial factor for the persistent convection and reducing the negative impacts of the dry air aloft.

5.4.2 2012 Hurricane Nadine

The precursor wave for Hurricane Nadine left the African coast on 7th September 2012. Development of the tropical depression took 3 days after leaving the coast. The analysis here will focus on that time frame to present the evolution of the AEW trough from over the continent to the early stages of genesis. Fig. 5.12 shows the evolution of precipitation associated with the trough of the wave overlaid on the precipitable water field for when the trough left West Africa. Comparable to Fig. 5.7 the tropical eastern Atlantic has moisture greater than 40 mm. The 300 hPa geopotential height contours shows the upper level ridge extending from over Africa over eastern Atlantic. This more zonal flow at upper levels matches the pattern as discussed with the genesis of Hurricane Leslie. Assocaited with the track of the trough over West Africa there is precipitation on the eastern side of the Guinea highlands, where although the accumulation amounts are less than those observed with the pre-Leslie trough they appear to have greater spatial coverage. Along the coastal region, over the ocean, there is substantial precipitation accumulation. After the trough moves away from the coast, there is a slight decrease in the precipitation accumulation during September 7th to 9th, though this is for less than 48 h (3 black trough lines).

Figure 5.13 shows the anomalous moisture and trough relative streamlines the pre-Nadine trough over the 36 h after leaving West Africa. In these snapshots both the low-level and jet-level have closed circulation at each time. At 600 hPa there was initially negative moisture anomalies to the west and east of the trough (Fig. 5.13c), though these remained outside the closed circulation at this level. As the trough moves west the negative moisture anomalies to the east propagate with the trough, however during at each time it remains outside the circulation of the trough (Fig. 5.13a,b). At 800 hPa, similar to pre-Leslie, the eastern Atlantic has a wide area of positive moisture anomalies with increased anomalies to the north (Fig. 5.13d-f).

The trough relative streamlines and 850 hPa relative vorticity, at 6 h interval presented in Fig. 5.14, highlight the evolution of the low-level vortex during the 36 h after the trough

leaves the continent. At 1200UTC on Sept 8th the low-level circulation is initially open to the environment to the west (Fig. 5.14a), while above this at the jet-level there was a small region of closed circulation slightly to the south-west of the low-level vortex center. Over the next 18 h both the jet-level and low-level circulation expand, but throughout this time the jet-level center remains displaced to the south-west (Fig. 5.14b-d) and thus located over low-level north-westerly relative flow. Between 1200UTC on the 9th and 0000UTC on the 10th the circulation centers become vertically aligned (Fig. 5.14e-g) centered around the trough axis.

Shortly after this vertical alignment of the circulation, at 1200UTC on the 10th, the system was declared as a tropical depression. Similar to the evolution of pre-Leslie, although negative moisture anomalies were present around the pre-Nadine trough they remained outside the region of closed circulation. At low levels there was an anomalously moist environment and through sustained convection and vorticity accretion the circulation expanded vertically and horizontally. Although the column was initially tilted to the SW with height, this positioned the jet-level circulation over the relative advection of increased moisture. Shortly after the vortex aligned vertically the tropical depression was recorded.

The pre-genesis trough associated with Hurricane Nadine showed a similar evolution to the trough associated with Hurricane Leslie. Both cases have shown that the initially cold core system is potentially susceptible to the environment. In the two cases here, the environment at low levels was favourable for sustaining convection within the trough. This sustained convection increases the strength of the vortex and associated circulation leading to the development of closed circulation through the lower troposphere. In both cases however the vortex exhibited vertical tilt of the column to the southwest. Due to anomalously moist environment at low levels this may have been beneficial for development. Downdrafts in the south-west quadrant associated with the mid-level dry air, would have had limited impact in the anomalously moist environment outside of the low-level circulation. As both the column aligned vertically and the closed circulation expanded horizontally it is expected that the

troughs then become more resilient to the environment. Shortly after vertical alignment in both cases the systems were declared to be of tropical depression strength and continued to intensify.

5.4.3 2013 Non-Developing Wave AEW33

On August 31st a well developed trough was located over the West African coast. Fig. 5.15 shows that over West Africa the trough was associated consistent convection over the previous 5 days. Similar to the pre-Nadine trough there was substantial coastal convection over the ocean. However within 24 h after leaving the coast the precipitation has reduced and very little signal is present around the trough. The background shading of total precipitable water shows that while the coastal region has moist conditions west of the Cape Verde islands was a region of TPW of less than 30 mm. This dry air extends northwards and is coincident with an upper-level trough to the northwest; matching the non-developing composite shown in chapter 3.

The evolution of the profile of relative vorticity in the column (Fig. 5.16) shows that between 7°W and the coastline, the vorticity throughout the column of the trough intensified, crossing the coast with well developed mid to low-level vorticity. The magnitude of vorticity and moisture within 300 km of the trough center then rapidly declines after leaving the continent. Within 2 days of leaving the coast the trough center has negative moisture anomalies at 700 hPa with deep relative westerly flow. This rapid decline of both moisture and vorticity within the trough is somewhat a result of the 300 km radial average and the horizontal displacement of the jet-level center with respect the low-level vortex.

Instantaneous cross sections reveal more details about the rapid decline in vorticity and moisture. Fig. 5.17a shows the strong vortex over the coastal region at 0000UTC on the 31st. In close proximity to the west of the vortex however, is a low-level region of negative moisture anomalies of around -8 g/kg with trough relative flow towards vortex below 800 hPa. At 1800UTC moisture in the lower levels of the trough has decreased slightly with continued

advection of negative moisture anomalies through the column below 800 hPa (Fig. 5.17b). At this time the vortex is projected onto the cross section as two distinct centers at 650 hPa, with the western center located above the entrained negative moisture anomalies. Following this initial separation of the vortex at the jet-level and interaction with the dry anomaly to the west, the column continues to weaken and the system returns to a jet-level maximum with a cold-core below by 1200UTC September 1st (Fig. 5.17b).

The trough relative streamlines and moisture anomalies for three times during the 36 h demise of the trough are shown in Fig. 5.18. As the trough approached the coast both the low-level and jet-level circulation show a closed region of recirculation (Fig. 5.18c,f). To the west of the low-level circulation was the large region of dry air which was starting to be advected around the south of the circulation. At 600 hPa the top of the dry layer was further away to the north but in a region of relative northwesterlies and therefore being advected towards the circulation. As the trough left the coast a large region of low-level positive moisture anomalies was present to the north of the trough axis (Fig. 5.18e), however these were in the trough relative southwesterlies to the northeast of the vortex being advected away from the circulation. The low-level inflow remained from the west through the region of strong negative moisture anomalies. The circulation at low levels became zonally elongated extending from over the Cape Verde islands back to the coast of West Africa (Fig. 5.18d), while the jet-level circulation remained smaller but centered with the trough axis over the Cape Verde islands (Fig. 5.18a). At both levels the negative moisture anomalies remained on the western boundary of the vortex in the region of inflow into the now open circulation.

The evolution of the circulation centers is shown more thoroughly at 6 h intervals in Fig. 5.19. Within 12 h of leaving the coast the low-level and jet-level closed circulation attain an initial westward tilt with height (Fig. 5.19a-c). During this 12 h period, the low-level vorticity initially ahead of the trough axis aggregates under the trough forming the zonally elongated circulation shown in (Fig. 5.18d). At this time however there were strong negative moisture anomalies to the west and the now open circulation has relative inflow from

this region (Fig. 5.19d). From 1200UTC on the 1st to 0600UTC on the 2nd, the circulation at both levels becomes more axisysmmetric though the column retains a slightly westward tilt with height (Fig. 5.19e-h). The westward tilt of the vortex keeps the jet-level circulation positioned above the strong negative moisture anomalies below and during this time there was little observed precipitation (Fig. 5.15).

Back trajectories reveal that the dry air west of the trough over the eastern Atlantic originates from subsidence of air from both the mid-latitudes and from over West Africa (Fig. 5.20). The 192 h back trajectories were initialised at 0000UTC on the day the trough reached the coastline (30th August). Trajectories were released from grid points with relative humidity less than 40% at 2000 metres above sea level (masl) approximately 800 hPa and 4000 masl (625 hPa). Trajectories initialised at 800 hPa are primarily from mid-latitude sources, subsiding from 500 hPa over the northeastern Atlantic and following the eastern edge of the subtropical ridge south between 700 - 800 hPa (Fig. 5.20). Fig. 5.15 showed that as the trough left West Africa there was a mid-latitude trough to the north at upper levels. These trajectories reveal that the dry air from mid-latitudes moves south into the tropics around 5 days before the trough reached the coast, therefore the direct relationship with the upper-level trough is unclear. Further research and trajectory analysis of the origins and variability of dry air over the eastern Atlantic is needed. These trajectories suggest that not all dry air over the Atlantic is of Saharan origin as was also shown by Braun (2010). The trajectories initialised at 600 hPa are predominantly sourced from West Africa and over the Sahara (Fig. 5.21, these trajectories also subside as they approach the eastern Atlantic, originating from near 400 hPa and descending 200 hPa over the 8 days. The evolution of the parcels initialised at 800 hPa and 625 hPa are similar over the 8 day integration (Figs. 5.22). In general both sets of trajectories subside around 200 hPa over the 192 hours. The low-level trajectories, or trajectories from mid-latitude origin, have a significantly lower moist static energy throughout the integration. Low-level trajectories have a mean MSE of 325 KJ/kg, while the mid-level trajectories have a mean MSE of around 332 KJ/kg (not

shown). Therefore although the dry air is likely a combination of two origins, the lower levels within the dry air has lower moist static energy and is therefore potentially more detrimental when entrained into the convective environment. .

The non-developing trough from 2013 presented here initially had favourable conditions within trough over West Africa but then moved into a hostile environment over the eastern Atlantic. As the vortex evolved the low levels were open to the environment to the west of the trough as also seen in the previous cases. In this case however, that environment had strong negative moisture anomalies. A westward tilt with height positioned the jet-level circulation over this low-level region of dry air. During this time convection ceased and the vortex became less symmetric horizontally and misaligned vertically. Although the vortex appears to align vertically and become develop a closed circulation around 72 h after leaving the coast, at this point the vortex has weakened and the moisture in the column has reduced.

5.4.4 2014 Non-Developing Wave AEW40

The non-developing wave in 2014 left West Africa on September 4th and was initially forecast at 50% genesis probability by NHC. The wave had intersected with a convectively active phase of a Kelvin wave over Central Africa and a weak suppressed phase of the Kelvin wave was present as the trough left the West African coast (Fig. 5.6). Accumulated precipitation along the track shows increased precipitation around 0° and again once the trough approached the Guinea Highlands and coastline. However once over the ocean there was only a narrow track of precipitation associated with the trough. The background moisture field for the day the trough left the coast resembles a similar structure to the previously discussed non-developing AEW in 2013, with a region of low TPW over the eastern Atlantic ahead of the AEW trough. As in the previous non-developing case an upper-level trough is present over the north-eastern Atlantic although this is weaker and further north that shown for the other non-developing wave. The presence of this upper-level trough and dry eastern Atlantic again matches the composite results in chapter 3.

The evolution of the relative vorticity profile shows that over West Africa, this trough was stronger around the jet-level than the previous 3 troughs analysed (Fig. 5.27). After leaving the coast however the vortex gradually weakened. Over Africa the trough relative winds shows strong low-level westerly flow through the low levels of the vortex however once over the ocean the low-level relative flow is below 1 m/s and thus not shown. The instantaneous cross sections show a large region of negative moisture anomalies ahead of the trough as it crosses the coast and eastern Atlantic (Fig. 5.25). At 1800UTC on the 4th the cross section shows the low-level dry air encroaching on the lower levels of the vortex however the trough relative winds are negligible and notable inflow in the cross section isn't evident(Fig. 5.25a). By 1200UTC on the 5th the positive moisture anomalies haven't decreased and the vortex retains its strength (Fig. 5.25b). The trough however is still cold-core in the lower levels with the vortex maximum around 700 hPa. As the trough approaches 30°W, 36 h after leaving the coast, the vortex has weakened slightly and still retains its low-level cold-core (Fig. 5.25c). While the cross-sections haven't shown relative inflow of the negative moisture anomalies to the west, there also wasn't relative easterlies to advect the dry air away from the trough. Therefore there is now a strong gradient of moisture along the western edge of the trough.

This trough had a well developed closed circulation at 600 hPa and 800 hPa after leaving the continent (Fig 5.26c,f) but had dry air to the west at low levels and to the west and east at 600 hPa. Due to the meridional extent of the jet-level circulation, the southern extent of the closed circulation is exposed to the relative westerly advection of negative moisture anomalies below (Fig 5.26b,e). By 1200UTC on the 6th (Fig 5.26a,d) although at low levels the negative anomalies have been mostly keep outside of the circulation to the west, the jet-level circulation has weakened and has persistently has at least a region aligned over the negative anomalies below.

Figure 5.27 shows the evolution of the circulation at two levels more clearly. As the trough leaves the coast, the initially open low-level circulation quickly develops a region of

closed streamline (Fig. 5.27a-c). Though even as this develops the two levels are already offset vertically. During September 5th, most of the jet-level circulation is situated south of the low-level center and positioned over the relative westerly advection of negative moisture anomalies shown previously (Fig. 5.27e-h). The magnitude of low-level vorticity during this time, although rather axisymmetric and colocated with the circulation, doesn't increase through this period due to the lack of sustained convection..

On September 5th the NASA hurricane and severe storm sentinel field program (HS3) was observing this system, (declared as invest AL90 by the NHC). Figure 5.28 shows the 850 hPa anomalous specific humidity and trough relative streamlines at 850 hPa and 700 hPa, with the locations of the dropsondes deployed. The initial transect from the northwest to southeast spanned approximately 1700 to 2100UTC (drop numbers 5 to 14). The cross section along this transect (Fig. 5.29) shows the dry low-level air being entrained underneath the jet-level circulation. At the right of the image (southeast corner of the transect) the moisture associated with the trough is evident from the boundary layer up to 550 hPa. At 600 hPa this moisture extends to the northwest over the lower layer of dry air. The overlayed vertical lines on Fig. 5.29 show the layers of aerosol along the transect detected by the CPL onboard the global hawk. In the dry air there is a lack of any detected aerosol layers suggested this was clear dry air and not the typical dusty air associated with the SAL. Imagery from MODIS on the same day confirms this lack of aerosol ahead of the trough, SAL outbreaks are typically associated with large areas of AOD values greater than 0.5 (Fig. 5.30).

Although both levels appear closed and direct entrainment isn't obvious as in the non-developing wave form 2013, the presence of dry negative anomalies below the jet-level circulation could still have detrimental impacts on the trough. If convection occurred in the region of overlap between jet-level circulation and low-level negative anomalies it would have to fall through the very dry lower levels. Evaporative cooling as the precipitation falls through this layer would strongly increase the likelihood of convective downdrafts in this region. Therefore rather than the needed diabatic heating and associated vorticity spin-

up, these troughs likely cooling the lower levels and flooding the boundary layer with low potential temperature by downdrafts. Further detailed analysis of this case, likely through numerical simulations, would be required to define the physical interaction between the convection and the vortex.

To evaluate the origin of the dry air ahead of the trough backward trajectories were initialised in the region west of the trough, at grid points with less than 50% relative humidity at 1500 masl (825 hPa) and 3000 masl (700 hPa), targeting the center and upper vertical limit of the main dry region. The 192 h back trajectories initialised at 825 hPa are shown in Fig. 5.31, over this integration time the low-level dry air remained over the tropical Atlantic. Trajectories shows that the air subsided over the eastern Atlantic from around 600 hPa (Fig. 5.32b). Once the trajectories were around 800 hPa, north of the Cape Verde islands, the air was advected south into the area ahead of the analysed non-developing trough. Dry air at higher elevations however shows a different route over the 192 h integration. Trajectories initialised at near 700 hPa almost exclusively originate from over West Africa and the Sahara (Fig. 5.33). These trajectories originate from low levels over the Sahara and are lifted as they leave the continent, then approaching the trough from around 700 hPa (Fig. 5.32a). While these trajectories show that the jet-level dry air was of Saharan origin, the CPL observations show that it was not the typical dusty SAL outbreak. The trajectories released from 700 hPa with Saharan origin represent the jet-level dry air that approaches from the north and east and has to wrap all the way round the closed circulation that was shown in chapter 4. The almost in-situ subsidence of the dry air over the Atlantic and then reaching the lower levels of the trough was not fully captured in the composite trajectory analysis in chapter 4, however a similar anticyclonic subsiding pattern was shown in Fig. 4.5c-f.

The non-developing wave analysed in 2014 showed a more gradual weakening of the vortex in time than compared to the non-developing wave in 2013. The strength of the vortex and the quick development of a closed circulation through the lower troposphere after leaving the continent likely helped the trough maintain its integrity. Due to the west and southwest

vertical tilt of the circulation though, the jet level closed circulation was consistently located over the trough relative westerly advection of negative moisture anomalies below. The causal impact of this is hypothesised to be through the occurrence of downdrafts being enhanced by the low-level layer of low equivalent potential temperature air (e.g Bister and Emanuel 1997). Fundamentally without the presence of continued deep convection the vortex is not able to intensify and gradually decays due to the vertical shear and horizontal deformation in the region.

5.5 Discussion and Conclusions

Three years of AEWs were reviewed including analysis of the influence of Kelvin and MJO filtered OLR anomalies. Throughout 2012, 2013 and 2014 around 50 AEWs were observed leaving the coast of Africa each year during July to October. Despite this consistency in the total number of waves, the three years had very contrasting behaviour with respect to tropical cyclogenesis over the MDR and eastern Atlantic.

During August and September 2012, 8 of 15 waves were classed as favourable for genesis. The genesis cases were however largely restricted to late August and early September, where 5 out of 6 consecutive AEWs developed over the eastern Atlantic. These genesis cases came from both marginal and favourable waves. During this period of enhanced TC genesis, multiple active Kelvin waves and a weak enhanced MJO signal were present over the Atlantic basin likely modulating convection within the AEW troughs. In 2013, similar to 2012, 8 of 16 waves were classed as favourable for development, however only 2 troughs were objectively tracked to genesis events. Only 1 of these was linked to a favourable wave. Weak equatorial wave signals crossed the basin but clear links with the waves or lack of genesis wasn't obvious. In 2014 only 4 of the 18 waves during August and September were characterised as favourable for development and these 4 did not develop. These seasonal and equatorial wave impacts of the genesis of AEWs reveal a potential weakness of the current logistic regression model to characterise the waves. Interaction with the eastward propagating equatorial waves can

influence the convective and dynamic structure (e.g. Aiyyer and Molinari 2008; Ventrice et al. 2012b; Schreck and Molinari 2011), likely modifying the structure of the trough and its genesis potential. For a prognostic statistical model of genesis from AEWs it may therefore be beneficial to include downstream equatorial wave signals, though the statistical impact of this would require further research.

Four cases were selected from the three years to document both developing and non-developing waves in the presence of negative moisture anomalies to their west and northwest. All four cases had dry air to the west of the trough at 600 hPa but had different profiles of moisture in the lower troposphere. The two developing cases, from 2012, had anomalously dry air between 700 and 500 hPa west of the trough, below this however was anomalously moist air extending from the surface up to around 800 hPa. In agreement with the previous chapters in this thesis, these two cases entrained lower troposphere environmental air from NW of the trough below the jet-level circulation. This low-level environment was anomalously moist and deep convection within the trough was sustained helping to develop a stronger and vertically aligned vortex within the trough. Conversely the two non-developing cases had dry air throughout the lower troposphere and the entrainment of this air is assumed to be a causal mechanism for the lack of sustained deep convection. The low-level vortex within the wave does not develop without the deep convection and succumbs to deformation due to the horizontal shear.

Trough relative streamline analysis has shown that in all four cases, when the trough initially leaves the West African coast the associated circulation is usually weak at low levels without a clear a region of recirculation. Despite the intensification, even in the developing cases, the circulation below the AEJ is initially open and takes around 48-72 h to develop and reach a comparable size to that of the jet-level circulation. This downward development of the closed circulation was observed in the composite results of chapter 4. All four cases also exhibit a vertical tilt in the circulation centers. The magnitude of the tilt varies with each case, but there is a consistent southwest tilt with height evident when the troughs

first leave the coast. This tilt in the vertical can be explained by the easterly vertical shear over the region, acting to initially tilt the vortex to the west. As the vortex begins to tilt the upper-level and low-level centers begin to rotate cyclonically around the jet-level center (Jones 1995). Given the resolution of the data, it is not possible to evaluate the nature by which the intensifying storms become vertically aligned (e.g. DeMaria 1996; Frank and Ritchie 1999; Jones 2004). Due to the weakness of the AEW troughs as they leave the West African coast, it is expected that the vortices will not be resilient to shear by dry dynamics (Reasor et al. 2004) and will require the additional effects of diabatic processes to aid in the alignment (Davis et al. 2008).

Dry air over the eastern Atlantic was present in the midlevels in all 4 cases analysed here. In the 2 developing cases the the mid-level dry air was undercut by a layer of moist oceanic air. Whereas, in the 2 non-developing cases the dry air extended throughout the lower troposphere and the moist boundary layer was restricted to a shallow layer below 900 hPa. Dry tropical air has been attributed to origins from the Sahara in numerous papers showing the detrimental impacts on tropical storm strength or genesis (e.g. Shu and Wu 2009; Sun et al. 2008; Reale et al. 2009; Dunion and Velden 2004). Analysis of the vertical structure has shown that the SAL generally rises and as it leaves West Africa with a base around 1 km over the eastern Atlantic. As the dry air propagates west over the Atlantic it gradually subsides and mixes vertically (Huang et al. 2010). Trajectory analysis here suggests that the lower layers of dry air over the eastern Atlantic are not of SAL origin within the back trajectories 192 h integration. The low-level dry air in both non-developing cases originated from subsidence over the eastern Atlantic, originally from either the tropical Atlantic or mid-latitude origins. The trajectory analysis highlights the multiples sources and vertical layers to the dry air over the eastern Atlantic and that previous analysis using vertical moisture gradients as a delineation for the base of the sal may have overlooked this. Carlson and Prospero (1972) noted this presence of low-level dry air under the dust laden Saharan outbreaks, originating from northern latitudes. Whether the origin of the dry air

is important is a further question that has not been addressed here. Further research into the vertical structure of dry air over the eastern Atlantic would benefit in understanding the origin, frequency and impact of these very low-level regions of dry air.

Fundamentally the analysis here confirms the hypothesis, that as AEWs leave the West African coast, they are especially sensitive to the environment to the northwest at elevations below the jet-level vortex maximum. Given a favourable (moist) low-level environment, advection of positive moisture anomalies into the low levels may aid in offsetting the other detrimental impacts felt by the trough through enhanced or sustained deep convection. Trajectories that originated from the Sahara were initialised at levels near the vortex maxima and thus at the level where recirculation was most robust and where the trough was most protected from the environment. Low-level dry air however is entrained under the jet-level vortex either through a misalignment of the circulation centers or due to the weaker vortex in the lower troposphere. As the vortex strengthens and extends through the lower troposphere the positive or negative impacts of the environment are likely to be reduced. In a region of low-level westerly storm-relative flow the main source region of entrained environmental air has been shown to be from the NW, in agreement with the simple kinematic results of Riemer and Montgomery (2011). Therefore when the AEW troughs leave the coast they are typically open to the environment to the northwest. Even as the vorticity in the trough intensifies, the trough relative low-level westerly flow and shallow easterly shear mean that the vortex remains open to the environment in the NW quadrant. During this period of sensitivity we hypothesis that the troughs can be subject to either a positive or negative feedback loop. If the environment to the NW is anomalously moist and thus advects high moist static energy into the trough, deep convection is more likely to be sustained. The sustained deep convection will increase the vorticity in the trough and thus increase the systems resiliency to the environment (Reasor et al. 2004). If the environment is unfavourable for TC genesis, with anomalously dry or low moist static energy, the environmental entrainment will reduce convection. Once over the ocean and without deep convection the vortex is unable to resist

the vertical shear, succumbing to deformation by the horizontal shear. The weakening vortex then makes the system more susceptible to the environment and thus the cycle continues.

5.6 Figures

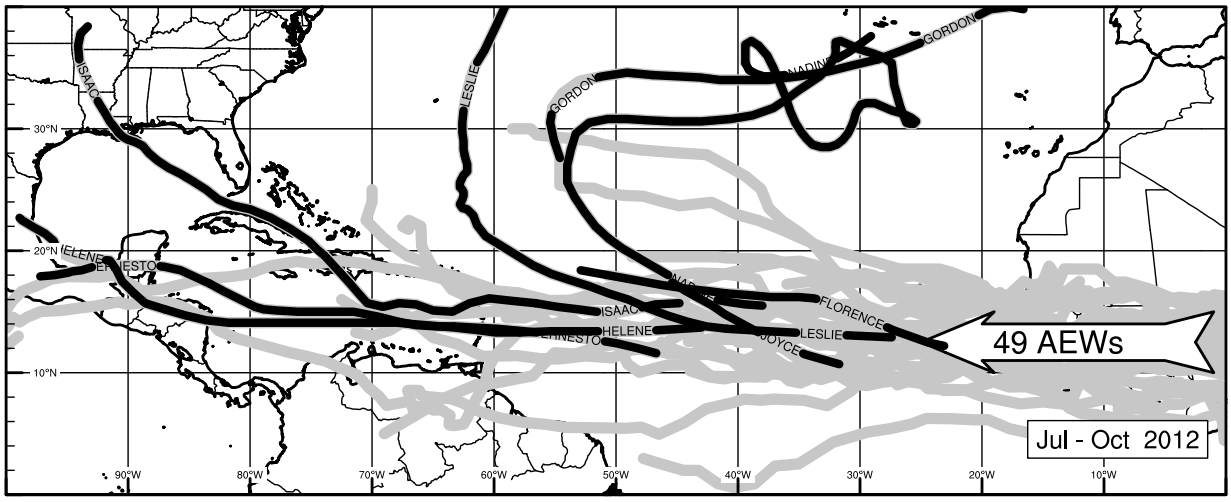

Figure 5.1: Tracks of all AEWs crossing 20°W during July-October 2012. Gray lines represent waves. Black tracks show official Tropical Depression or stronger that was objectively associated with an AEW track. Arrow displays the total count of AEWs leaving Africa during JJASO for the year.

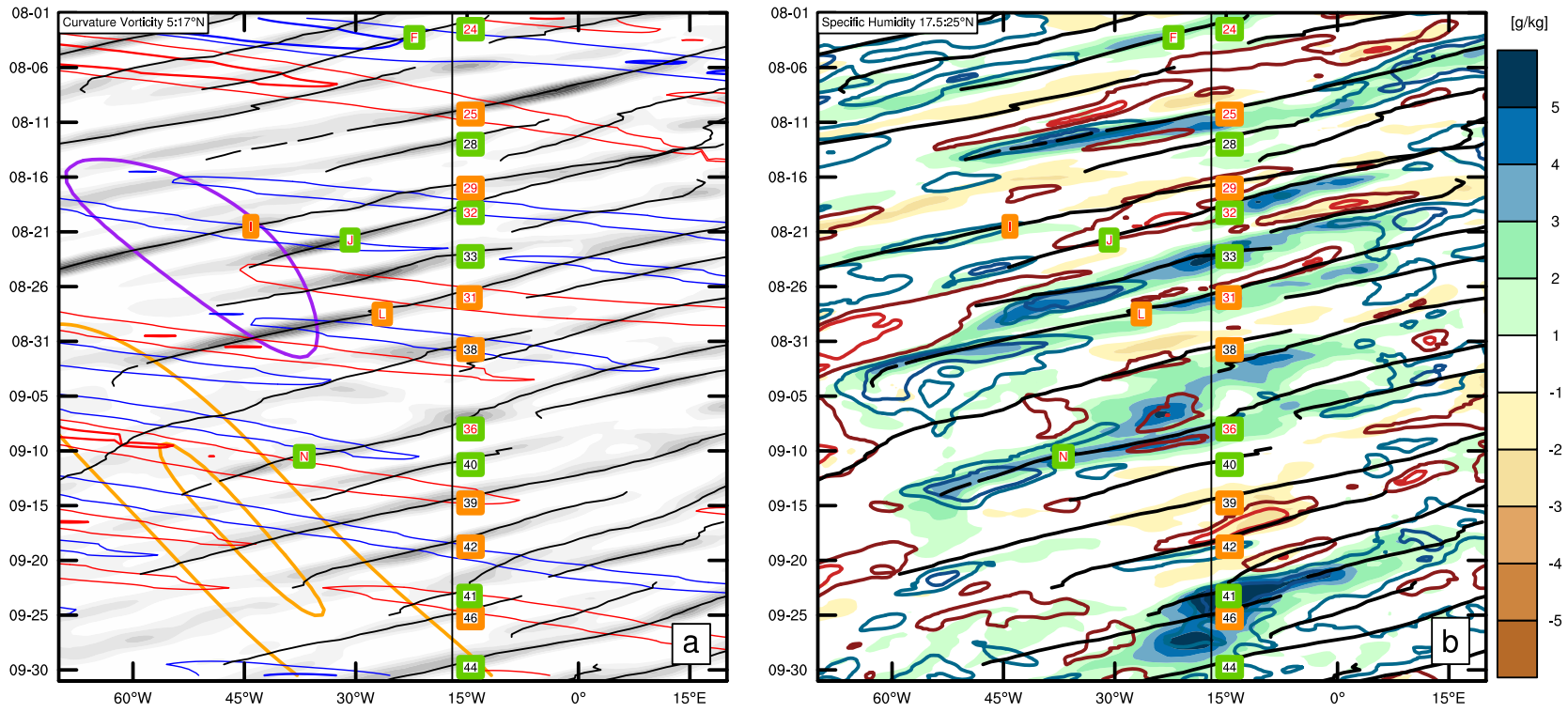

Figure 5.2: Hovmöllers covering August and September 2012. Left: Grayscale shading depicts 2-10 day filtered curvature vorticty averaged over 5:17°N. Objective tracks are overlayed. Tracks are shown as sold when south of 20°N and dashed south of 25°N. Red (blue) contours shows positive (negative) Kelvin Filtered OLR anomalies indicating suppressed (active) convection. Orange (purple) contours show positive (negative) MJO filtered OLR anomalies indication. Boxes at coast display the arbitrary identification number assigned to each wave. Red numbers indicate the wave was associated with genesis downstream. Red/orange/green perimeter to the box indicates the tercile of favourability the wave was characterised as by the logistic regression model. Red indicates unfavourable conditions for genesis, orange moderate favourability, green favourable. Right: Shading (contours) shows anomalous specific humidity averaged over 17.5° to 22.5°N for 850 hPa (600 hPa). Line intervals are at 1g/kg. Red (Blue) contours indicate negative (positive) anomalies.

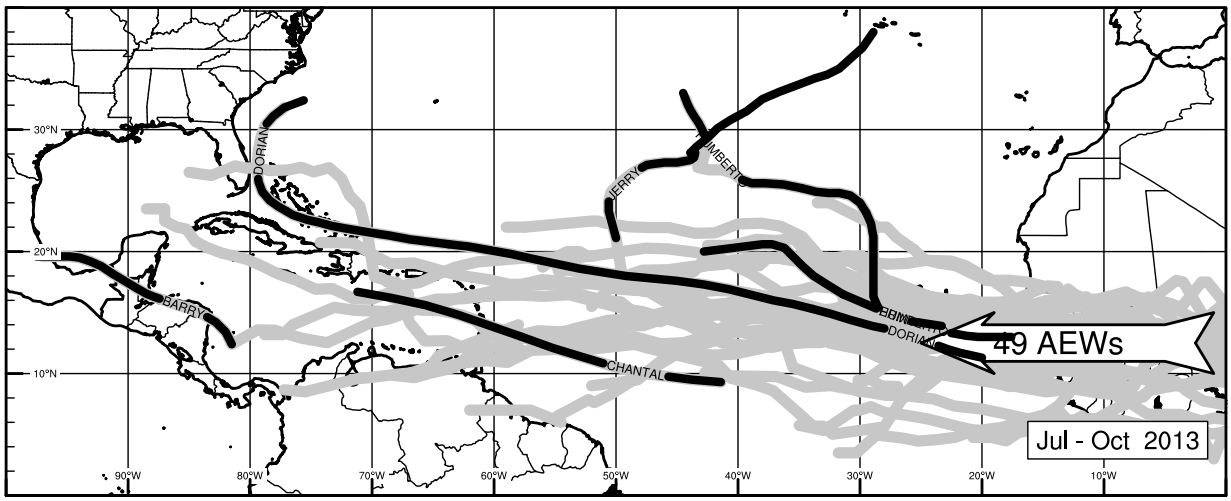

Figure 5.3: Tracks of all AEWs crossing 20°W during July-October 2013. Gray lines represent waves. Black tracks show official Tropical Depression or stronger that was objectively associated with an AEW track. Arrow displays the total count of AEWs leaving Africa during JJASO for the year.

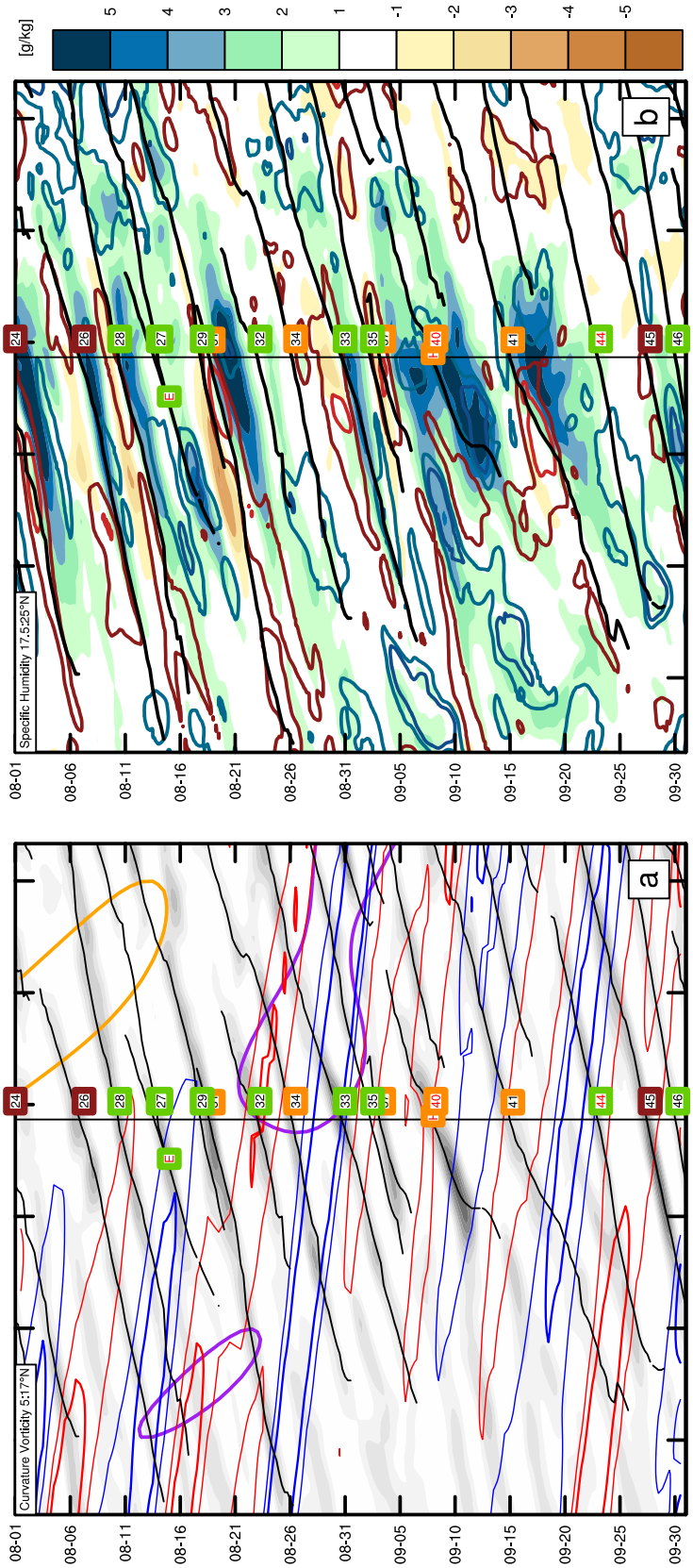

Figure 5.4: As Fig. 5.2 for August September 2013.

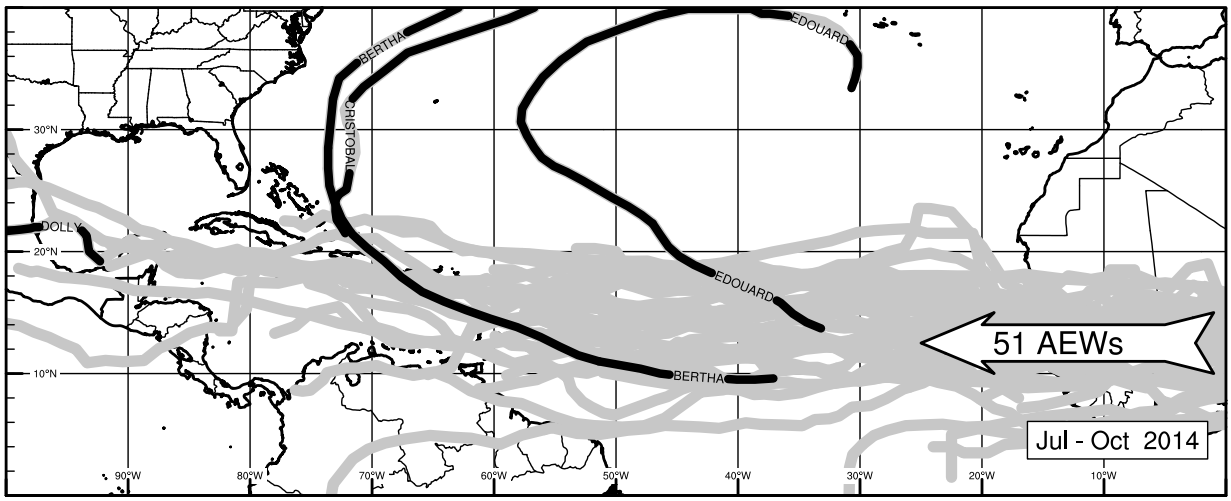

Figure 5.5: Tracks of all AEWs crossing 20°W during July-October 2014. Gray lines represent waves. Black tracks show official Tropical Depression or stronger that was objectively associated with an AEW track. Arrow displays the total count of AEWs leaving Africa during JJASO for the year.

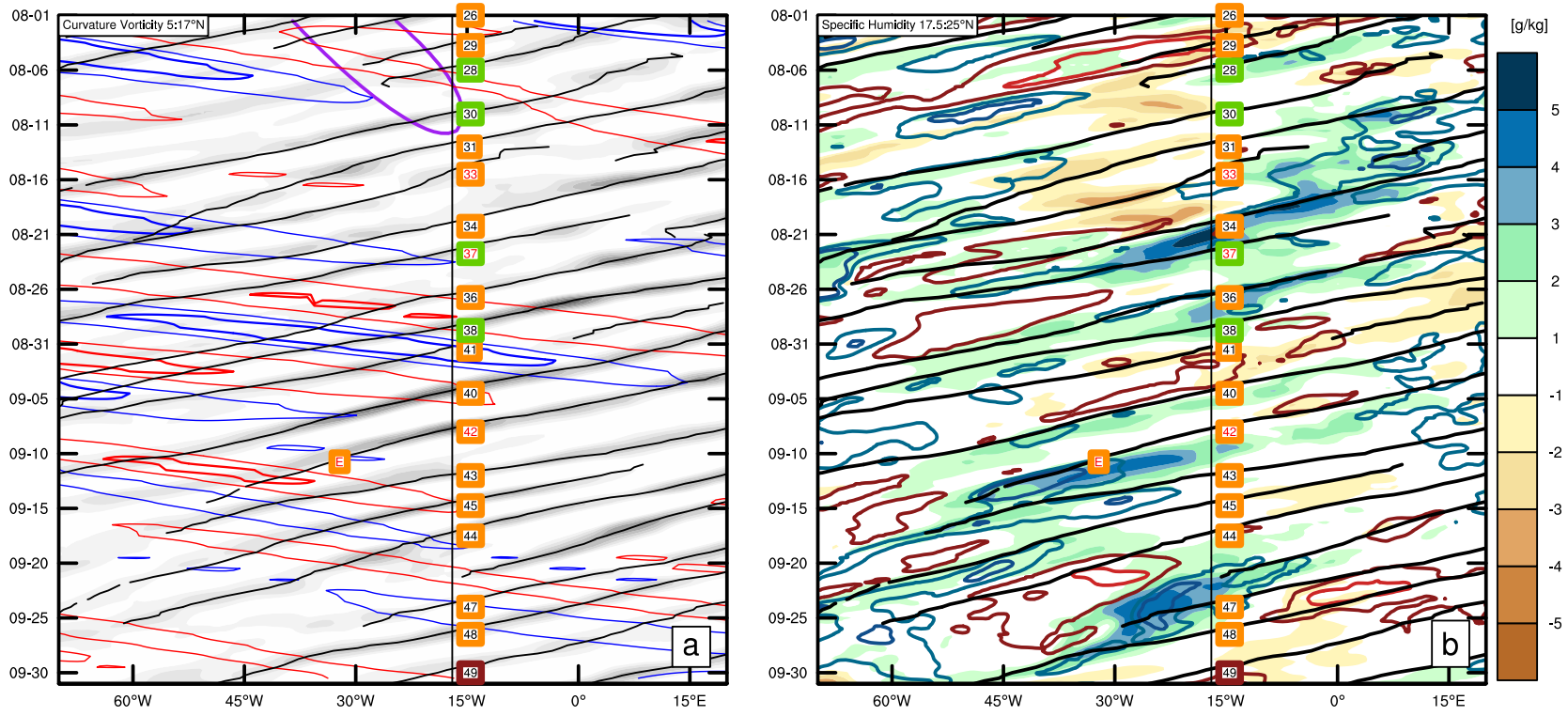

Figure 5.6: As Fig. 5.2 for August September 2014.

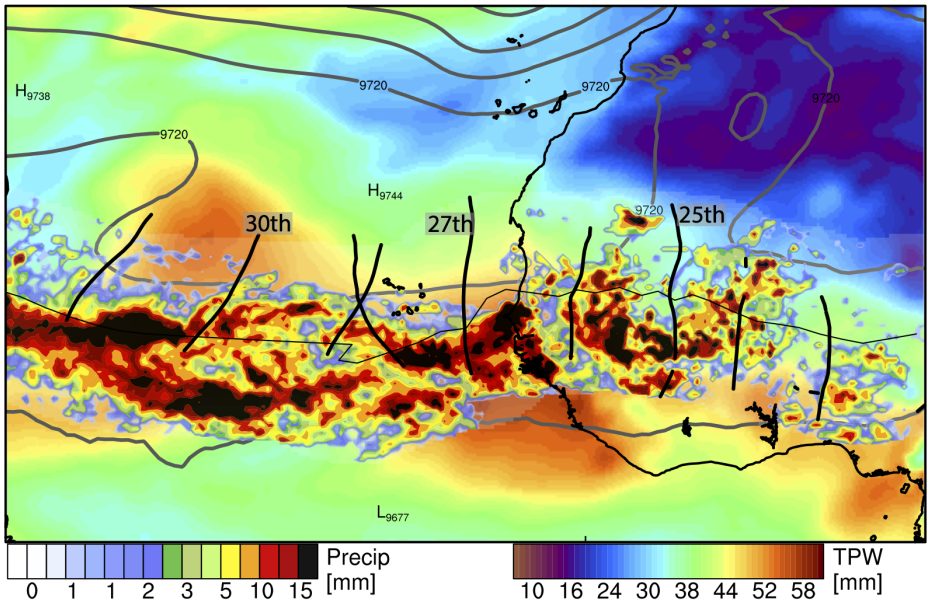

Figure 5.7: Evolution of AEW associated with genesis of Hurricane Leslie (2012). Accumulated precipitation within 750 km of trough center along track at 3 h intervals. Objective trough lines plotted at 24 h intervals with 6 h track of vortex center also shown. Shading and contours show the 36 h mean total precipitable water and 300 hPa geopotential height, respectively. Temporal averages are centered on the time the trough axis crosses the coast line.

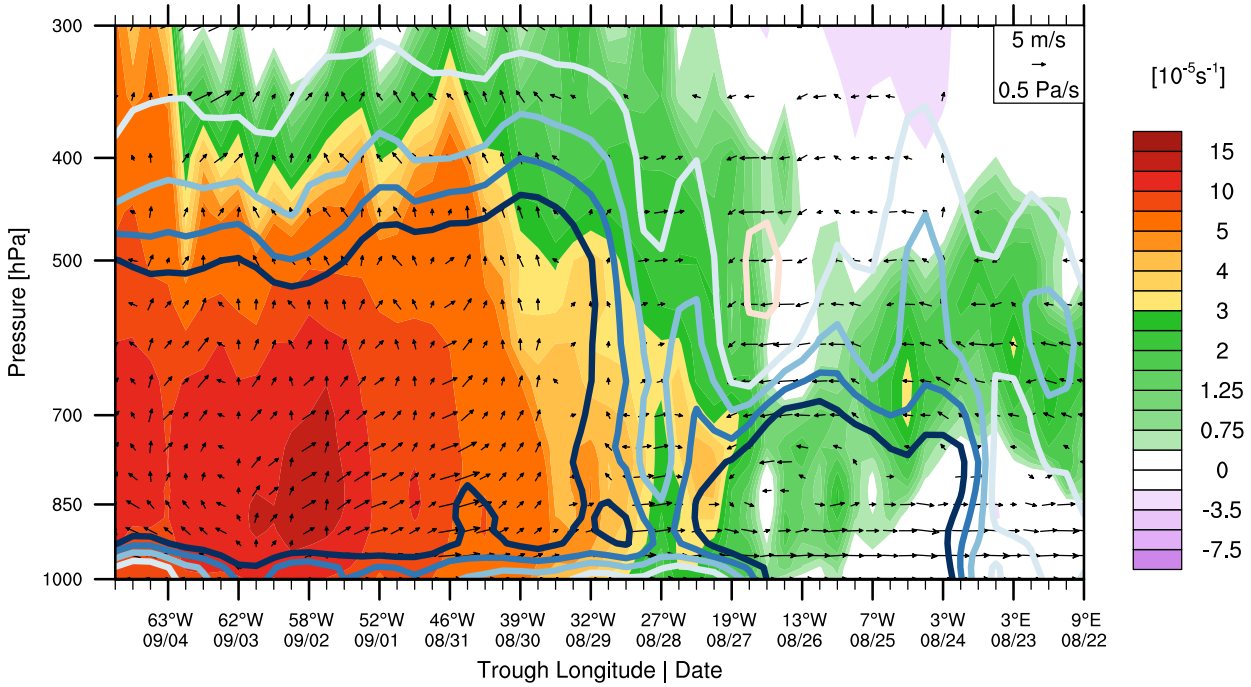

Figure 5.8: Vertical evolution of trough centric (300 km radius circular average) relative vorticity (shading) and anomalous specific humidity (contours) for pre-Leslie in 2012. Contours at 1g/kg intervals, red (blue) indicate negative (positive) anomalies. Zero contour is not shown. Wind vectors display trough relative zonal wind and vertical wind. X-axis represents the time (or longitudinal) evolution of the trough.

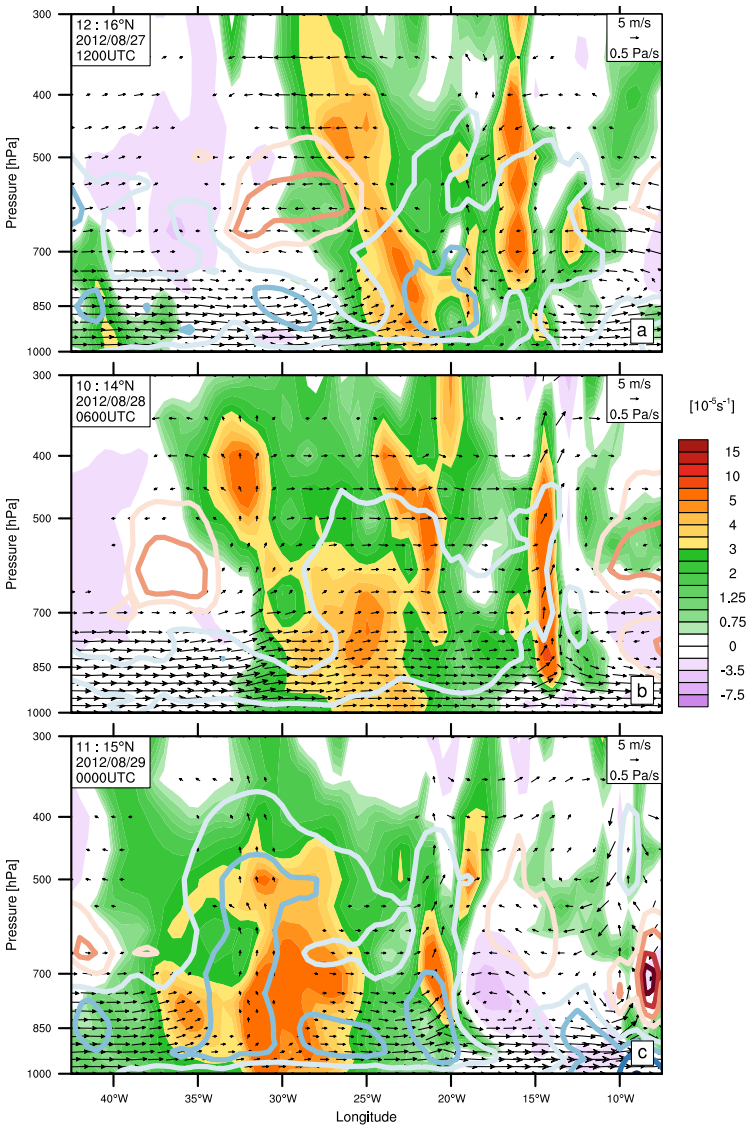

Figure 5.9: Relative vorticity (shading) and anomalous specific humidity (contours). Contours at 2g/kg intervals, red (blue) indicate negative (positive) anomalies for pre-Leslie in 2012. Zero contour is not shown. Wind vectors display trough relative zonal wind and vertical wind. Panels show instantaneous fields at 18 hour intervals. Meridionally averaged over 4°N centered on the trough latitude.

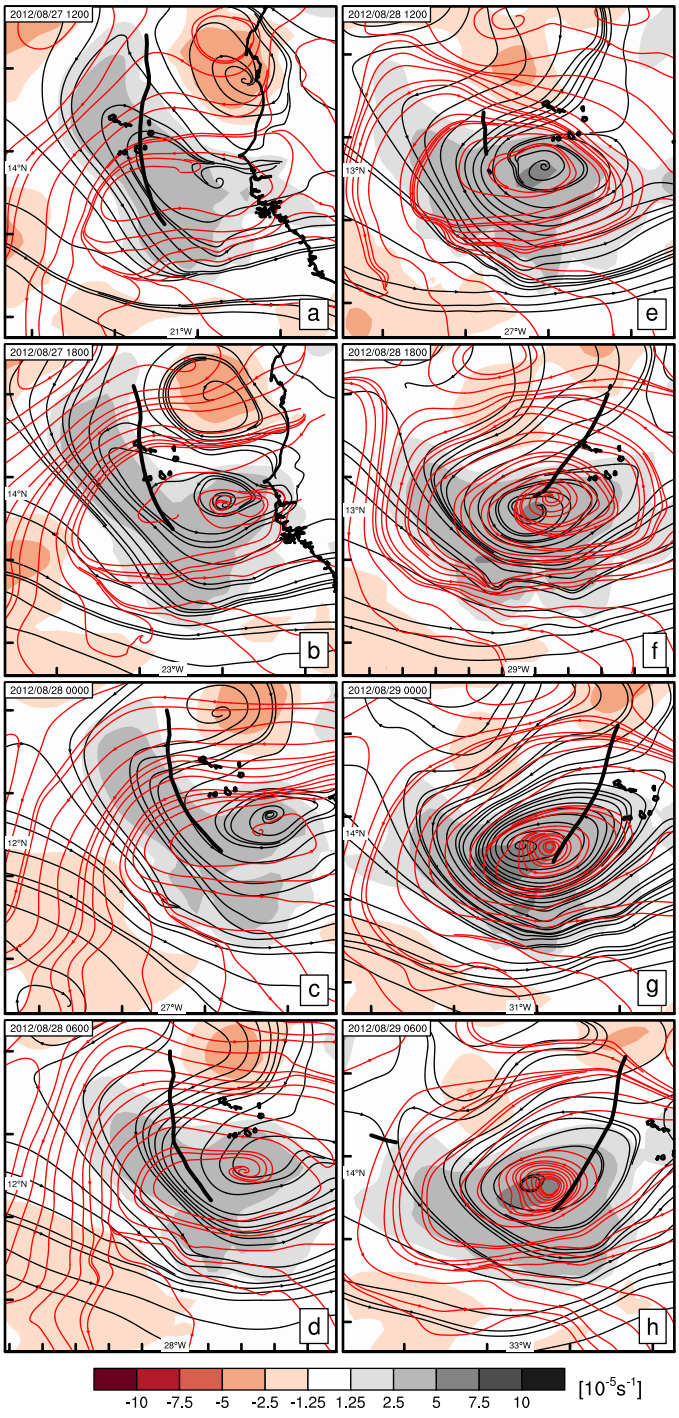

Figure 5.10: Evolution of pre-Leslie in 2012 at 6 hour intervals. Shading shows Relative vorticity at 850 hPa. Black (red) streamlines represent the wave relative flow at 850 hPa (600 hPa). Thick black contours indicates the AEW trough axis at 700 hPa.

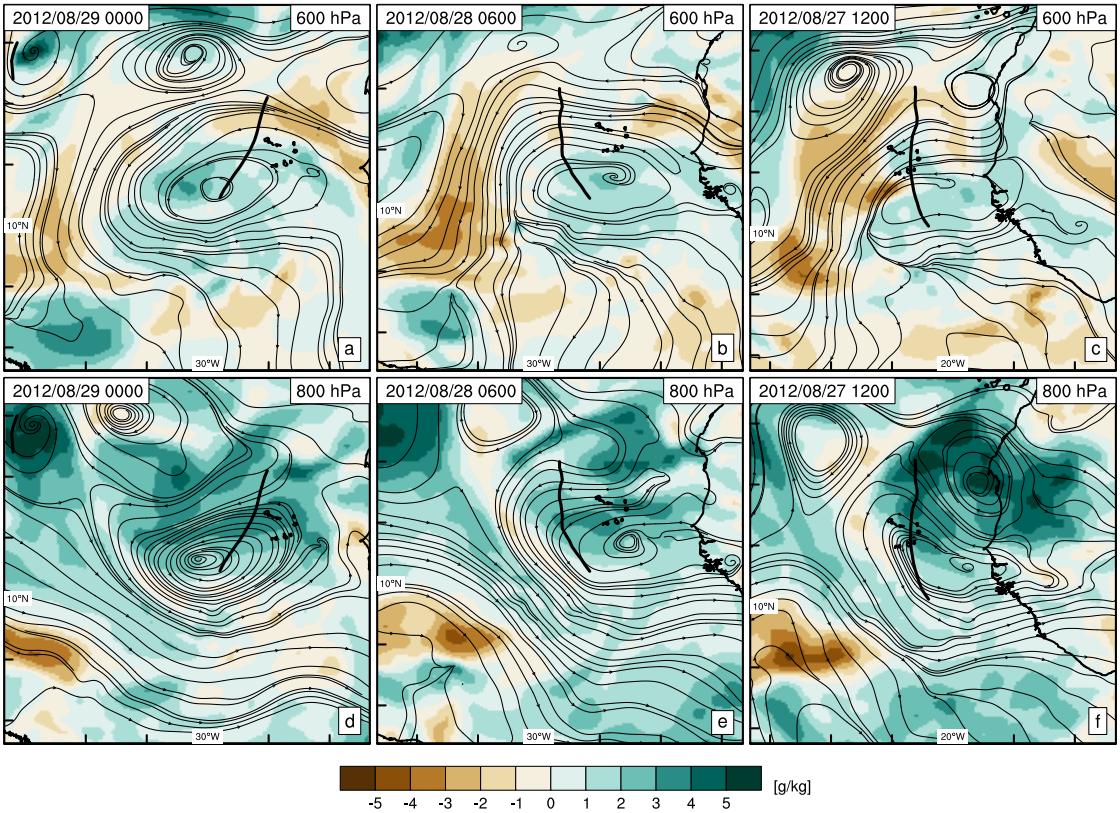

Figure 5.11: Evolution of pre-Leslie in 2012 at 18 hour intervals. Shading shows anomalous specific humidity (g/kg), streamlines show the trough relative flow for the corresponding level. Top row shows 600 hPa variables, bottom row shows 800 hPa variables. Rows are organised right to left in 18 h intervals. Times correspond to those plotted in Fig. 5.9. Thick black contour shows the trough axes at 700 hPa.

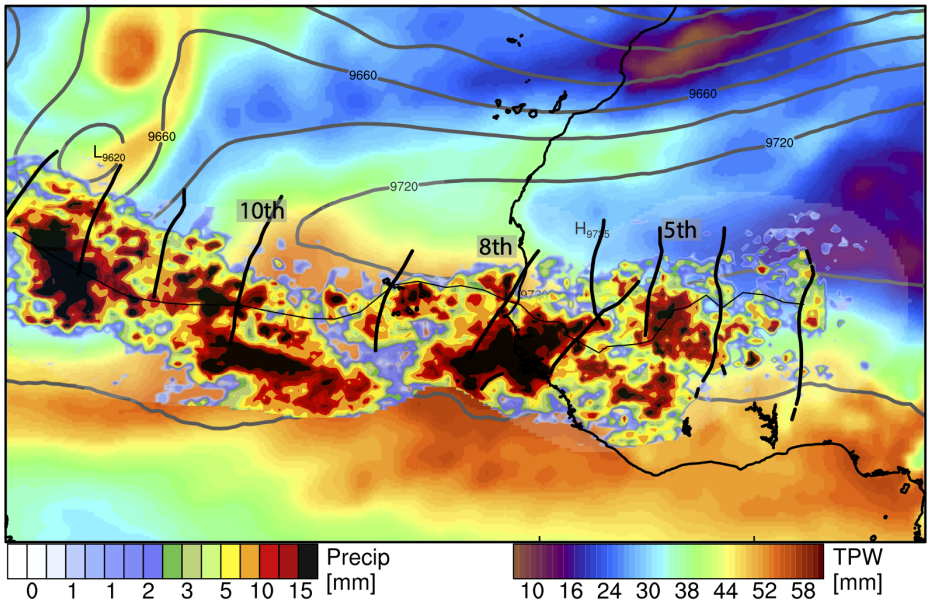

Figure 5.12: Evolution of AEW associated with genesis of Hurricane Nadine (2012). Accumulated precipitation within 750 km of trough center along track at 3 h intervals. Objective trough lines plotted at 24 h intervals with 6 h track of vortex center also shown. Shading and contours show the 36 h mean total precipitable water and 300 hPa geopotential height, respectively. Temporal averages are centered on the time the trough axis crosses the coast line.

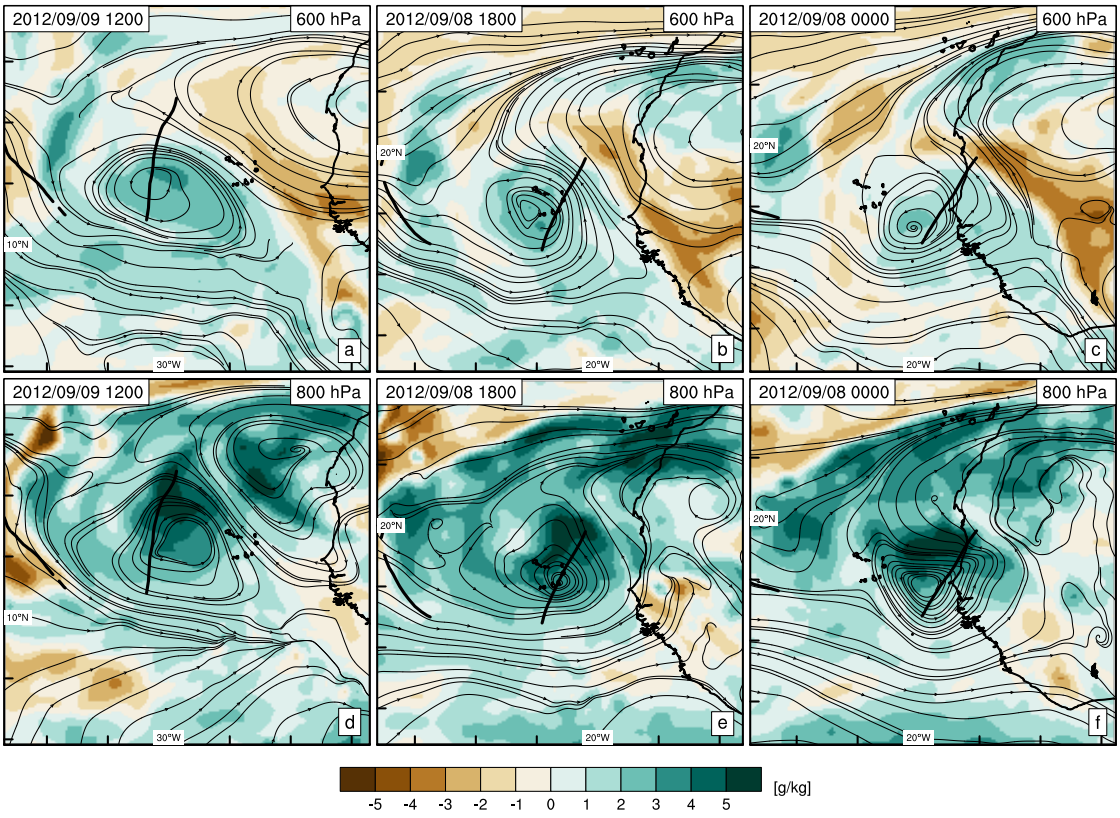

Figure 5.13: Evolution of pre-Nadine in 2012 at 18 hour intervals. Shading shows anomalous specific humidity (g/kg), streamlines show the trough relative flow for the corresponding level. Top row shows 600 hPa variables, bottom row shows 800 hPa variables. Rows are organised right to left in 18 h intervals. Thick black contour shows the trough axes at 700 hPa.

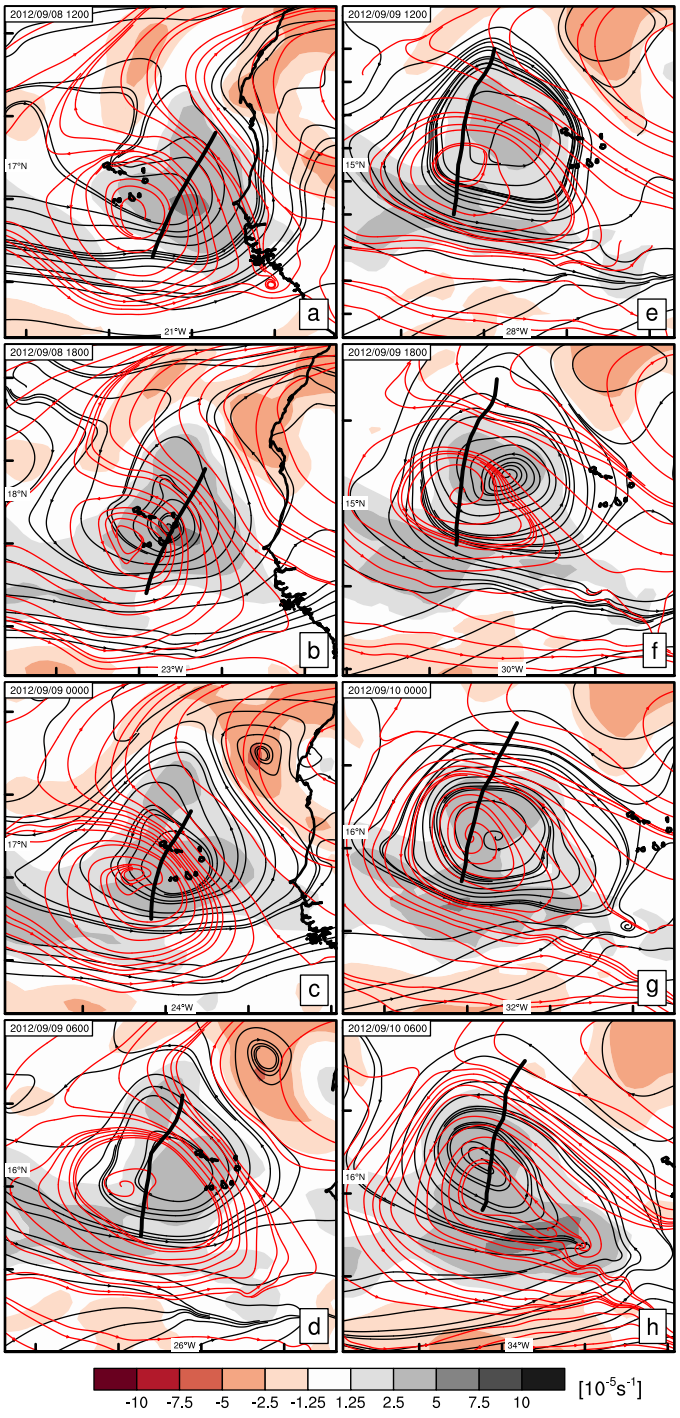

Figure 5.14: Evolution of pre-Nadine in 2012 at 6 hour intervals. Shading shows Relative vorticity at 850 hPa. Black (red) streamlines represent the wave relative flow at 850 hPa (600 hPa). Thick black contours indicatesAEW trough axis at 700 hPa.

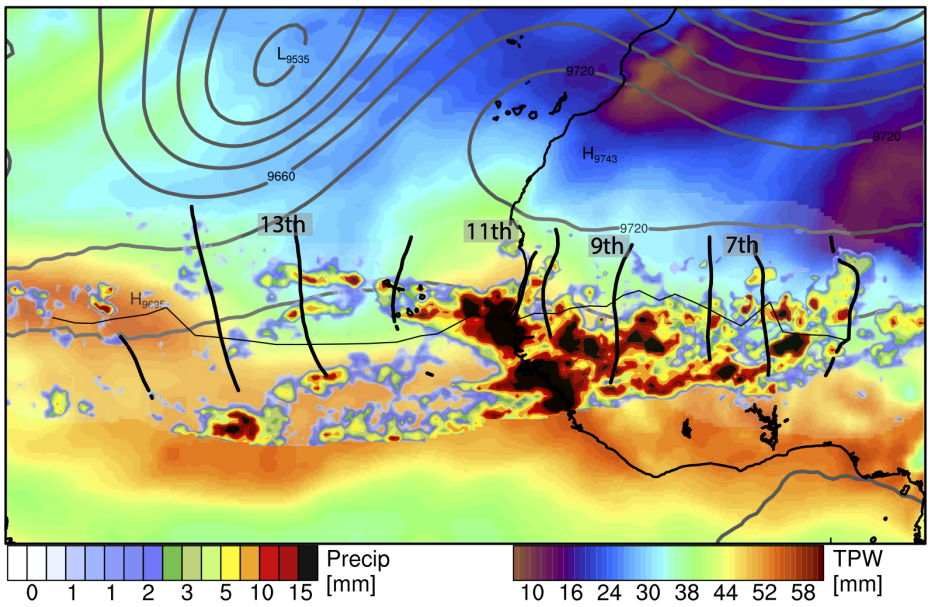

Figure 5.15: Evolution of a non-developing AEW in 2013. Accumulated precipitation within 750 km of trough center along track at 3 h intervals. Objective trough lines plotted at 24 h intervals with 6 h track of vortex center also shown. Shading and contours show the 36 h mean total precipitable water and 300 hPa geopotential height, respectively. Temporal averages are centered on the time the trough axis crosses the coast line.

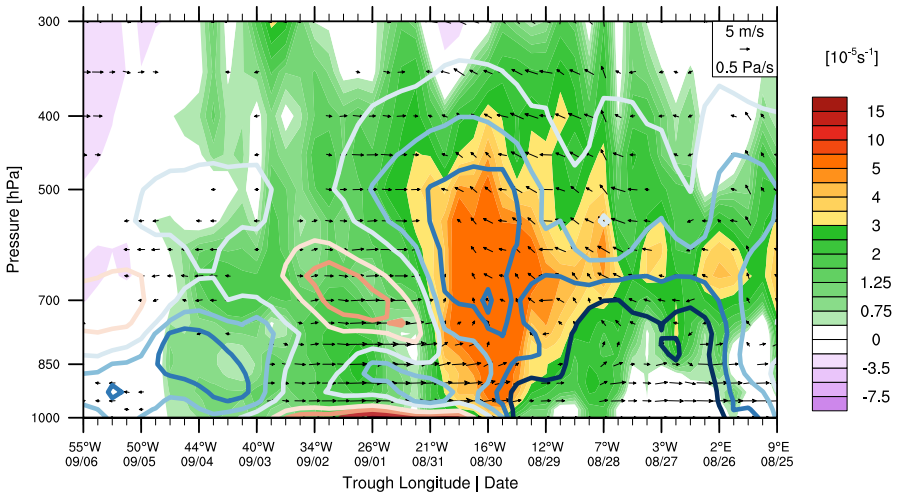

Figure 5.16: Vertical evolution of trough centric (300 km radius circular average) relative vorticity (shading) and anomalous specific humidity (contours). Contours at 1g/kg intervals, red (blue) indicate negative (positive) anomalies. Zero contour is not shown. Wind vectors display trough relative zonal wind and vertical wind. X-axis represents the time (or longitudinal) evolution of the trough.

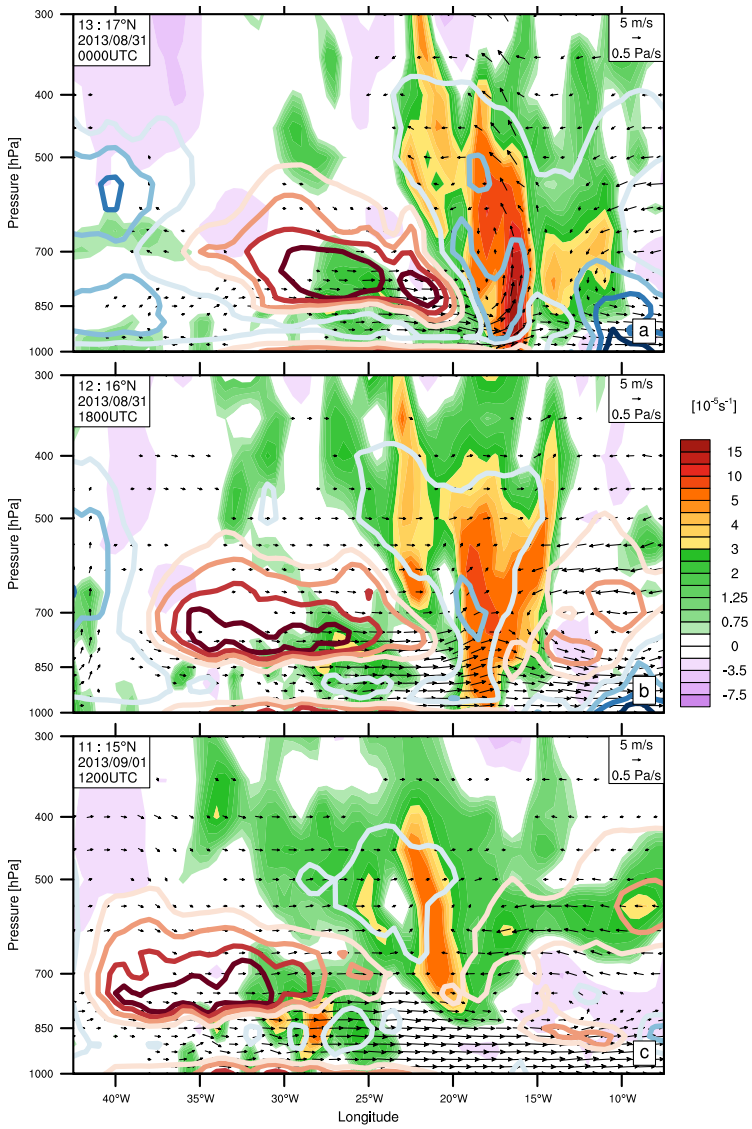

Figure 5.17: Relative vorticity (shading) and anomalous specific humidity (contours). Contours at 2g/kg intervals, red (blue) indicate negative (positive) anomalies. Zero contour is not shown. Wind vectors display trough relative zonal wind and vertical wind. Panels show instantaneous fields at 18 hour intervals. Meridionally averaged over 4° centered on the trough latitude.

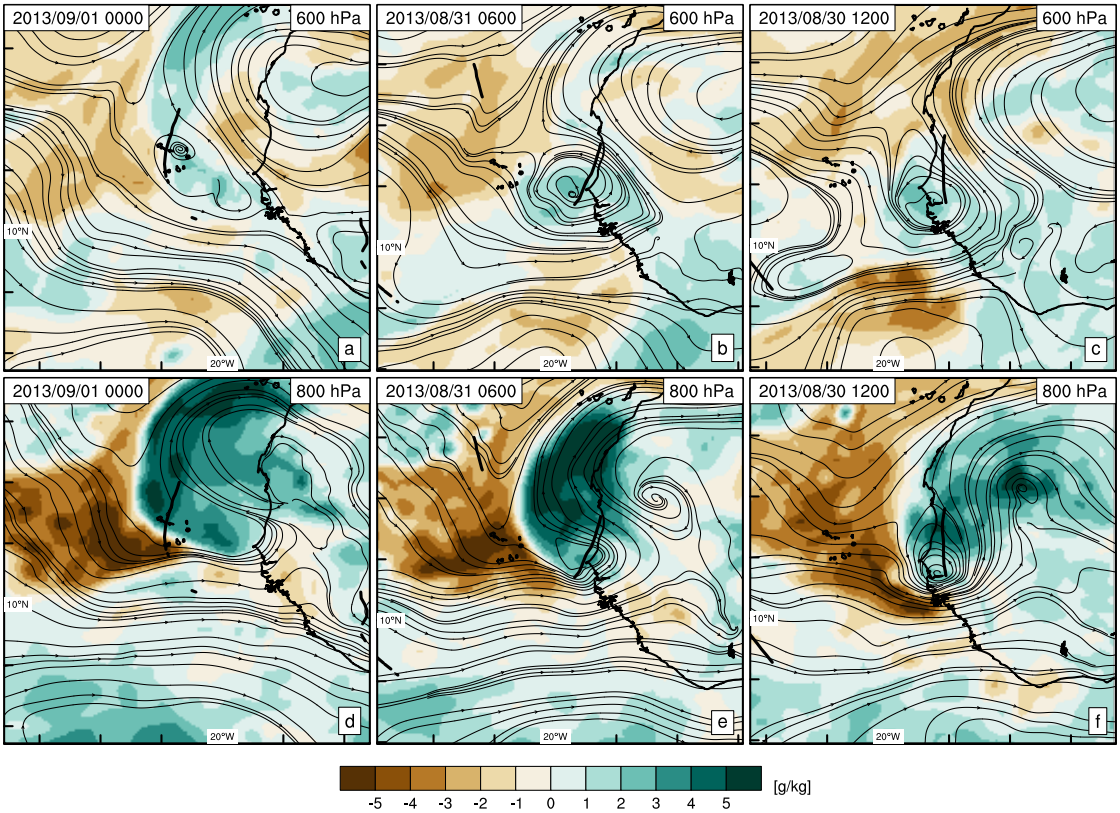

Figure 5.18: Evolution of non-developing AEW in 2013 at 18 hour intervals. Shading shows anomalous specific humidity (g/kg), streamlines show the trough relative flow for the corresponding level. Top row shows 600 hPa variables, bottom row shows 800 hPa variables. Rows are organised right to left in 18 h intervals. Thick black contour shows the trough axes at 700 hPa.

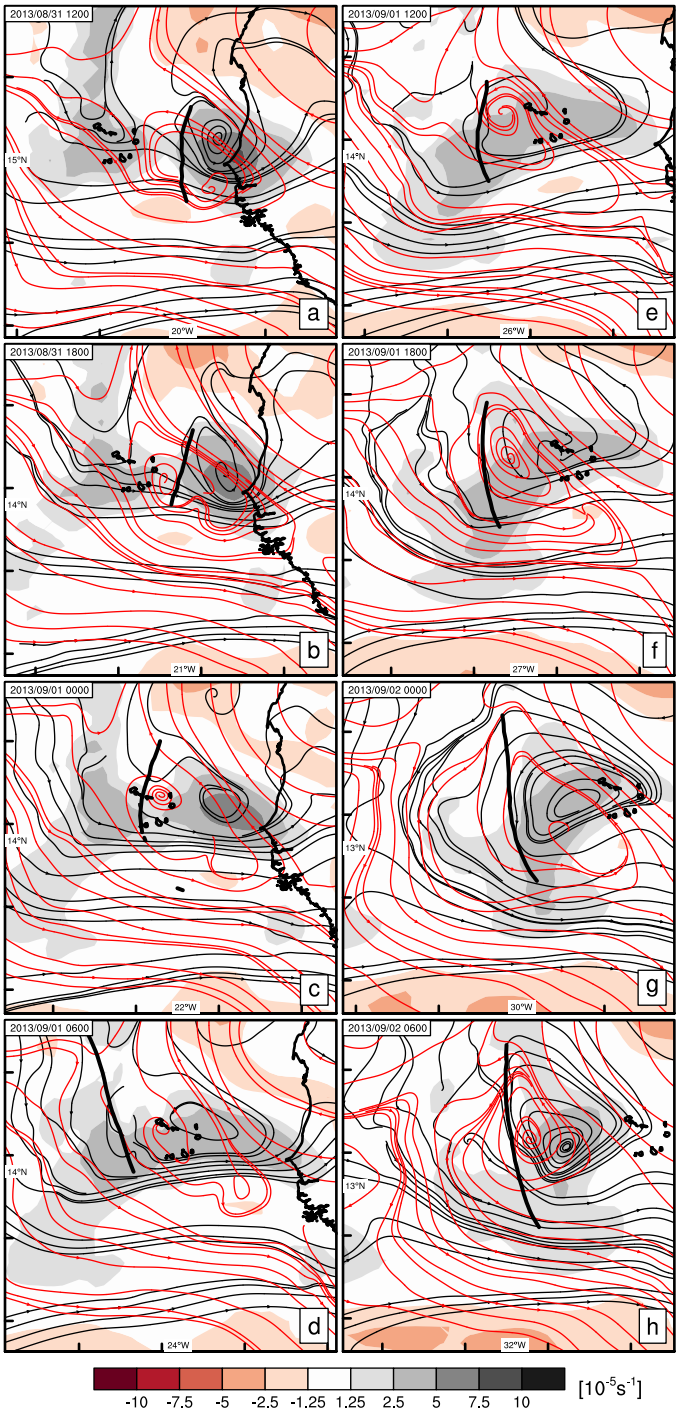

Figure 5.19: Evolution of AEW33 in 2013 at 6 hour intervals. Shading (contours) show Relative vorticity at 850 hPa (600 hPa). Dashed contours show negative values. Interval for contours and shading are equivalent. Thick black contours indicates the AEW trough axis at 700 hPa.

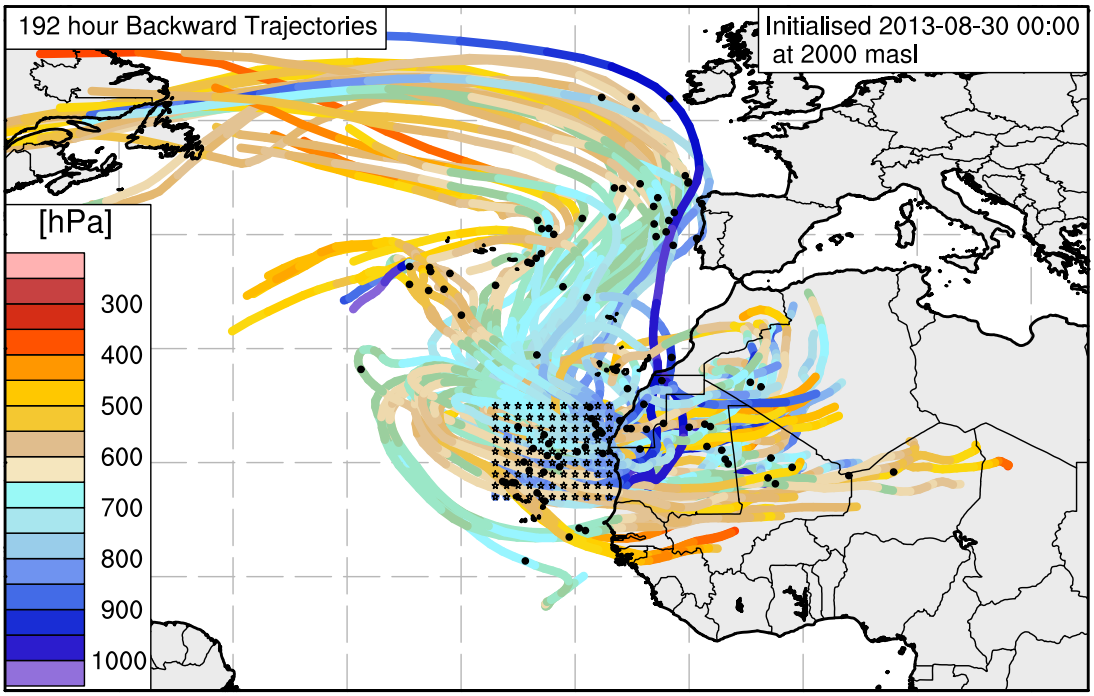

Figure 5.20: Trajectories initialised at 2000 metres above sea level on 30th August 2013 at 0000UTC as AEW33 was situated over the coastal region. Colour of trajectories represents the pressure level at that location. Grid of stars shows the starting location of the trajectories. Black dots show the -120 hour position. Trajectories were integrated for a total of 192 hours.

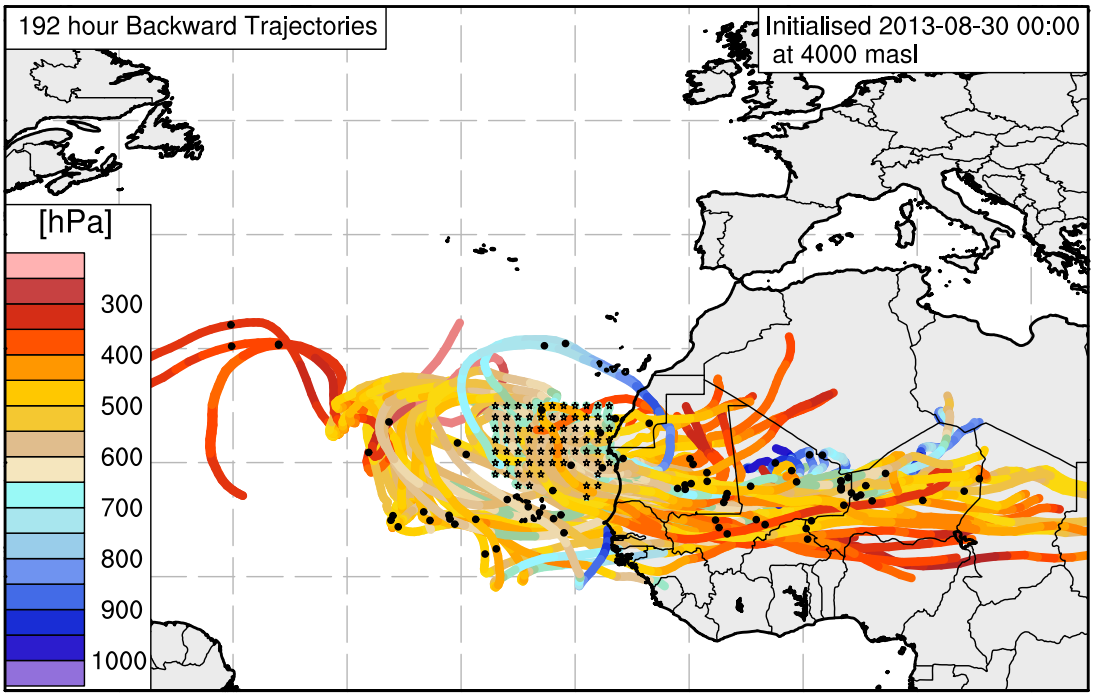

Figure 5.21: Trajectories initialised at 4000 metres above sea level on 30th August 2013 at 0000UTC as AEW33 was situated over the coastal region. Colour of trajectories represents the pressure level at that location. Grid of stars shows the starting location of the trajectories. Black dots show the -120 hour position. Trajectories were integrated for a total of 192 hours.

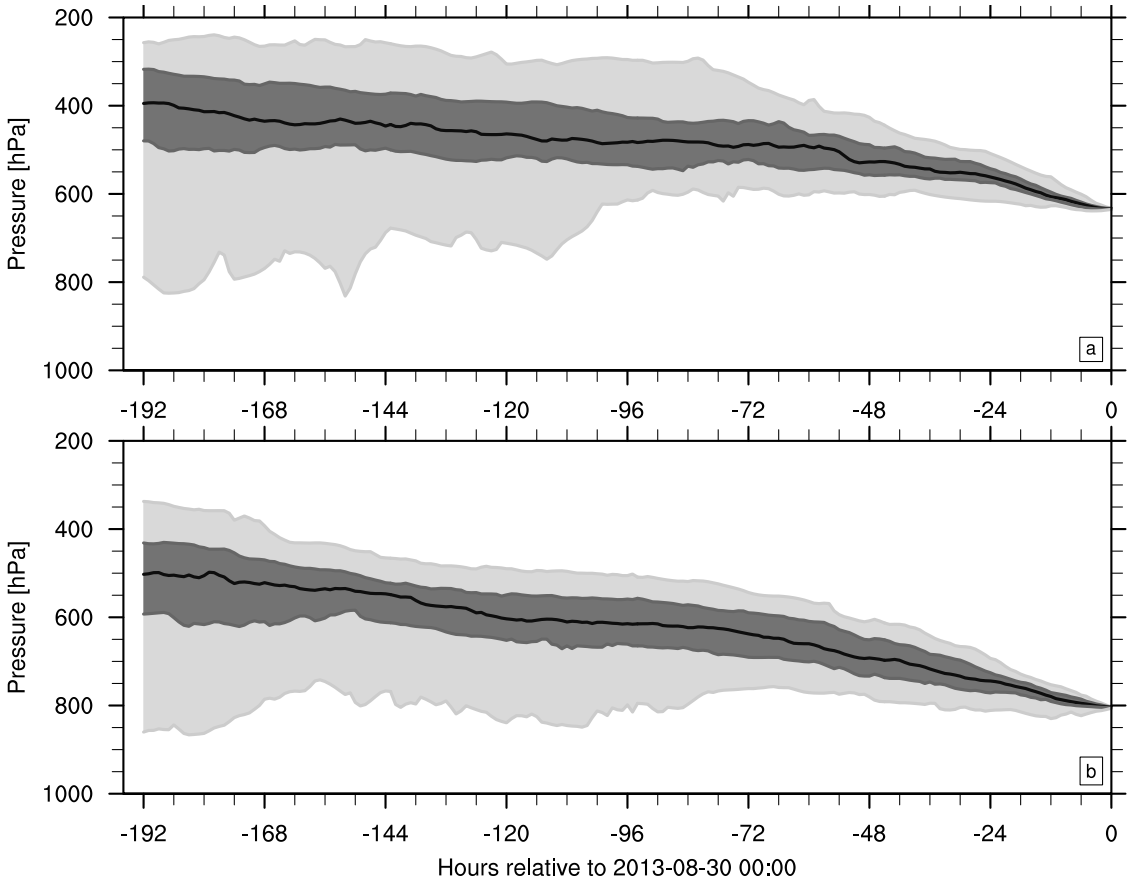

Figure 5.22: Distribution of trajectory pressures over the 192 hour backward integration initiased from 4000 masl (a) and 2000 masl (b), 600 and 800 hPa respectively. Percentile of distribution shaded at 5%, 25%, 75% and 95%. Dark central line represents the median.

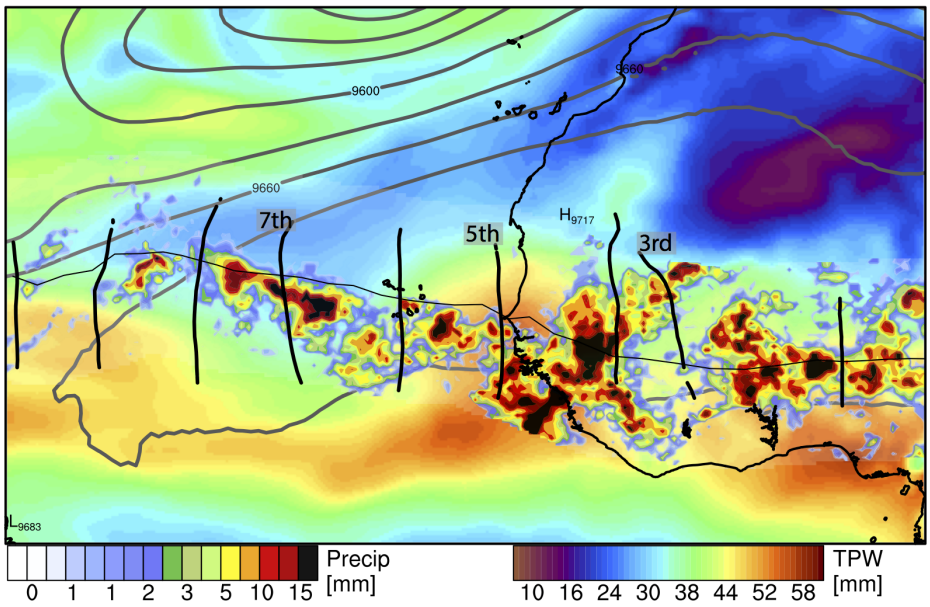

Figure 5.23: Evolution of a non-developing AEW in 2014. Accumulated precipitation within 750 km of trough center along track at 3 h intervals. Objective trough lines plotted at 24 h intervals with 6 h track of vortex center also shown. Shading and contours show the 36 h mean total precipitable water and 300 hPa geopotential height, respectively. Temporal averages are centered on the time the trough axis crosses the coast line.

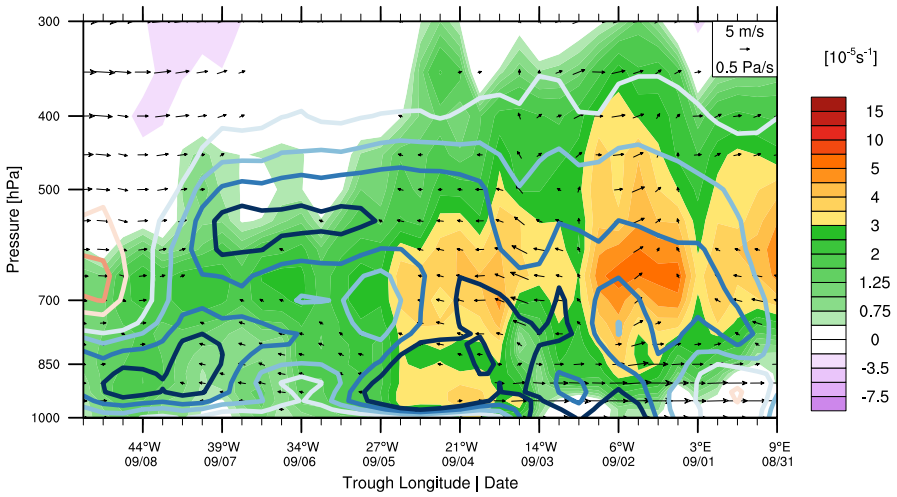

Figure 5.24: Vertical evolution of trough centric (300 km radius circular average) variables, for AEW40 in 2014, relative vorticity (shading) and anomalous specific humidity (contours). Contours at 1g/kg intervals, red (blue) indicate negative (positive) anomalies. Zero contour is not shown. Wind vectors display trough relative zonal wind and vertical wind. X-axis represents the time (or longitudinal) evolution of the trough.

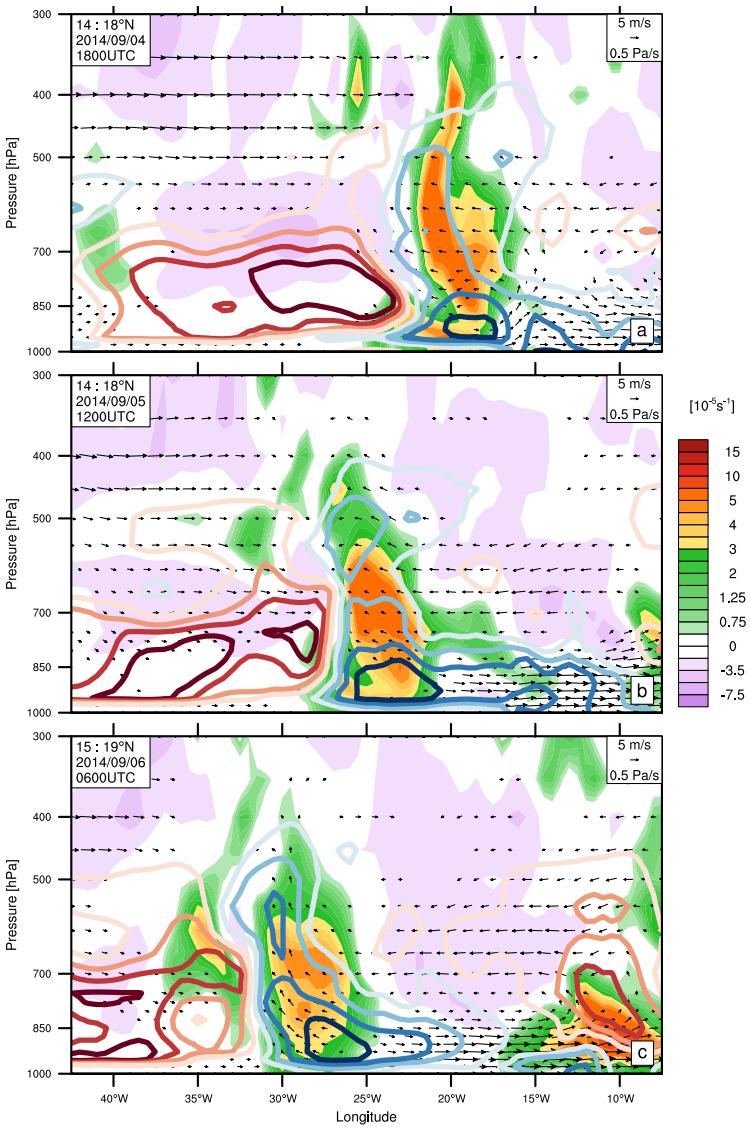

Figure 5.25: Height - longitude plots of AEW40 in 2012 at 18 hour intervals. Relative vorticity (shading) and anomalous specific humidity (contours). Contours at 2g/kg intervals, red (blue) indicate negative (positive) anomalies. Zero contour is not shown. Wind vectors display trough relative zonal wind and vertical wind. Meridionally averaged over 4° centered on the trough latitude.

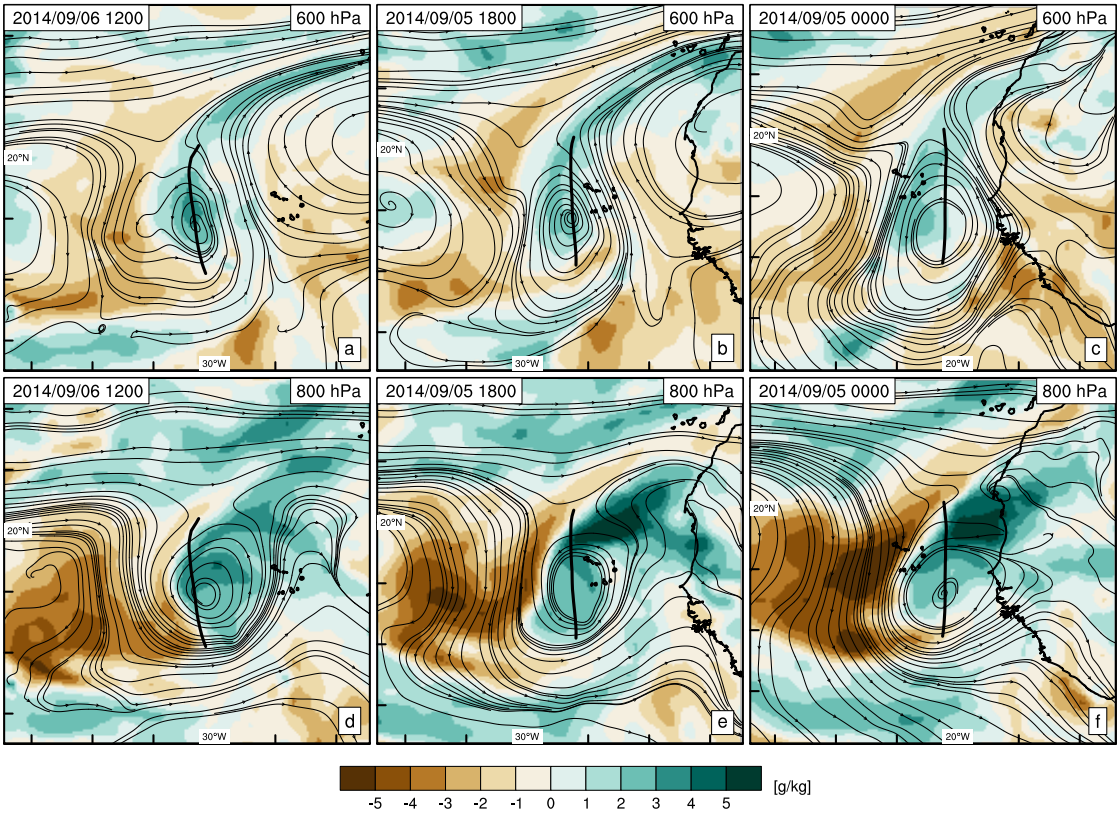

Figure 5.26: Evolution of non-developing AEW in 2014 at 18 hour intervals. Shading shows anomalous specific humidity (g/kg), streamlines show the trough relative flow for the corresponding level. Top row shows 600 hPa variables, bottom row shows 800 hPa variables. Rows are organised right to left in 18 h intervals. Thick black contour shows the trough axes at 700 hPa.

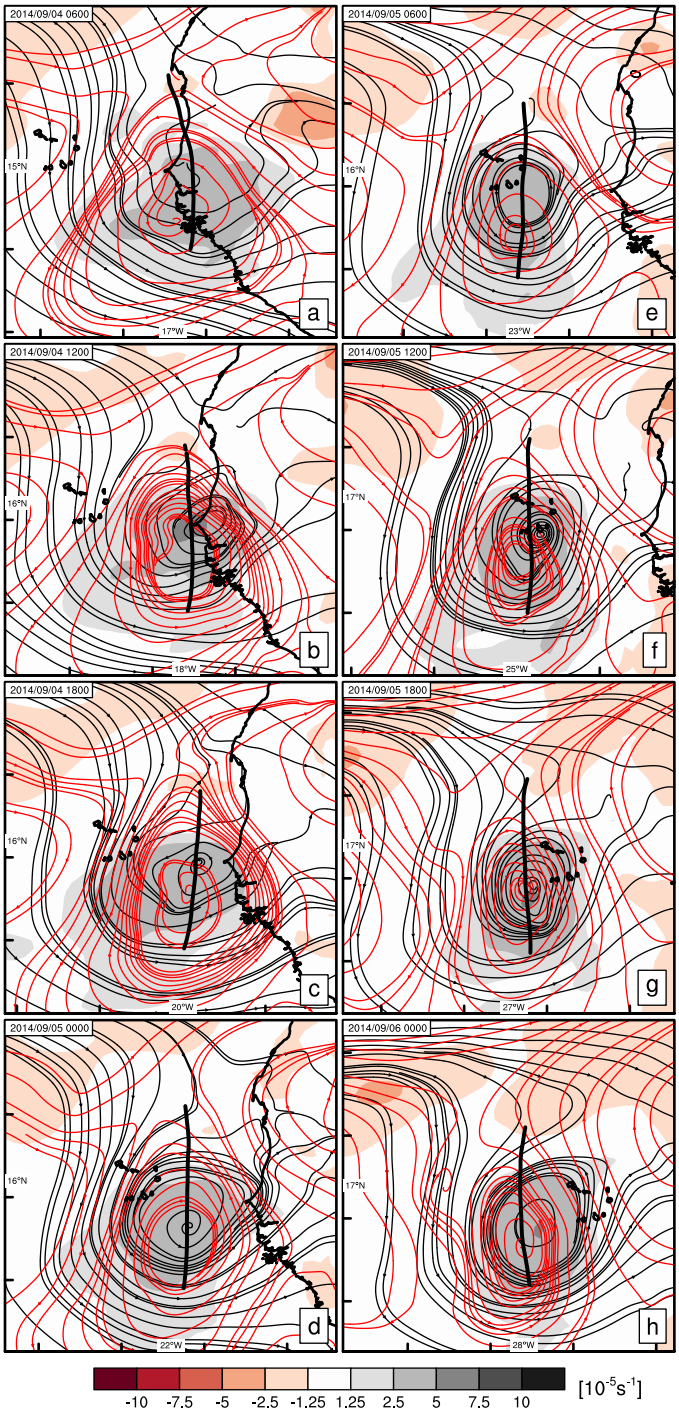

Figure 5.27: Evolution of AEW40 in 2014 at 6 hour intervals. Shading (contours) show Relative vorticity at 850 hPa (600 hPa). Dashed contours show negative values. Interval for contours and shading are equivalent. Thick black contours indicates the AEW trough axis at 700 hPa.

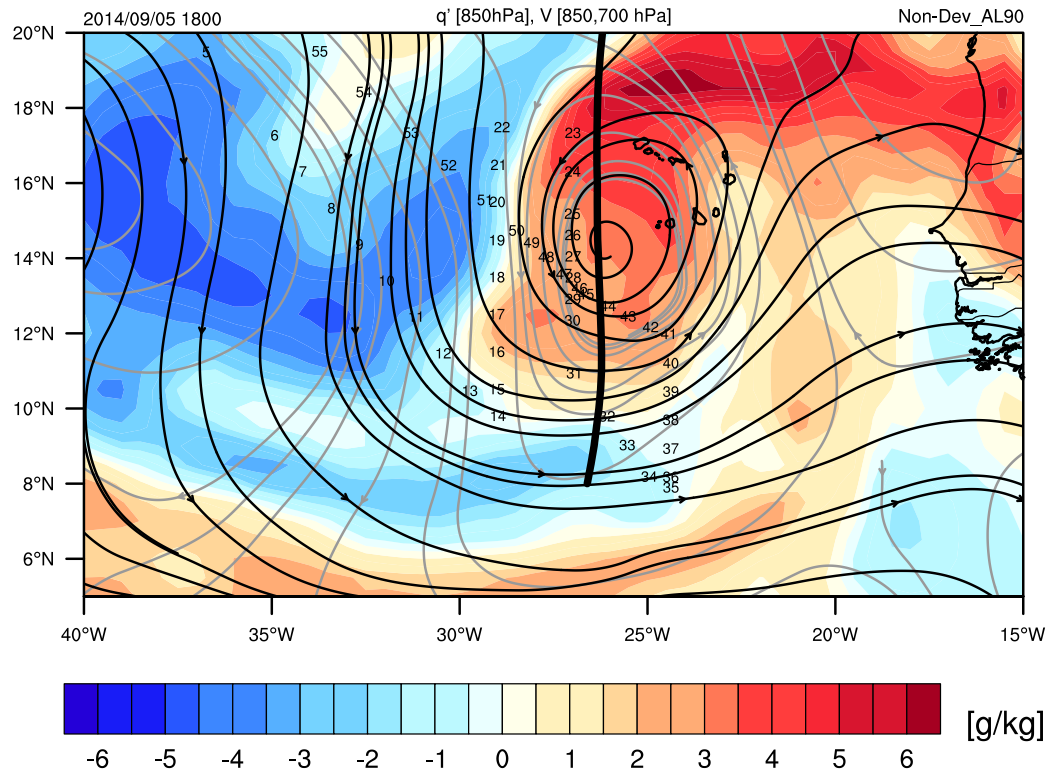

Figure 5.28: Location of Dropsondes overlaid on anomalous specific humidity at 850 hPa and trough relative streamlines at 850 hPa (Black) and 700 hPa (Grey). Humidity and wind vectors taken from CFSR at 1800UTC approximately when drop 5 was released for reference drop 14 was released at 2114UTC.

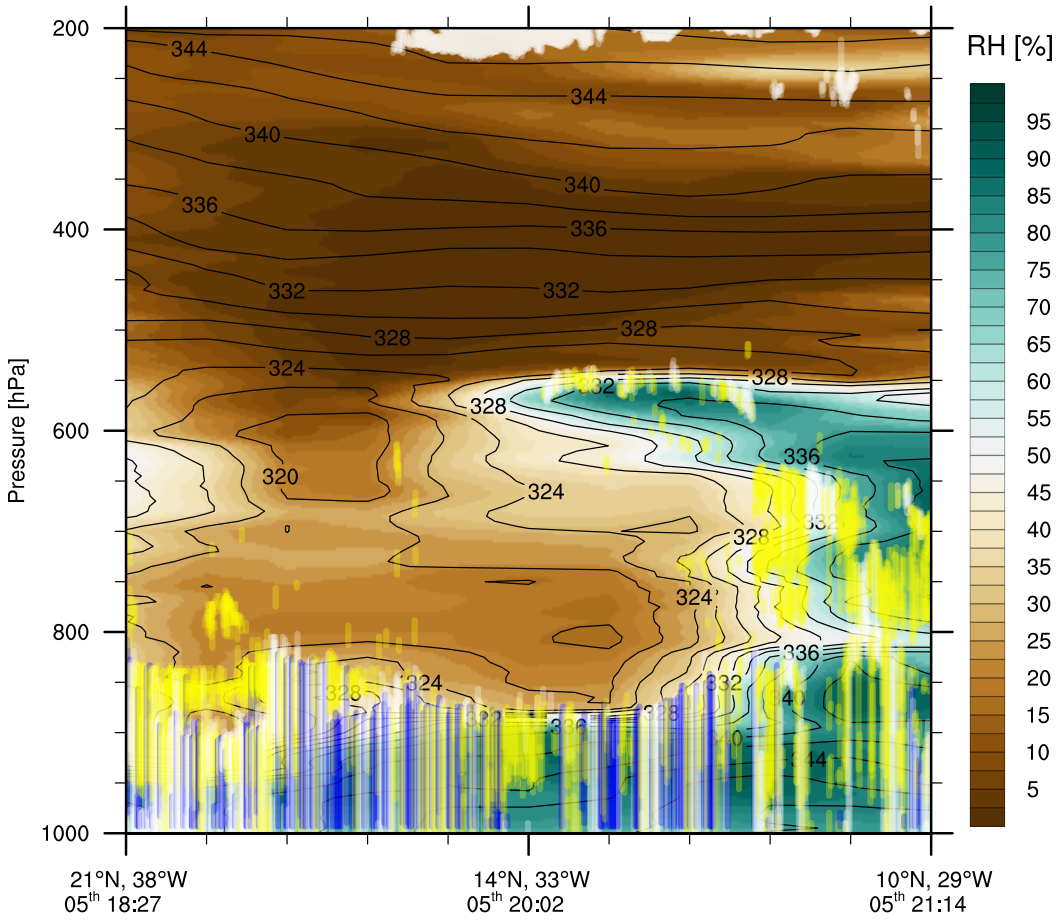

Figure 5.29: Cross section of Relative humidity (shading), equivalent potential temperature (contour lines) and overlaid layer detection as measured by CPL. CPL detects upto 8 layers of three types; cloud (white), elevated aerosol (yellow) and boundary layer (blue). Transect spans from drop 5 to drop 14 as shown in Fig. 5.28.

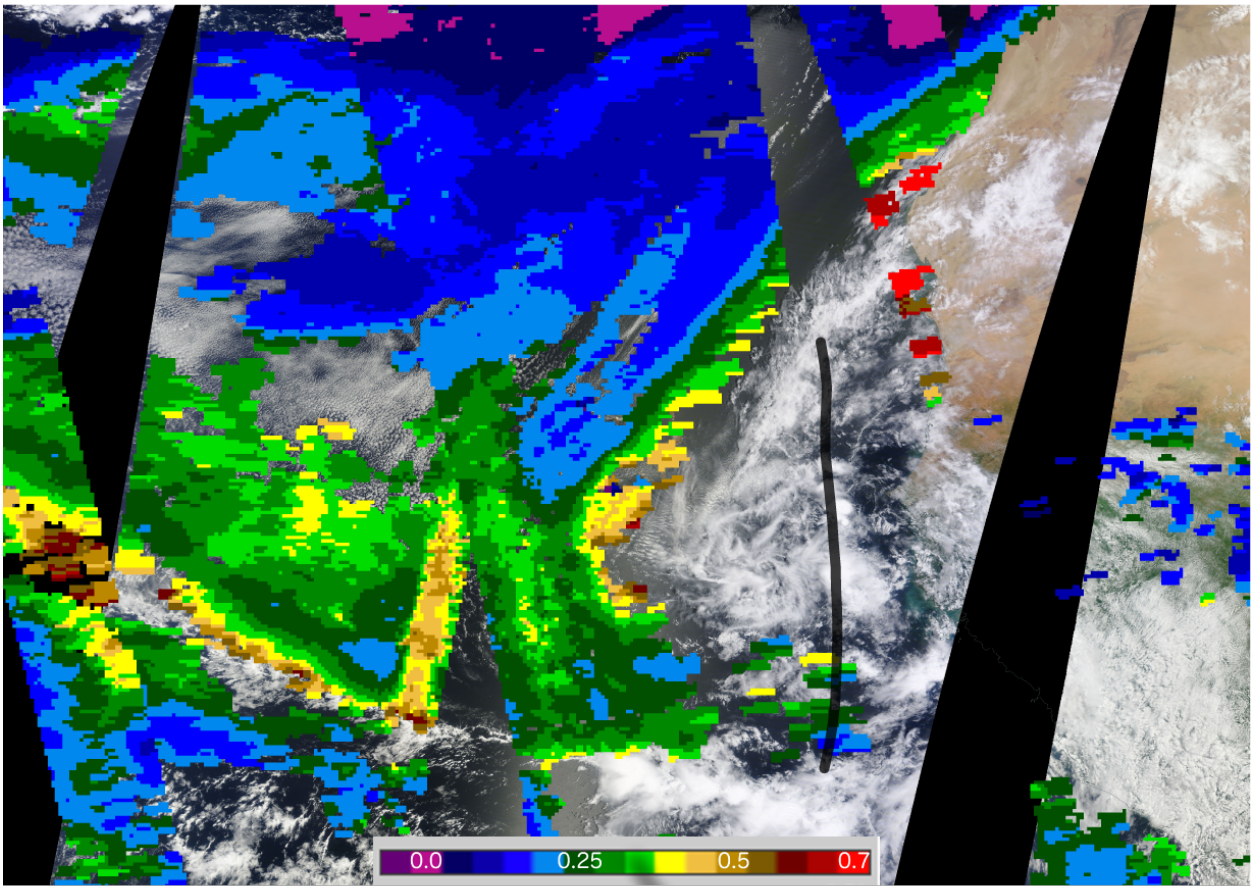

Figure 5.30: Aerosol optical depth and corrected reflectance for September 4th 2014 merged from Terra and Aqua on MODIS. Image downloaded from NASA worldview website. Black trough line overlaid manually using 1200UTC location.

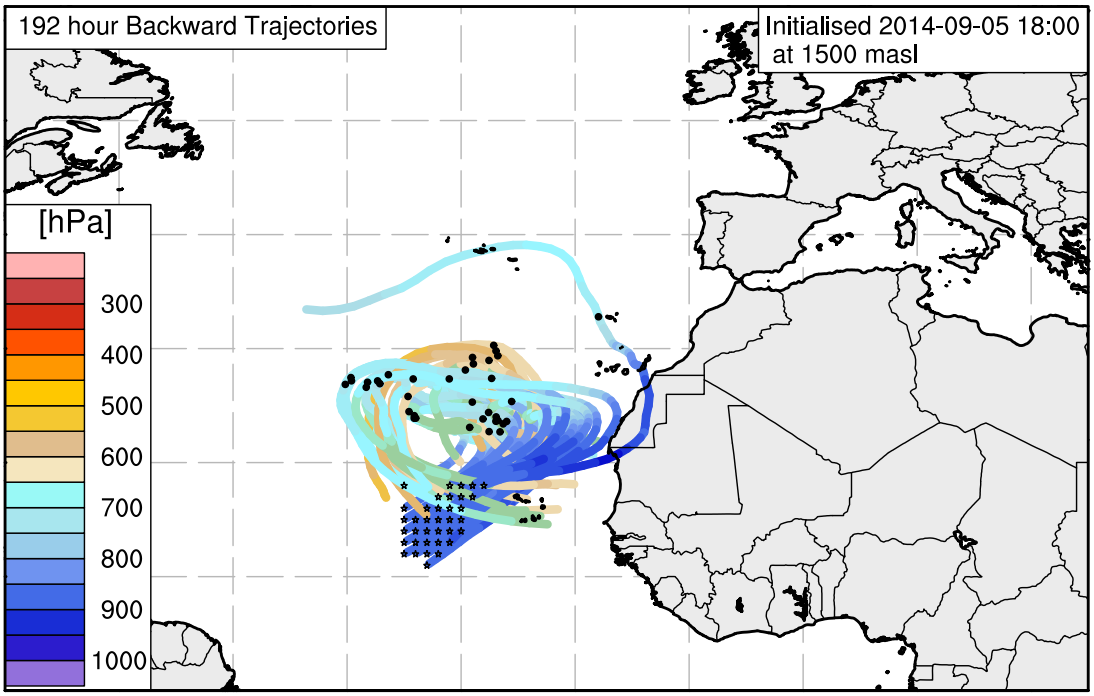

Figure 5.31: Trajectories initialised at 1500 metres above sea level on 5th September 2014 at 1800UTC west of AEW40. Colour of trajectories represents the pressure level at that location. Grid of stars shows the starting location of the trajectories. Black dots show the -120 hour position. Trajectories were integrated for a total of 192 hours.

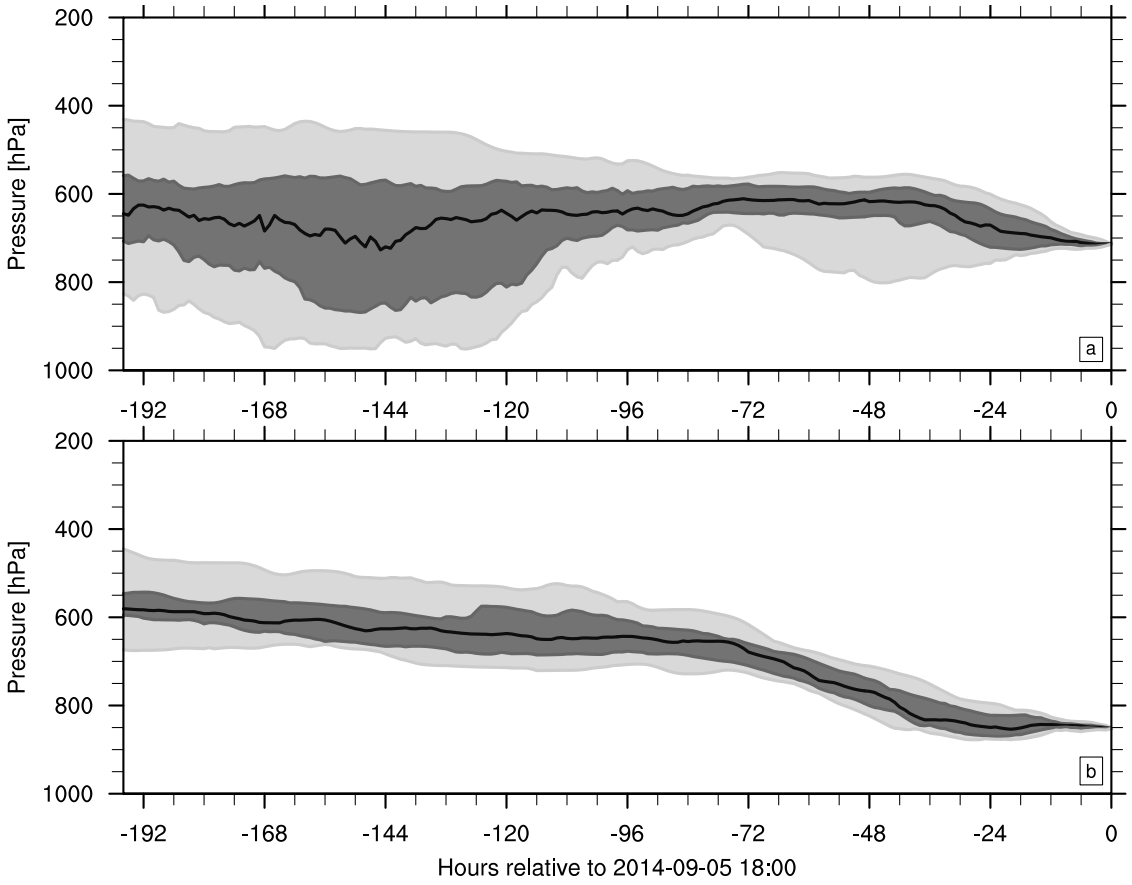

Figure 5.32: Distribution of trajectory pressures over the 192 hour backward integration initialised from 3000 masl (a) and15000 masl (b), 700 and 850 hPa respectively. Percentile of distribution shaded at 5%, 25%, 75% and 95%. Dark central line represents the median.

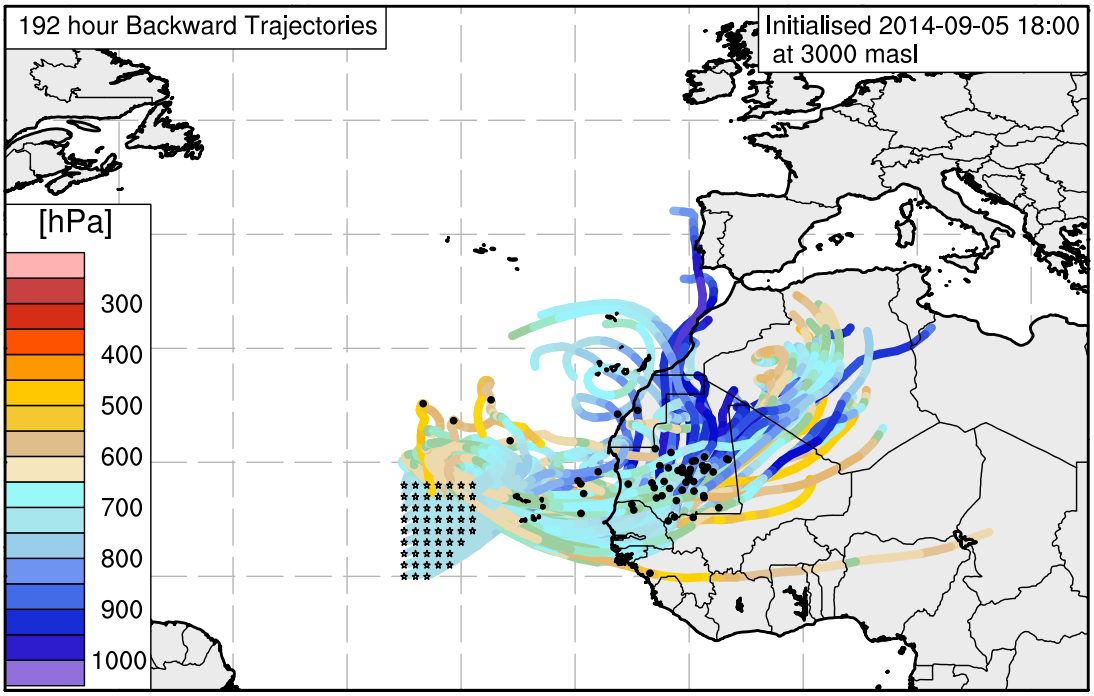

Figure 5.33: Trajectories initialised at 3000 metres above sea level on 5th September 2014 at 1800UTC west of AEW40. Colour of trajectories represents the pressure level at that location.. Colour of trajectories represents the pressure level at that location. Grid of stars shows the starting location of the trajectories. Black dots show the -120 hour position. Trajectories were integrated for a total of 192 hours.

6. Conclusions

6.1 Discussion of Results

This thesis has presented research regarding AEWs and their relationship with tropical cyclogenesis over the eastern Atlantic. The aim of this research has been to provide more detail about the evolution of developing and non-developing AEW troughs. The research aimed to address how distinguishable developing waves were from the population of AEWs leaving West Africa. As well as how many AEW troughs could be characterised as favourable for genesis and also why a number of these did not then develop. Previous research has presented differences between samples of all developing and non-developing disturbances, this thesis attempted to refine that question further by analysing only troughs that were already favourable for development.

This research has developed an objective tracking methodology of the synoptic scale AEWs. This was developed to track the large-scale center of the trough of the wave rather than the mesoscale vortices embedded within. Three dimensional tracks of the AEWs enabled detailed analysis of the evolution of the troughs across West Africa and to any possible downstream genesis events. The tracks also enabled the evolution of each disturbance to be analysed rather than relying on analysis of troughs around a base point. The research used the Lagrangian framework of the AEWs to compare the structure of the troughs that are involved in the development of tropical cyclones over the eastern Atlantic and the troughs that show no development after leaving the West African coast.

Composite analysis in Chapter 3 presented the mean differences and variability of developing and non-developing troughs over West Africa and the eastern Atlantic. Mean differences between the subsets confirmed previous results (e.g Hopsch et al. 2010), showing that the small number of developing waves are significantly different from the large population of non-developing waves over West Africa as early as 5°W. Variability within the subsets

however, revealed a large overlap in the distributions of the subsets. This suggests that a large number of the non-developing waves may be characteristically similar to the developing waves.

Rather than subjectively choosing a single variable to then select strong non-developing waves, a logistic regression model was used to determine the optimum combination of trough scale variables with respect to the probability of development over the eastern Atlantic. In developing the statistical model both satellite measures of convection and reanalysis variables were tested separately and together. There was no significant improvement in the diagnostic through inclusion of the satellite observations, therefore a model was developed using only reanalysis variables. The two models were very similar however, and more testing with satellite observations may prove beneficial if the approach were to be used in a real-time prognostic sense, similar to the current generation of statistical hurricane models (e.g. DeMaria and Kaplan 1994; Dunion et al. 2013).

The statistical diagnostic revealed that around 75% of all waves analysed do not possess characteristics associated with the developing waves as they leave West Africa. This suggests that composite analyses including all of these non-developing waves is limited for results outside of the trough; as many of the troughs are unfavourable for TC genesis over the eastern Atlantic. This diagnostic was used to objectively select the most favourable developing and non-developing waves based on a combination of variables averaged around each waves trough.

Chapter 3 made use of the statistical diagnostic to refine the composite analysis of developing and non-developing waves using equal size subsets from waves characterised as favourable for genesis. This analysis revealed differences on a larger scale than the AEW troughs, revealing a role of the environment in influencing the outcome of the subsets. The main differences found were lower-tropospheric moisture to the northwest of the AEW troughs and the strength of an upper-tropospheric trough over the northeastern Atlantic. Developing waves were associated with positive anomalous moisture in the lower troposphere

ahead of the AEW trough. This was associated with a consistent downstream wave drawing moisture poleward on the eastern side of its trough. Non-developing waves exhibited a more climatological structure with dry air to the northwest potentially associated with the presence of the mid-latitude trough to the north.

Trough relative streamlines showed that as the AEW troughs moved over the ocean, both subsets had similar flow around the trough with the lower levels of the vortex open to the environment to the northwest. Recirculation within the trough of the AEW has been hypothesised as an important precursor to TC genesis by enabling the system to become protected from the surrounding environment (e.g Dunkerton et al. 2009). The composite results in chapter 3 showed that as the troughs left the coast, while they had closed circulation at the level of the jet, due to the easterly shear in the region and the cold-core nature of the waves, the low levels of the vortex were still entraining environmental air from the northwest. Trajectory analysis confirmed this ingestion of environmental air from up to 2000 km to the northwest of the troughs; during the 48 h after the troughs had moved over the ocean. For developing waves this meant that the trough was ingesting anomalously moist air throughout this time. This flux of high moisture into the lower levels of the trough is hypothesised to be a major factor in sustaining the deep convection within the trough and thus intensifying the vortex. Conversely non-developing waves were ingesting drier air into the lower levels of the vortex. This direct flux of dry air through the low levels is expected to inhibit extent and depth of convection (Braun et al. 2012), increasing the frequency of downdrafts around the trough and further decreasing the ability for the system to extend downwards to the boundary layer (e.g Bister and Emanuel 1997).

This composite analysis showed that not only do AEWs need to have associated convective activity over West Africa to create a favourable wave. The favourable waves also needed to move over an eastern Atlantic with anomalously moist conditions in the lower troposphere. Both developing and non-developing waves were initially cold core at lower levels and thus open to the environment to the north-west. This interaction with environ-

mental entrainment is viewed as either a positive or negative feedback loop. In the presence of anomalously moist low-level environment convection is sustained and the vortex extends down increasing the resiliency to the environment. However likely more typical over the eastern Atlantic is the ingestion of dry air into the low levels, hindering convection and the development of the vortex. This leaves the vortex open to the environment for longer further ingesting dry air and inhibiting convection.

Chapter 4 analysed the relative flow around the AEW troughs over West Africa and the eastern Atlantic. An objective analysis of the occurrence of closed circulation within the AEW troughs was initially presented. Over West Africa the occurrence of recirculation was maximised around the level of the AEJ. After leaving the coast the vertical extent of recirculation increased over the first 72 h, with the occurrence of closed circulation equally distributed through the lower troposphere by this time. During this vertical expansion in closed circulation, the horizontal area of recirculation at low levels was also shown to increase and reach an equivalent size to the jet-level circulation. These results highlighted the cold core nature of the the AEWs as they leave West Africa and the downward extension of circulation after the troughs have left West Africa. The vertical alignment of the vortex was also assessed using the closed circulation to determine vertical tilt and consequently the overlap of the closed circulations in the vertical. The vertical alignment of the developing vortex has shown to be an important factor for genesis in both observations and idealised simulations (e.g. Davis and Ahijevych 2012; Rappin and Nolan 2012). The composite tilt diagnosed from the AEW closed circulations showed an initially substantial tilt to the southwest with height (over 200 km). During the 72 h evolution from the coast, the vertical tilt reduced and the mean circulation centers of the waves were within 100 km of alignment in the lower troposphere. This vertical tilt is likely due to the vertical shear imposed by the AEJ and low-level monsoonal inflow towards Africa. An intiial westward tilt with height of the column would then induce precession of the column as the upper and lower level centers rotate slowly around the mid-level vortex (Jones 1995). Due to the weakness of the vortices

at this point this precession is likely slow resulting in a quasi-constant southwestward tilt. As the troughs move away from Africa the low-level vortex typically intensifies (Janiga and Thorncroft 2012) and the the background easterly shear weakens helping to reduce the mean tilt of the vortex column.

To evaluate the relative flow around the waves more completely and to analyse the various source regions of environmental air reaching the AEW troughs a large sample of backward trajectories were released from within the trough of the favourable waves analysed in Chapter 3. The large scale trajectory analysis revealed that over West Africa the AEWs experience inflow into the trough from either the southwest or east/northeast. As the troughs approach the eastern Atlantic, northerly flow over the eastern Atlantic becomes a dominant source for trajectories that reach the low levels of the trough. This northerly flow was also a dominant source of low humidity air at low levels. Over Africa trajectories around the level of the AEJ propagated at a comparable rate to the AEW trough, however the number of trajectories that remained within 500 km of the center was less than 10%. These trajectories approached the trough from the east and then wrapped around the north and west of the vortex. At low levels the monsoonal inflow approached the troughs from the southwest, advecting high humidity air over the continent and into the low levels of the troughs.

As the troughs approached the coast the ingestion of dry air from the north increased. Variability in the trajectories from this low-level source of dry air was related to the differences between the developing and non-developing troughs. The trajectories suggested that the main source of this low-level dry air was from the subtropical eastern Atlantic. This dry air was likely associated with subsidence of mid-latitude air over the subtropics which is then advected south on the eastern edge of the subtropical ridge. The origin of dry air over the tropical Atlantic has been questioned previously by Braun (2010), the trajectory analysis here agrees with the notion that dry air over the tropical Atlantic is not necessarily of Saharan origin. A major route of dry air over the eastern Atlantic shown here is in the low-level northerlies from the subtropics. The 120 h back trajectories presented here did

not reveal the longer term origin of this dry air however. Though it is expected that this low-level dry air is associated with subsidence over the region, which is potentially enhanced by the midlatitude upper-level trough shown in the non-developing composite analysis.

To refine the details of the results from chapter 3 and chapter 4, analysis of 4 events was presented in chapter 5. The cases provided more detail in the evolution of the troughs and their embedded vortices. The two developing cases resemble large scale patterns observed in the composite analysis. These showed increase anomalous moisture in the lower-levels of the troposphere over the eastern Atlantic and zonal flow through the upper levels over the subtropics. The non-developing waves conversely both had an upper-level trough present over the northeastern Atlantic and a large region of dry air extending through the lower troposphere to the west of the AEW trough as it left West Africa. In all four cases when the trough initially left the continent, the vortex below the AEJ was open to the environment and subject to relative northwesterly flow through the lower levels. Although closed circulation developed in all cases, a consistent vertical tilt of the vortex to the south-west was also observed. Due to this misalignment of the circulations, the jet-level circulation is located over the relative northwesterly flow of the low-level circulation. In both developing and non-developing cases the jet-level circulation was located near negative moisture anomalies. While this dry air was outside the closed circulation of the vortex, downdrafts can flood the inflow at lower levels with the low equivalent potential temperature air (Bister and Emanuel 1997). Vertical shear of the vortex can enhance this effect by enhancing the ventilation of the system at lower levels and increasing the inflow of the low θ_e air (Riemer et al. 2010; Tang and Emanuel 2012).

In the developing cases, the positive moisture anomalies at low levels are hypothesised to have negated the potential detrimental impacts of any downdrafts. The horizontal flux of positive moisture anomalies would have been sufficient to offset the vertical transport of dry air by the downdrafts. When the circulation was open at low levels this also meant that the developing cases were ingesting increased moisture at a time when the surface fluxes are

assumed to be small due to the weakness of the circulation at the surface. This increased moisture flux into the system is expected to have positive effects on helping sustain deep convection, thus intensifying the vortex and helping to develop a more resilient system. For non-developing cases this feedback mechanism is hypothesised to act to weaken the vortex and cause decay. As the trough leaves the continent, the circulation is typically open at low levels. As was seen in the 2013 non-developing case, this resulted in advection of low-level dry air through the lower levels of the trough inhibiting deep convection. The non-developing wave analysed from 2014 developed a low-level closed circulation very quickly after leaving the coast. However the vertical tilt of the vortex meant the jet-level circulation overlapped with the dry northwesterly flow of the low-level circulation. The combination of dry air around the jet-level circulation and dry air below would have likely have resulted significant number of downdrafts throughout the southwestern quadrant of the storm increasing the likelihood of entrainment and mixing of low θ_e air into the vortex. Surface fluxes associated with these weak systems are expected to be insufficient to counteract these negative environmental impacts.

A schematic of the main hypothesis developed from this work is shown in Fig. 6.1. Building on the simple kinematic model proposed by Riemer and Montgomery (2011), as the AEW troughs leave the West African coast they are in a region of easterly vertical shear resulting in relative inflow from the northwest. Typically the vortex is open to the environment below the level of the AEJ, as vorticity extends down to the boundary layer the system remains in easterly shear and thus there is slight vertical tilt towards the west. Although the vorticity in the column is weak, the westward tilt imposes slight precession resulting in the column tilted towards the southwest. The tilt coupled with the low-level relative flow makes this southwest quadrant susceptible to the low-level environment from the northwest for an extended period of time after the troughs have left the West African coast. The meridional gradients over the eastern Atlantic are typically quite strong with unfavourable environmental conditions to the north. This sensitivity to the environment may

therefore typically result in a weakening of convection resulting in the decay of most AEWs. In cases where the environment is anomalously moist however, entrainment of favourable environmental air is expected to help the system and provide the necessary thermodynamic support in an otherwise hostile environment.

The results within this thesis highlight a potential role in the interaction between the environment and the AEW trough. While the potential causality of the results has been hypothesised, the scale of the analysis and the datasets used are limiting. The mesoscale interactions and effects on convection will not be captured by a global model used for reanalysis, so questions about causal links between the environment and mesoscale vortex remain. The interactions observed in these results are in agreement with observations across other basins and in idealised simulations so there is confidence in the results and the proposed causal mechanisms.

6.2 Future Work

6.2.1 Characteristics of AEWs

The variability in AEW trough characteristics in Chapter 3 showed that there was a wide distribution in the characteristics of AEWs. Many papers concerned with the interannual or climate scale variability of AEWs have focussed on the mean characteristics of individual variables within the troughs. Based on the results here it is proposed that the logistic regression model approach (or other method of combining variables) enables a more complete picture of the AEW troughs to be determined. The seasonal analysis in chapter 5 showed large differences in the number of favourable waves leaving West Africa. This characterisation could therefore provide a useful diagnostic for interpreting interannual variability in the structure of AEWs. Through use of this diagnostic, the results on the developing and non-developing waves have been refined in this thesis. In a similar manner variability on the interannual timescale could be refined by objectively characterising the AEW troughs. This analysis could also benefit research in climate projections of AEW variability. Climate mod-

els have been shown to struggle to reproduce AEW characteristics and variability compared to historic simulations (e.g. Crétat et al. 2014; Martin and Thorncroft 2015). As AEWs are a large source of tropical cyclogenesis seedlings over the Atlantic it is important to understand how the simulations capture both the frequency and the characteristics of the AEW troughs. Research has shown the potential changes in the tropical cyclone activity when seedling disturbances are randomly generated across the globe (e.g. Emanuel 2013). Though this methodology assumes that the projected variability in the seedlings is less important. Whether this assumption is valid is unclear, however the location and longevity of tropical cyclones may be significantly influenced by the origins of the pre-genesis systems. As such, understanding the variability in AEW trough characteristics is viewed as an important consideration for climate projections and the use of a statistical model to characterise the waves provides a simple way to analyse this.

6.2.2 Origin of Environmental Air Around the AEWs

The trajectory analysis in chapter 4 highlighted potential routes for environmental air to impact the AEW troughs. The low-level dry air from the northeastern Atlantic, that was shown to have a significant impact on TC genesis from AEWs, is not typically considered when evaluating dry air over the Atlantic. In agreement with the results of Braun (2010), the trajectories throughout this thesis have shown the importance of dry air from multiple origins besides the Sahara. The trajectories here focussed on the interaction of the environment with the AEW troughs, however it would be interesting to focus rather on the dry air over the eastern Atlantic. Recent research has provided a clearer view of the structure and variability over the eastern Atlantic and the fluxes of dry air over West Africa (Roca et al. 2005; Casey et al. 2009; Huang et al. 2010; Ben-Ami et al. 2012). However the variability in the origins of dry air is still unclear. Improving the knowledge of the interactions between mid-latitude subsidence, tropical subsidence and the more typical Saharan air layer will provide clearer understanding of the seasonal impacts of each route as well whether the impacts of the dry

air differ based on its origin.

While the trajectories here provided a novel view of the environmental flow approaching the AEWs, this could be extended to analyse whether this large-scale flow is associated with differences in the evolution of the AEW troughs over West Africa. Waves included here were those diagnosed as favourable for genesis at the coast thus possibly reducing the variability in the origin of the back trajectories. Comparison of the large-scale flow with weaker and less favourable waves may reveal large-scale differences in the environment associated with favourable and unfavourable waves. Understanding how changes in the large-scale flow influences the characteristics of the AEW troughs may reveal clearer dynamical links in the influence of seasonal and equatorial wave variability on the AEWs.

6.2.3 Interaction of the Environment and Vortex

The research presented here is limited in the temporal and spatial resolution of the results. The analysis has shown interesting potential interactions between the environment and the vortex but can not answer the direct causal links between the correlations presented. The role of dry air on tropical cyclogenesis remains an active research topic in both observational and numerical simulations. Idealised simulations using a background flow equivalent to the relative flow experienced by the AEW troughs and a vertical shear profile dominated by the AEJ may produce more realistic conditions that more generalised or idealised simulations (e.g. Braun et al. 2012; Rappin and Nolan 2012). The role of the vertical tilt of the vortex after leaving the coast and the relative flow of the environmental air through or under regions of closed circulation remain a potentially critical influence for the AEW troughs. The sensitivity to the environment proposed here however may also have a limited temporal span. As the height of low-level cold core is reduced the circulation is expected to become more resilient to entrainment of the environment. Sippel et al. (2011) showed that in simulations of Tropical Storm Debby (2006) while the system was sensitive to the environment initially, this only delayed genesis and as the storm intensified the environmental moisture has less

impact on the rate of intensification.

Understanding these interactions and the timeframe over which they occur is expected to be useful knowledge not only for future research but also forecasting tropical cyclogenesis from these systems. Global models currently struggle with forecasting genesis over the eastern Atlantic (Halperin et al. 2013), therefore refined understanding of the trough characteristics and surrounding environment would be useful for interpreting individual cases and the potential deficiencies of the forecasts.

To better answer these interactions, combinations of idealised and case study numerical simulations would be proposed. Utilisation of ensemble techniques and evaluating the sensitivities within individual cases would help focus the results on the specific interactions in play. These simulations however rely on a full understanding of the biases within the model and the models ability to properly resolve the dynamics of the AEWs and associated vortex and convection.

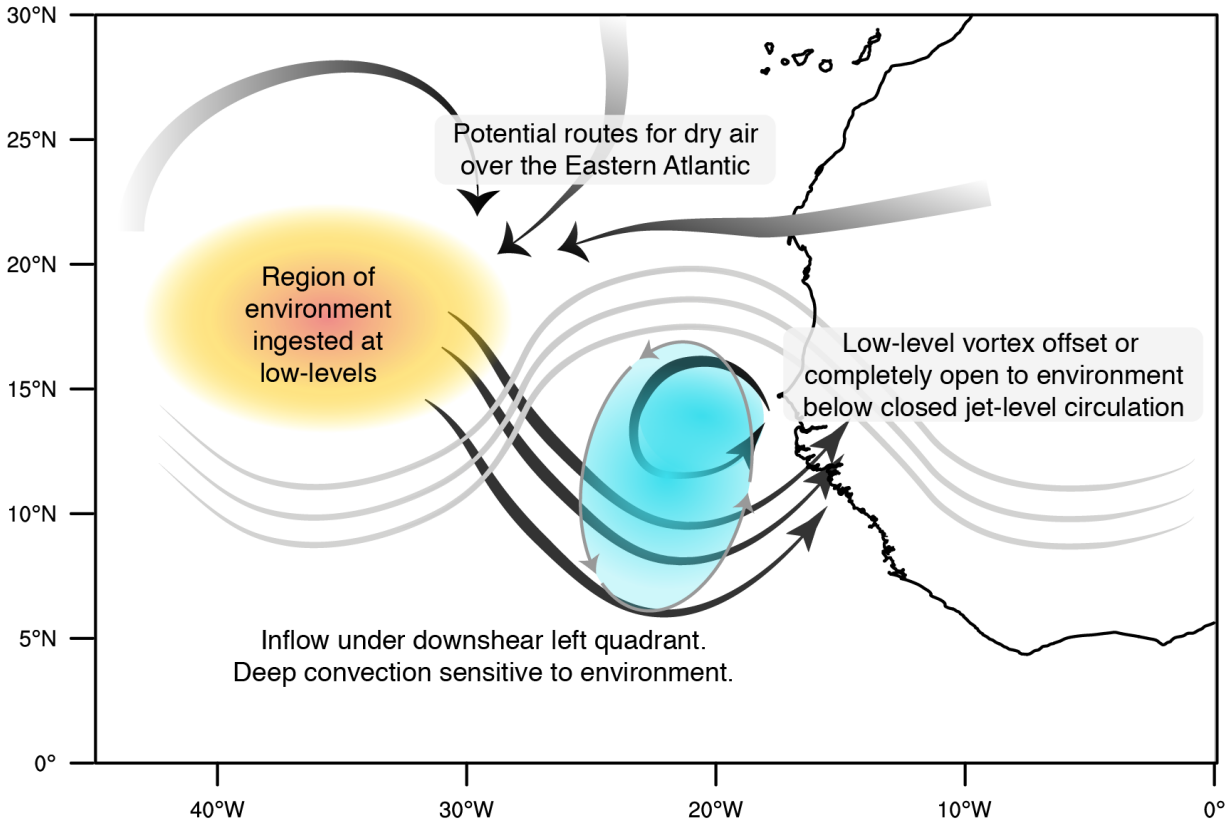

Figure 6.1: Schematic of the interaction of low-level environmental air and an AEW trough. Lighter gray shade throughout represents lower pressure. Low-level dry air was shown to originate from subsidence from multiple regions. Troughs ingested environmental air from NW (orange oval), flow shown by black arrows. Low-level closed circulation typically offset to NE initially. Jet-level circulation (grey arrows) therefore is over the advection of environmental air below.

BIBLIOGRAPHY

Agudelo, P., C. D. Hoyos, J. Curry, and P. J. Webster, 2011: Probabilistic discrimination between large-scale environments of intensifying and decaying African Easterly Waves. *Clim Dyn*, **36 (7)**, 1379–1401.

Aiyyer, A., and J. Molinari, 2008: MJO and tropical cyclogenesis in the Gulf of Mexico and eastern Pacific: Case study and idealized numerical modeling. *J. Atmos. Sci.*, **65 (8)**, 2691–2704.

Arnault, J., and F. Roux, 2009: Case study of a developing African easterly wave during NAMMA: An energetic point of view. *J. Atmos. Sci.*, **66 (10)**, 2991–3020.

Arnault, J., and F. Roux, 2010: Failed Cyclogenetic Evolution of a West African Monsoon Perturbation Observed during AMMA SOP-3. *J. Atmos. Sci.*, **67 (6)**, 1863–1883.

Avila, L. A., and R. Pasch, 1995: Atlantic tropical systems of 1993. *Mon. Wea. Rev.*, **123 (3)**, 887–896.

Bain, C. L., K. D. Williams, S. F. Milton, and J. T. Heming, 2014: Objective tracking of African Easterly Waves in Met Office models. *Quart. J. Roy. Meteor. Soc.*, **140 (678)**, 47–57.

Ben-Ami, Y., I. Koren, O. Altaratz, A. Kostinski, and Y. Lehahn, 2012: Discernible rhythm in the spatio/temporal distributions of transatlantic dust. *Atmospheric Chemistry and Physics*, **12 (5)**, 2253–2262.

Berry, G. J., and C. D. Thorncroft, 2005: Case study of an intense African easterly wave. *Mon. Wea. Rev.*, **133**, 752–766.

Berry, G. J., and C. D. Thorncroft, 2012: African Easterly Wave Dynamics in a Mesoscale Numerical Model: The Upscale Role of Convection. *J. Atmos. Sci.*, **69 (4)**, 1267–1283.

Berry, G. J., C. D. Thorncroft, and T. Hewson, 2007: African Easterly Waves during 2004—Analysis Using Objective Techniques. *Mon. Wea. Rev.*, **135 (4)**, 1251–1267.

Bister, M., and K. A. Emanuel, 1997: The genesis of Hurricane Guillermo: TEXMEX analyses and a modeling study. *Mon. Wea. Rev.*, **125 (10)**, 2662–2682.

Brammer, A., and C. D. Thorncroft, 2015: Variability and Evolution of African Easterly Wave Structure and the Relationship with Tropical Cyclogenesis over the Eastern Atlantic. *Mon. Wea. Rev.*, eView.

Braun, S. A., 2010: Reevaluating the Role of the Saharan Air Layer in Atlantic Tropical Cyclogenesis and Evolution. *Mon. Wea. Rev.*, **138 (6)**, 2007–2037.

Braun, S. A., J. A. Sippel, and D. S. Nolan, 2012: The Impact of Dry Midlevel Air on Hurricane Intensity in Idealized Simulations with No Mean Flow. *J. Atmos. Sci.*, **69 (1)**, 236–257.

Briegel, L. M., and W. Frank, 1997: Large-scale influences on tropical cyclogenesis in the western North Pacific. *Mon. Wea. Rev.*, **125 (7)**, 1397–1413.

Burpee, R., 1972: The origin and structure of easterly waves in the lower troposphere of North Africa. *J. Atmos. Sci.*, **29**, 77–90.

Burpee, R., 1974: Characteristics of North African easterly waves during the summers of 1968 and 1969. *J. Atmos. Sci.*, **31**, 1556–1570.

Camargo, S. J., K. A. Emanuel, and A. H. Sobel, 2007: Use of a Genesis Potential Index to Diagnose ENSO Effects on Tropical Cyclone Genesis. *J. Clim.*, **20 (19)**, 4819–4834.

Carlson, T. N., 1969a: Some remarks on African disturbances and their progress over the tropical Atlantic. *Mon. Wea. Rev.*, **97 (10)**, 716–726.

Carlson, T. N., 1969b: Synoptic histories of three African disturbances that developed into Atlantic hurricanes. *Mon. Wea. Rev.*, **97 (3)**, 256–276.

Carlson, T. N., and J. M. Prospero, 1972: The Large-Scale Movement of Saharan Air Outbreaks over the Northern Equatorial Atlantic. *J. Appl. Meteor.*, **11 (2)**, 283–297.

Casey, S. P. F., A. E. Dessler, and C. Schumacher, 2009: Five-Year Climatology of Midtroposphere Dry Air Layers in Warm Tropical Ocean Regions as Viewed by AIRS/ Aqua. *J. Appl. Meteor. Climatol.*, **48 (9)**, 1831–1842.

Charney, J. G., and M. E. Stern, 1962: On the Stability of Internal Baroclinic Jets in a Rotating Atmosphere. *J. Atmos. Sci.*, **19 (2)**, 159–172.

Chen, S.-H., S.-H. Wang, and M. Waylonis, 2010: Modification of Saharan air layer and environmental shear over the eastern Atlantic Ocean by dust-radiation effects. *Journal of Geophysical Research: Atmospheres*, **115 (D21)**, D21 202.

Chen, T.-C., S.-Y. Wang, and A. J. Clark, 2008: North Atlantic Hurricanes Contributed by African Easterly Waves North and South of the African Easterly Jet. *J. Clim.*, **21 (24)**, 6767–6776.

Crétat, J., E. K. Vizy, and K. H. Cook, 2014: The relationship between African easterly waves and daily rainfall over West Africa: observations and regional climate simulations. *Clim Dyn*, **44 (1-2)**, 385–404.

Davis, C. A., and D. A. Ahijevych, 2012: Mesoscale Structural Evolution of Three Tropical Weather Systems Observed during PREDICT. *J. Atmos. Sci.*, **69 (4)**, 1284–1305.

Davis, C. A., S. C. Jones, and M. Riemer, 2008: Hurricane Vortex Dynamics during Atlantic Extratropical Transition. *J. Atmos. Sci.*, **65 (3)**, 714–736.

DeMaria, M., 1996: The effect of vertical shear on tropical cyclone intensity change. *J. Atmos. Sci.*, **53 (14)**, 2076–2088.

DeMaria, M., and J. Kaplan, 1994: A statistical hurricane intensity prediction scheme (SHIPS) for the Atlantic basin. *Weather and Forecasting*, **9 (2)**, 209–220.

Dieng, A. L., L. Eymard, S. M. Sall, A. Lazar, and M. Leduc-Leballeur, 2014: Analysis of Strengthening and Dissipating Mesoscale Convective Systems Propagating off the West African Coast. *Mon. Wea. Rev.*, **142 (12)**, 4600–4623.

Draxler, R. R., and G. D. Hess, 1997: *Description of the HYSPLIT4 modeling system.* NOAA Technical Memorandum ERL ARL-224, NOAA Air Resources Laboratory, Silver Spring, MD.

Draxler, R. R., and G. D. Hess, 1998: An overview of the HYSPLIT 4 modelling system for trajectories. *Australian Meteorological Magazine*, **47 (4)**.

Dunion, J. P., J. Kaplan, A. Schumacher, J. Cossuth, and M. DeMaria, 2013: Development

of a Probabilistic Tropical Cyclone Genesis Prediction Scheme. JHT Year 2 End of Year Report. Tech. rep.

Dunion, J. P., and C. S. Velden, 2004: The Impact of the Saharan Air Layer on Atlantic Tropical Cyclone Activity. *Bull. Amer. Meteor. Soc.*, **85 (3)**, 353–365.

Dunkerton, T., M. Montgomery, and Z. Wang, 2009: Tropical cyclogenesis in a tropical wave critical layer: easterly waves. *Atmospheric Chemistry and Physics*, **9**, 5587–5646.

Emanuel, K. A., 1989: The finite-amplitude nature of tropical cyclogenesis. *J. Atmos. Sci.*, **46 (22)**, 3431–3456.

Emanuel, K. A., 2013: Downscaling CMIP5 climate models shows increased tropical cyclone activity over the 21st century. *PNAS*, **110 (30)**, 12 219–12 224.

Erickson, C., 1963: An incipient hurricane near the West African coast. *Mon. Wea. Rev.*, **91 (2)**, 61–68.

Fink, A. H., and A. Reiner, 2003: Spatiotemporal variability of the relation between African easterly waves and West African squall lines in 1998 and 1999. *J. Geophys. Res.*, **108 (D11)**, 4332.

Fink, A. H., D. G. Vincent, and P. M. Reiner, 2004: Mean state and wave disturbances during Phases I, II, and III of GATE based on ERA-40. *Mon. Wea. Rev.*, **132 (7)**, 1661–1683.

Frank, N. L., 1969: The "Inverted V" Cloud Pattern—an Easterly Wave? *Mon. Wea. Rev.*, **97 (2)**, 130–140.

Frank, W., and P. Roundy, 2006: The role of tropical waves in tropical cyclogenesis. *Mon. Wea. Rev.*, **134 (9)**, 2397–2417.

Frank, W. M., and E. A. Ritchie, 1999: Effects of Environmental Flow upon Tropical Cyclone Structure. *Mon. Wea. Rev.*, **127 (9)**, 2044–2061.

Fritz, C., and Z. Wang, 2013: A Numerical Study of the Impacts of Dry Air on Tropical Cyclone Formation: A Development Case and a Nondevelopment Case. *J. Atmos. Sci.*, **70 (1)**, 91–111.

Ge, X., T. Li, and M. Peng, 2013: Effects of Vertical Shears and Midlevel Dry Air on Tropical Cyclone Developments. *J. Atmos. Sci.*, **70 (12)**, 3859–3875.

Gray, W., 1968: Global view of the origin of tropical disturbances and storms. *Mon. Wea. Rev.*, **96 (10)**, 669–700.

Gray, W., 1988: Environmental influences on tropical cyclones. *Australian Meteorological Magazine*, **36**, 127–139.

Gray, W., and C. Landsea, 1992: African rainfall as a precursor of hurricane-related destruction on the US east coast. *Bull. Amer. Meteor. Soc.*, **73**, 1352–1352.

Gray, W. M., C. W. Landsea, P. W. Mielke, and K. J. Berry, 1994: Predicting Atlantic Basin Seasonal Tropical Cyclone Activity by 1 June. *Weather and Forecasting*, **9 (1)**, 103–115.

Halperin, D. J., H. E. Fuelberg, R. E. Hart, J. H. Cossuth, P. Sura, and R. J. Pasch, 2013: An Evaluation of Tropical Cyclone Genesis Forecasts from Global Numerical Models. *Weather and Forecasting*, **28 (6)**, 1423–1445.

Hodges, K., B. J. Hoskins, J. Boyle, and C. D. Thorncroft, 2003: A Comparison of Recent Reanalysis Datasets Using Objective Feature Tracking: Storm Tracks and Tropical Easterly Waves. *Mon. Wea. Rev.*, **131 (9)**, 2012–2037.

Hopsch, S. B., C. D. Thorncroft, K. Hodges, and A. R. Aiyyer, 2007: West African Storm Tracks and Their Relationship to Atlantic Tropical Cyclones. *J. Clim.*, **20 (11)**, 2468–2483.

Hopsch, S. B., C. D. Thorncroft, and K. R. Tyle, 2010: Analysis of African Easterly Wave Structures and Their Role in Influencing Tropical Cyclogenesis. *Mon. Wea. Rev.*, **138 (4)**, 1399–1419.

Huang, J., C. Zhang, and J. M. Prospero, 2010: African dust outbreaks: A satellite perspective of temporal and spatial variability over the tropical Atlantic Ocean. *J. Geophys. Res.*, **115 (D5)**, D05 202.

Huffman, G. J., and Coauthors, 2007: The TRMM Multisatellite Precipitation Analysis (TMPA): Quasi-Global, Multiyear, Combined-Sensor Precipitation Estimates at Fine Scales. *J. Hydrometeor*, **8 (1)**, 38–55.

Intrieri, J. M., and Coauthors, 2014: Global Hawk dropsonde observations of the Arctic atmosphere during the Winter Storms and Pacific Atmospheric Rivers (WISPAR) field campaign. *Atmospheric Measurement Techniques Discussions*, **7**, 3917–3926.

Janiga, M. A., 2013: Interactions between African Easterly Waves and Moist Convection. Ph.D. thesis, University At Albany, NY, University At Albany, NY.

Janiga, M. A., and C. D. Thorncroft, 2012: Regional differences in the kinematic and thermodynamic structure of African easterly waves. *Quart. J. Roy. Meteor. Soc.*, **139 (675)**, 1598–1614.

Jones, S. C., 1995: The evolution of vortices in vertical shear. I: Initially barotropic vortices. *Quart. J. Roy. Meteor. Soc.*, **121 (524)**, 821–851.

Jones, S. C., 2004: On the ability of dry tropical-cyclone-like vortices to withstand vertical shear. *J. Atmos. Sci.*, **61 (1)**, 114–119.

Kampstra, P., 2008: Beanplot: A boxplot alternative for visual comparison of distributions. *Journal of Statistical Software*, **28**, Code Snippet 1.

Karyampudi, V. M., and T. N. Carlson, 1988: Analysis and numerical simulations of the Saharan air layer and its effect on easterly wave disturbances. *J. Atmos. Sci.*, **45 (21)**, 3102–3136.

Karyampudi, V. M., and H. F. Pierce, 2002: Synoptic-Scale Influence of the Saharan Air Layer on Tropical Cyclogenesis over the Eastern Atlantic. *Mon. Wea. Rev.*, **130 (12)**, 3100–3128.

Kiladis, G. N., C. D. Thorncroft, and N. M. J. Hall, 2006: Three-Dimensional Structure and Dynamics of African Easterly Waves. Part I: Observations. *J. Atmos. Sci.*, **63 (9)**, 2212–2230.

Klotzbach, P. J., 2014: The Suprisingly Quiet 2013 Atlantic Basin Hurricane Season. *Science and Technology Infusion Climate Bulletin*, 38th NOAA Annual Climate Diagnostics and Prediction Workshop College Park–MD– 21–24.

Knapp, K. R., and NOAA CDR Program, 2014: NOAA Climate Data Record (CDR) of Gridded Satellite Data from ISCCP B1 (GridSat-B1) 11 micron Brightness Temperature, Version 2. . NOAA National Climatic Data Center.

Knapp, K. R., and Coauthors, 2011: Globally Gridded Satellite Observations for Climate Studies. *Bull. Amer. Meteor. Soc.*, **92 (7)**, 893–907.

Laing, A. G., R. Carbone, V. Levizzani, and J. Tuttle, 2008: The propagation and diurnal cycles of deep convection in northern tropical Africa. *Quart. J. Roy. Meteor. Soc.*, **134**, 93–109.

Laken, B. A., H. Parviainen, and E. Pallé, 2014: Saharan mineral dust outbreaks observed over the North Atlantic island of La Palma in summertime between 1984 and 2012. *Quart. J. Roy. Meteor. Soc.*, **140 (680)**, 1058–1068.

Landsea, C. W., 1993: A climatology of intense (or major) Atlantic hurricanes. *Mon. Wea. Rev.*, **121 (6)**, 1703–1713.

Landsea, C. W., A. Hagen, W. Bredemeyer, C. Carrasco, D. A. Glenn, A. Santiago, D. Strahan-Sakoskie, and M. Dickinson, 2014: A Reanalysis of the 1931–43 Atlantic Hurricane Database*. *Mon. Wea. Rev.*, **27 (16)**, 6093–6118.

Leppert, K. D., II, D. J. Cecil, and W. A. Petersen, 2013: Relation Between Tropical Easterly Waves, Convection, and Tropical Cyclogenesis: A Lagrangian Perspective. *Mon. Wea. Rev.*, **141**, 2649–2668.

Ling, J., and C. Zhang, 2013: Diabatic heating profiles in recent global reanalyses. *J. Clim.*, **26 (10)**, 3307–3325.

Martin, E. R., and C. D. Thorncroft, 2013: The impact of the AMO on the West African monsoon annual cycle. *Quart. J. Roy. Meteor. Soc.*, **140 (678)**, 31–46.

Martin, E. R., and C. D. Thorncroft, 2015: Representation of African Easterly Waves in CMIP5 Models. *J. Clim.*, **28 (19)**, 7702–7715.

Matthews, A. J., and G. N. Kiladis, 1999: The tropical-extratropical interaction between

high-frequency transients and the Madden-Julian oscillation. *Mon. Wea. Rev.*, **127 (5)**, 661–677.

McBride, J. L., 1995: Tropical Cyclone Formation. *Global Perspectives on Tropical Cyclones*, World Meteorological Organisation.

McGill, M., and D. L. Hlavka, 2015: Hurricane and Severe Storm Sentinel (HS3) Global Hawk Cloud Physics Lidar (CPL). NASA Global Hydrology Resource Center DAAC, Huntsville, Alabama, U.S.A.

McGill, M. J., D. L. Hlavka, W. D. Hart, E. J. Welton, and J. R. Campbell, 2003: Airborne lidar measurements of aerosol optical properties during SAFARI-2000. *Journal of Geophysical Research: Atmospheres*, **108 (D13)**.

McTaggart-Cowan, R., G. D. Deane, L. F. Bosart, C. A. Davis, and T. J. Galarneau Jr., 2008: Climatology of Tropical Cyclogenesis in the North Atlantic (1948–2004). *Mon. Wea. Rev.*, **136 (4)**, 1284–1304.

Montgomery, M. T., L. L. Lussier III, R. W. Moore, and Z. W. Wang, 2010: The genesis of Typhoon Nuri as observed during the Tropical Cyclone Structure 2008 (TCS-08) field experiment. Part 1: The role of the easterly wave critical layer . *Atmospheric Chemistry and Physics*, **10 (20)**, 9879–9900.

Montgomery, M. T., M. E. Nicholls, and T. A. Cram, 2006: A vortical hot tower route to tropical cyclogenesis. *J. Atmos. Sci.*, **63 (1)**, 355–386.

Neumann, C. J., M. B. Lawrence, and E. L. Caso, 1977: Monte Carlo Significance Testing as Applied to Statistical Tropical Cyclone Prediction Models. *J. Appl. Meteor.*, **16 (11)**, 1165–1174.

Norquist, D. C., E. E. Recker, and R. J. Reed, 1977: The Energetics of African Wave Disturbances as observed During Phase III of GATE. *Mon. Wea. Rev.*, **105 (3)**, 334–342.

Powell, M. D., 1990: Boundary layer structure and dynamics in outer hurricane rainbands. Part II: Downdraft modification and mixed layer recovery. *Mon. Wea. Rev.*, **118 (4)**, 918–938.

Pytharoulis, I., and C. D. Thorncroft, 1999: The Low-Level Structure of African Easterly Waves in 1995. *Mon. Wea. Rev.*, **127 (10)**, 2266–2280.

Rappin, E. D., and D. S. Nolan, 2012: The effect of vertical shear orientation on tropical cyclogenesis. *Quart. J. Roy. Meteor. Soc.*, **138 (665)**, 1035–1054.

Rappin, E. D., D. S. Nolan, and K. A. Emanuel, 2010: Thermodynamic control of tropical cyclogenesis in environments of radiative-convective equilibrium with shear. *Quart. J. Roy. Meteor. Soc.*, **136 (653)**, 1954–1971.

Raymond, D. J., and C. L. Carrillo, 2011: The vorticity budget of developing typhoon Nuri (2008). *Atmospheric Chemistry and Physics*, **11 (1)**, 147–163.

Raymond, D. J., and S. L. Sessions, 2007: Evolution of convection during tropical cyclogenesis. *Geophys. Res. Lett.*, **34 (6)**, L06 811.

Reale, O., W. K. Lau, K.-M. Kim, and E. Brin, 2009: Atlantic Tropical Cyclogenetic Processes during SOP-3 NAMMA in the GEOS-5 Global Data Assimilation and Forecast System. *J. Atmos. Sci.*, **66 (12)**, 3563–3578.

Reasor, P. D., M. T. Montgomery, and L. D. Grasso, 2004: A new look at the problem of tropical cyclones in vertical shear flow: Vortex resiliency. *J. Atmos. Sci.*, **61 (1)**, 3–22.

Reed, R. J., D. C. Norquist, and E. E. Recker, 1977: The Structure and Properties of African Wave Disturbances as Observed During Phase III of GATE. *Mon. Wea. Rev.*, **105 (3)**, 317–333.

Riemer, M., and M. T. Montgomery, 2011: Simple kinematic models for the environmental interaction of tropical cyclones in vertical wind shear. *Atmospheric Chemistry and Physics*, **11 (17)**, 9395–9414.

Riemer, M., M. T. Montgomery, and M. E. Nicholls, 2010: A new paradigm for intensity modification of tropical cyclones: thermodynamic impact of vertical wind shear on the inflow layer. *Atmospheric Chemistry and Physics*, **10 (7)**, 3163–3188.

Rios-Berrios, R., R. D. Torn, and C. A. Davis, 2015: An Ensemble Approach to Investigate Tropical Cyclone Intensification in Sheared Environments. Part I: Katia (2011). *J. Atmos. Sci.*, e–View.

Ritchie, E., and G. J. Holland, 1993: On the interaction of tropical-cyclone-scale vortices. II: Discrete vortex patches. *Quart. J. Roy. Meteor. Soc.*, **119 (514)**, 1363–1379.

Roca, R., J. P. Lafore, C. Piriou, and J.-L. Redelsperger, 2005: Extratropical dry-air intrusions into the West African monsoon midtroposphere: An important factor for the convective activity over the Sahel. *J. Atmos. Sci.*, **62 (2)**, 390–407.

Ross, R. S., and T. N. Krishnamurti, 2009: Energy Transformation and Diabatic Processes in Developing and Nondeveloping African Easterly Waves Observed during the NAMMA Project of 2006. *Weather and Forecasting*, **24**, 1524–1548.

Ross, R. S., and T. N. Krishnamurti, 2012: Interactions of Diabatic Heating in Convective

Superbursts with Energy Conversion Processes in the Genesis of Cape Verde Hurricanes from African Easterly Waves. *Mon. Wea. Rev.*, **140**, 748–773.

Saha, S., and Coauthors, 2010: The NCEP Climate Forecast System Reanalysis. *Bull. Amer. Meteor. Soc.*, **91 (8)**, 1015–1057.

Saha, S., and Coauthors, 2014: The NCEP Climate Forecast System Version 2. *J. Clim.*, **27 (6)**, 2185–2208.

Schenkel, B. A., and R. E. Hart, 2012: An examination of tropical cyclone position, intensity, and intensity life cycle within atmospheric reanalysis datasets. *J. Clim.*, **25 (10)**, 3453–3475.

Schreck, C. J., and J. Molinari, 2011: Tropical Cyclogenesis Associated with Kelvin Waves and the Madden–Julian Oscillation. *Mon. Wea. Rev.*, **139 (9)**, 2723–2734.

Schreck, C. J., L. Shi, J. P. Kossin, and J. J. Bates, 2013: Identifying the MJO, Equatorial Waves, and Their Impacts Using 32 Years of HIRS Upper-Tropospheric Water Vapor. *J. Clim.*, **26 (4)**, 1418–1431.

Schumacher, C., R. A. Houze Jr., and I. Kraucunas, 2004: The tropical dynamical response to latent heating estimates derived from the TRMM precipitation radar. *J. Atmos. Sci.*, **61 (12)**, 1341–1358.

Shu, S., and L. Wu, 2009: Analysis of the influence of Saharan air layer on tropical cyclone intensity using AIRS/Aqua data. *Geophys. Res. Lett.*, **36 (9)**, L09 809.

Sippel, J. A., S. A. Braun, and C.-L. Shie, 2011: Environmental Influences on the Strength of Tropical Storm Debby (2006). *J. Atmos. Sci.*, **68 (11)**, 2557–2581.

Stohl, A., G. Wotawa, P. Seibert, and H. Kromp-Kolb, 1995: Interpolation Errors in Wind Fields as a Function of Spatial and Temporal Resolution and Their Impact on Different Types of Kinematic Trajectories. *J. Appl. Meteor.*, **34 (10)**, 2149–2165.

Sun, D., K. M. Lau, and M. Kafatos, 2008: Contrasting the 2007 and 2005 hurricane seasons: Evidence of possible impacts of Saharan dry air and dust on tropical cyclone activity in the Atlantic basin. *Geophys. Res. Lett.*, **35 (15)**, L15 405.

Tang, B., and K. A. Emanuel, 2010: Midlevel Ventilation's Constraint on Tropical Cyclone Intensity. *J. Atmos. Sci.*, **67 (6)**, 1817–1830.

Tang, B., and K. A. Emanuel, 2012: A Ventilation Index for Tropical Cyclones. *Bull. Amer. Meteor. Soc.*, **93 (12)**, 1901–1912.

Thorncroft, C. D., and K. Hodges, 2001: African easterly wave variability and its relationship to Atlantic tropical cyclone activity. *J. Clim.*, **14 (6)**, 1166–1179.

Thorncroft, C. D., and B. J. Hoskins, 1994a: An idealized study of African easterly waves. I: A linear view. *Quart. J. Roy. Meteor. Soc.*, **120 (518)**, 953–982.

Thorncroft, C. D., and B. J. Hoskins, 1994b: An idealized study of African easterly waves. II: A nonlinear view. *Quart. J. Roy. Meteor. Soc.*, **120 (518)**, 983–1015.

Tory, K. J., and W. Frank, 2010: Tropical Cyclone Formation. *Global Perspectives on Tropical Cyclones*, J. Chan, and J. D. Kepert, Eds., World Meteorological Organisation, 55–91.

TRMM, 2011: *TRMM/TMPA 3B42 TRMM and Others Rainfall Estimate Data V7,version 7*. Greenbelt, MD:Goddard Space Flight Center Distributed Active Archive Center (GSFC DAAC).

Ventrice, M. J., C. D. Thorncroft, and M. A. Janiga, 2012a: Atlantic Tropical Cyclogenesis: A Three-Way Interaction between an African Easterly Wave, Diurnally Varying Convection, and a Convectively Coupled Atmospheric Kelvin Wave. *Mon. Wea. Rev.*, **140 (4)**, 1108–1124.

Ventrice, M. J., C. D. Thorncroft, and C. J. Schreck, 2012b: Impacts of Convectively Coupled Kelvin Waves on Environmental Conditions for Atlantic Tropical Cyclogenesis. *Mon. Wea. Rev.*, **140 (7)**, 2198–2214.

Vizy, E. K., and K. H. Cook, 2009: Tropical storm development from African easterly waves in the eastern Atlantic: A comparison of two successive waves using a regional model as part of NASA AMMA 2006. *J. Atmos. Sci.*, **66 (11)**, 3313–3334.

Wang, J., L. Zhang, A. Dai, F. Immler, M. Sommer, and H. Vömel, 2013: Radiation Dry Bias Correction of Vaisala RS92 Humidity Data and Its Impacts on Historical Radiosonde Data. *J. Atmos. Oceanic Technol.*, **30 (2)**, 197–214.

Wang, J., and Coauthors, 2010a: Water vapor variability and comparisons in the subtropical Pacific from The Observing System Research and Predictability Experiment-Pacific Asian Regional Campaign (T-PARC) Driftsonde, Constellation Observing System for Meteorology, Ionosphere, and Climate (COSMIC), and reanalyses. *J. Geophys. Res.*, **115 (D21)**, D21 108.

Wang, Z., M. T. Montgomery, and T. Dunkerton, 2010b: Genesis of Pre–Hurricane Felix (2007). Part I: The Role of the Easterly Wave Critical Layer. *J. Atmos. Sci.*, **67 (6)**, 1711–1729.

Wilks, D. S., 2011: *Statistical Methods in the Atmospheric Sciences*. Academic Press.

Xu, K.-M., and K. A. Emanuel, 1989: Is the tropical atmosphere conditionally unstable? *Mon. Wea. Rev.*, **117 (7)**, 1471–1479.

Yorks, J. E., D. L. Hlavka, W. D. Hart, and M. J. McGill, 2011: Statistics of Cloud Optical Properties from Airborne Lidar Measurements. *J. Atmos. Oceanic Technol.*, **28 (7)**, 869–883.

Zehr, R. M., 1992: Tropical Cyclogenesis in the Western North Pacific. Ph.D. thesis, National Environmental Satellite, Data, and Information Service.

Zhang, C., and S. M. Hagos, 2009: Bi-modal Structure and Variability of Large-Scale Diabatic Heating in the Tropics. *J. Atmos. Sci.*, **66 (12)**, 3621–3640.

Zhang, C., and J. Pennington, 2004: African dry air outbreaks. *J. Geophys. Res.*, **109 (D20)**, D20 108.